

Benchmarking of Thermal-Hydraulic Loop Models for Lead-Alloy-Cooled Advanced Nuclear Energy Systems

Phase II: Natural Convection



Organisation for Economic Co-operation and Development

NEA/NSC/R(2018)1

Unclassified

English - Or. English

10 September 2018

NUCLEAR ENERGY AGENCY
NUCLEAR SCIENCE COMMITTEE

Benchmarking of Thermal-Hydraulic Loop Models for Lead-Alloy-Cooled Advanced Nuclear Energy Systems

Information Note: This document exists only in pdf.

stephanie.cornet@.oecd.org

JT03435464

Foreword

Under the auspices of the Nuclear Energy Agency (NEA) Nuclear Science Committee (NSC), the Working Party on Scientific Issues of the Fuel Cycle (WPFC) has been established to co-ordinate scientific activities regarding various existing and advanced nuclear fuel cycles, including advanced reactor systems, associated chemistry and flowsheets, development and performance of fuel and materials, as well as accelerators and spallation targets. The WPFC has set up different expert groups to cover a wide range of scientific issues in the field of the nuclear fuel cycle.

The Task Force on Lead-Alloy-Cooled Advanced Nuclear Energy Systems (LACANES) was launched in 2007 to study the thermal-hydraulic characteristics of heavy liquid metal coolant loops. The objectives of the task force are: 1) to validate thermal-hydraulic loop models for application to LACANES design analysis in participating organisations by benchmarking with a set of well-characterised lead-alloy coolant loop test data; 2) to establish guidelines for quantifying thermal-hydraulic modelling parameters related to friction and heat transfer by lead-alloy coolant; and 3) to identify specific issues, either in modelling and/or in loop testing, which need to be addressed in possible future work.

Nine participants from seven different institutes took part in the first phase of the benchmarking on forced convection. The related report provided details of the benchmark specifications, method and code characteristics, as well as a comparison and analysis of the calculation results of the preliminary study, i.e. the pressure loss coefficients [1]. In Phase II on natural convection, five participants from five different institutes were involved in the study. Similar to the Phase I report, this document describes details of the benchmark specifications, method and code characteristics. The present report summarises the results of Phase II, which focuses on the comparison between experimental data from the HELIOS (Heavy eutectic liquid metal loop for integral test of operability and safety) facility at Seoul National University, Korea, and calculation results for natural circulation (NC) tests.

Reference

- [1] NEA (2007), *Handbook on Lead-bismuth Eutectic Alloy and Lead Properties, Materials Compatibility, Thermal-hydraulics and Technologies*, OECD, Paris.

Acknowledgements

The NEA would like to acknowledge the contributions of members of the Task Force on Lead-Alloy-Cooled Advanced Nuclear Energy Systems (LACANES). In particular, to Professor Il Soon Hwang (Seoul National University, Korea), the Chair of this task force, and to all the experts who contributed to the realisation of this work and the preparation of this report: Y.H. Shin (Seoul National University, Korea), M. Polidori (National Agency for New Technologies, Energy and Sustainable Economic Development [ENEA], Italy), V. Cassamassima (RSE, Italy), L. Barrucca (Ansaldo, Italy), and M. Jin (Institute of Nuclear Energy Safety Technology [INEST], China).

Table of contents

List of abbreviations and acronyms	8
1. Introduction	10
2. Benchmark specifications	12
2.1 The HELIOS facility	12
2.2 The NACIE facility	18
2.3 Guidelines for pressure loss coefficient evaluation and comparison	25
3. Method of the benchmark	27
3.1 Approach	27
3.2 RSE, Italy	27
4. Experiments and results	72
4.1 HELIOS	72
4.2 NACIE	83
5. Comparison and discussion	89
5.1 HELIOS	89
5.2 NACIE	98
6. Summary and conclusion	108
6.1 Summary	108
6.2 Conclusion	109
Appendix A: NACIE drawings	110
Appendix B: HELIOS pressure loss result comparison tables	115

List of figures

Figure 2.1	Schematic (left) and photograph (right) of HELIOS [4]	12
Figure 2.2	Natural circulation flow path in the HELIOS: Birds-eye view from top, natural circulation bypass in detail.	14
Figure 2.3	Component map of the HELIOS primary loop in natural circulation test campaigns.	15
Figure 2.4	NACIE Loop Layout.	18
Figure 2.5	Vertical section of the NACIE Bundle and grids.	20
Figure 2.6	Picture of the NACIE spacer grid (before operate)	22
Figure 2.7	Scheme of the HX and view of the expansion joint.	23
Figure 2.8	Scheme of heating section position in the loop.	24
Figure 2.9	Scheme of NACIE with section lengths.	24
Figure 3.1	Graphical description of the HELIOS model in the LegoPST environment.	28
Figure 3.2	Graphical representation of the model of HELIOS heat exchanger in LegoPC environment.	29
Figure 3.3	Graphical representation of the model of HELIOS core mockup in LegoPC environment.	29
Figure 3.4	Standard test set up for valve sizing	30
Figure 3.5	LACANES phase I – Pressure loss at gate valve	31
Figure 3.6	Graphical description of the NACIE model in the LegoPST environment	32
Figure 3.7	NACIE heat exchanger open loop model – graphical representation in LegoPC environment.	33

Figure 3.8	Main pressure losses accounted by the Lego PC model of the NACIE facility.....	34
Figure 3.9	HELIOS nodalisation for RELAP5 (ENEA).....	37
Figure 3.10	Comparison of the thermal conductivity (ENEA).....	38
Figure 3.11	Comparison of the heat capacity (ENEA).....	39
Figure 3.12	NACIE nodalisation for RELAP5 (ENEA).....	39
Figure 3.13	HELIOS nodalisation prepared for MARS-LBE simulation.....	43
Figure 3.14	NACIE nodalisation prepared for MARS-LBE simulation.....	46
Figure 3.15	RELAP5 geometrical configuration scheme (Ansaldo).....	51
Figure 3.16	Sections of the elements in the riser (Ansaldo).....	52
Figure 3.17	Details of expansion vessel nodalisation and initial configuration.....	52
Figure 3.18	RELAP5 nodalisation model of HELIOS NC loop.....	59
Figure 3.19	RELAP5 nodalisation model of NACIE NC loop.....	67
Figure 4.1	Test procedure for HELIOS non-isothermal natural circulation test campaigns.....	73
Figure 4.2	Position of orifice flow meter and thermocouples in HELIOS.....	74
Figure 4.3	Case I (15.0 kW) results: variation of power given to main loop, temperature distributions and mass flow rates of the HELIOS.....	76
Figure 4.4	Case I (15.0 kW) steady-state results: HELIOS temperature distributions.....	77
Figure 4.5	Case I (15.0 kW) steady-state results: HELIOS mass flow rates.....	77
Figure 4.6	Case I (15.0 kW) steady-state results: HELIOS primary loop temperature distribution.....	78
Figure 4.7	Case II (9.8 kW) results: variation of power given to main loop, temperature distributions and mass flow rates of the HELIOS.....	79
Figure 4.8	Case II (9.8 kW) steady-state results: HELIOS temperature distributions.....	80
Figure 4.9	Case II (9.8 kW) steady-state results: HELIOS mass flow rates.....	80
Figure 4.10	Case II (9.8 kW) steady-state results: HELIOS primary loop temperature distribution.....	81
Figure 4.11	Synoptic view of NACIE facility.....	84
Figure 4.12	Sketch of the Induction flow meter MP101 installed in the NACIE primary loop.....	85
Figure 4.13	Test 301: LBE mass flow rate measured (MP101) and estimated with thermal balance.....	87
Figure 4.14	Test 301: LBE and water temperatures.....	87
Figure 5.1	Calculated LBE temperature distributions along main loop: Case I (15.0kW).....	91
Figure 5.2	Calculated LBE temperature distributions along main loop: Case II (9.8kW).....	92
Figure 5.3	LBE mass flow rate comparisons on Case I (15.0kW) and Case II (9.8kW).....	93
Figure 5.4	Comparisons on average temperature differences between hot leg and cold leg in Case I (15.0kW) and Case II (9.8kW).....	93
Figure 5.5	Graphical illustration of pressure loss comparison groups for HELIOS loop.....	95
Figure 5.6	Comparison of total and local pressure loss of HELIOS for (a) Case I (15.0kW) and (b) Case II (9.8kW).....	96
Figure 5.7	Comparison of accumulated pressure loss of HELIOS for (a) Case I (15.0kW) and (b) Case II (9.8kW).....	97
Figure 5.8	Comparison of total and partial pressure loss of NACIE Test 301.....	104
Figure 5.9	Comparison of the accumulated pressure loss of NACIE Test 301.....	104
Figure 5.10	Qualitative comparison of the temperature distributions of NACIE Test 301.....	106
Figure 5.11	Comparison of the inlet/outlet water temperatures of NACIE Test 301.....	106
Figure 5.12	Comparison of mass flow rates in natural circulation of NACIE Test 301.....	107

List of tables

Table 1.1	List of participants and codes for the second phase of the NEA Benchmark on LACANES.....	11
Table 2.1	Thermophysical properties of Dowtherm® RP thermal fluid [5].....	13
Table 2.2	List of components and parts of the HELIOS primary loop in natural circulation test campaigns.....	16
Table 2.3	NACIE Main Geometrical Data.....	19
Table 2.4	NACIE Bundle Characteristics.....	19

Table 2.5	Height and azimuthal position of the TCs installed along the active length of the pins	22
Table 2.6	NACIE HX Pipes Dimension.....	23
Table 2.7	Main section lengths.	25
Table 3.1	Reference physical properties of AISI316L, AISI304 [10].....	30
Table 3.2	Form loss coefficient calculated by the LegoPC model of NACIE.	35
Table 3.3	Thermophysical properties of stainless steel 316L included in MARS-LBE simulations	44
Table 3.4	Thermophysical properties of stainless steel 304 and stainless steel powder used for MARS-LBE input for NACIE.....	47
Table 3.5	Projected area, undisturbed area, and form loss coefficient of the NACIE spacer grid.	48
Table 3.6	HS 1041 characteristics.	54
Table 3.7	HS 1121 characteristics.	55
Table 3.8	Concentrated hydraulic loss coefficients overview	59
Table 3.9	Pb-Bi property correlations	60
Table 3.10	Oil property correlations [9].....	60
Table 3.11	The grids loss coefficients correlation	61
Table 3.12	The core grids loss coefficients correlation.....	62
Table 3.13	The heat exchanger grids loss coefficients correlation	62
Table 3.14	The bend loss coefficients correlation.....	63
Table 3.15	The 90° elbows loss coefficients correlation values.....	63
Table 3.16	The 45° elbows loss coefficients correlation values.....	64
Table 3.17	The area change loss coefficients correlation	64
Table 3.18	The gasket loss coefficients correlation.....	65
Table 3.19	The orifice loss coefficients correlation.....	66
Table 3.20	The tee loss coefficients correlation.....	66
Table 3.21	AISI 304 thermal property table	68
Table 4.1	Thermocouple locations in HELIOS in terms of accumulated length.	75
Table 4.2	Case definition for HELIOS natural circulation tests.....	75
Table 4.3	Averaged steady-state test results for Case I: 15.0 kW core power.....	78
Table 4.4	Averaged steady-state test results for Case II: 9.8 kW core power.....	81
Table 4.5	Modified benchmark specifications for HELIOS natural circulation tests.	82
Table 4.6	Test matrix of the experimental campaign in the NACIE loop	83
Table 4.7	Test 301 main averaged experimental data (1 h).....	88
Table 5.1	Summary of benchmark results from participants: Case I (15.0kW).....	90
Table 5.2	Summary of benchmark results from participants: Case II (9.8kW).....	90
Table 5.3	Grouping of HELIOS sub-parts for pressure loss comparison.....	94
Table 5.4	Comparison of total and local pressure loss of HELIOS for (a) Case I (15.0kW) and (b) Case II (9.8kW).	96
Table 5.5	ENEA pressure loss results of NACIE Test 301 (RELAP5 mod3.3).	99
Table 5.6	RSE pressure loss results of NACIE Test 301 (LegoPST).....	100
Table 5.7	SNU pressure loss results of NACIE Test 301 (MARS).....	100
Table 5.8	Ansaldo pressure loss results of NACIE Test 301 (RELAP5 mod3.3.2b).....	101
Table 5.9	INEST pressure loss results of NACIE Test 301 (RELAP5 mod4.0).....	101
Table 5.10	Comparison of the partial and total pressure loss of NACIE Test 301.....	102
Table 5.11	Comparison of the experimental data against simulations of NACIE Test 301.....	105
Table B.1	Friction loss coefficient (f/d) at Case I: 15.0 kW.....	116
Table B.2	Form loss coefficient (K) at Case I: 15.0 kW	122
Table B.3	Friction loss coefficient (f/d) at Case II: 9.8 kW.....	131
Table B.4	Form loss coefficient (K) at Case II: 9.8 kW	137

List of abbreviations and acronyms

ADS	Accelerator-driven systems
ALFRED	Advanced Lead Fast Reactor European Demonstrator
CAD	Computer aided design
CFD	Computational fluid dynamics
CLEAR	China lead-based reactor
EFIT	European Facility for Industrial Transmutation
ELSY	European lead system
ENEA	Italian National Agency for New Technologies, Energy and Sustainable Economic Development
FPS	Fuel pin simulator
GEC	Gas enhanced circulation
HELIOS	Heavy eutectic liquid metal loop for integral test of operability and safety
HLM	Heavy liquid metal
HMI	Human machine interface
HS	Heat structure
HX	Heat exchanger
HZDR	Helmholtz-Zentrum Dresden-Rossendorf (German research laboratory, Dresden)
IEMTP	Information Exchange Meeting on Transmutation and Partitioning
INEST	Institute of Nuclear Energy Safety Technology (Chinese Academy of Sciences, China)
KAERI	Korea Atomic Energy Research Institute
KIMM	Korea Institute of Machinery and Materials
LACANES	Lead-Alloy-Cooled Advanced Nuclear Energy Systems
LBE	Lead-bismuth eutectic
LegoPC	Lego Process CAD
LegoPST	Lego plant simulation tools
LegoSM	Lego simulation manager
LFR	Lead fast reactor

LWR	Light water reactor
MARS	Multi-dimensional analysis reactor safety
MEGAPIE	Megawatt pilot experiment
NACIE	Natural circulation experiment
NC	Natural circulation
NSC	Nuclear Science Committee
P&I	Piping and instrumentation
PEACER	Proliferation-resistant, environment-friendly, accident-tolerant, continual and economical reactor
PWR	Pressurised water reactor
PSI	Paul Scherrer Institute (research institute, Switzerland)
RELAP	Reactor Excursion and Leak Analysis Programme
RSE	Ricerca sul Sistema Energetico (Italy)
SAAS GmbH	Systemanalyse and Automatisierungsservice GmbH (Bannewitz, Germany)
SBLOCAs	Small-break loss-of-coolant accidents
SNU	Seoul National University (Korea)
TBMFR	Thermal balance mass flow rate
TC	Thermocouple
THT	Tetrahydrothiophen
WPFC	Working Party on Scientific Issues of the Fuel Cycle (NEA)
XADS	EXperimental accelerator-driven system

1. Introduction

Lead and lead alloys are very attractive nuclear reactor coolants because of their positive combination of properties important to safety and economy, including low melting temperature, high boiling temperature, chemical stability and neutron transparency. In particular, lead-bismuth eutectic (LBE) is a very efficient spallation target for neutron generation via a high-energy proton accelerator. For this reason, lead and lead-alloy coolants are becoming the subject of expanding research in the United States, Europe and Asia, as well as Russia, with a focus on the development of Generation IV lead fast reactors (LFRs) and accelerator-driven nuclear transmutation systems. Examples include SVBR-100 and BREST-300 in Russia, G4M and SSTAR in the United States, ALFRED and MYRRHA in Europe, and PEACER-300 and URANUS in Korea, as well as CLEAR in China.

The Nuclear Energy Agency has published a comprehensive handbook on lead-bismuth eutectic (LBE) alloy and lead properties, materials compatibility, thermal-hydraulics and technologies in 2007 [1] and its revised edition in 2015 [2] to integrate available information on such heavy liquid metals (HLMs). Meanwhile, a systematic study on HLM was proposed, which covers thermal-hydraulic safety issues of Lead-Alloy-Cooled Advanced Nuclear Energy Systems (LACANES). This study mainly characterises thermal-hydraulic behaviours of LACANES under the steady-state forced and natural convection, which is of critical importance for the system design development effort, while such studies have been extensively carried out for sodium coolants.

By utilising large-scale lead-alloy coolant loop test facilities, experimental data can be examined and qualified in the benchmarking of these models. Hence, two HLM loop test facilities named HELIOS (heavy eutectic liquid metal loop for integral test of operability and safety of PEACER) of Seoul National University in Korea and NACIE (NAtural Circulation Experiment) of the Italian National Agency for New Technologies, Energy and Sustainable Economic Development (ENEA) Brasimone Research Centre are benchmarked.

Originally, the benchmarking programme was to be divided into two phases:

- Phase I – Isothermal steady-state forced convection case;
- Phase II – Non-isothermal steady-state natural circulation (NC) case.

During Phase I, a comparative study on the pressure loss coefficient of each part of HELIOS under isothermal forced circulation conditions was performed. The report for Phase I suggested hydraulic loss coefficients of several hydrodynamic components and geometries. In Phase II, by using the suggestion from the former (Phase I) results, comparison studies on the calculation results of non-isothermal NC conditions of HELIOS and NACIE were conducted. This report presents the characteristics of the facilities considered and the benchmark specifications. Finally, the calculation results from the participants are compared, mainly focusing on the temperature distributions along the flow direction and mass flow rates. All thermophysical properties of LBE coolant are based on the NEA LBE Handbook [1].

The complete list of participants and codes used in this phase are shown in Table 1.1.

Table 1.1 – List of participants and codes for the second phase of the NEA Benchmark on LACANES.

Country	Institute	Participant	Code*
Italy	Ansaldo Nucleare	Luciana BARUCCA	RELAP5/Mod3.2.2b
Italy	ENEA	Paride MELONI and Massimiliano POLIDORI	RELAP5/Mod3.3
Italy	RSE	Vincenzo CASAMASSIMA	LEGO-PST
China	INEST	Ming JIN	RELAP5/Mod4.0
Korea	SNU	Il Soon HWANG and Yong-Hoon SHIN	MARS-LBE

* References for employed computer codes are given in Chapter 3.

References

- [1] NEA (2007), *Handbook on Lead-bismuth Eutectic Alloy and Lead Properties, Materials Compatibility, Thermal-hydraulics and Technologies*, OECD, Paris.
- [2] NEA (2015), *Handbook on Lead-Bismuth Eutectic Alloy and Lead Properties, Materials Compatibility, Thermal-Hydraulics and Technology*, NEA No. 7268, OECD, Paris.

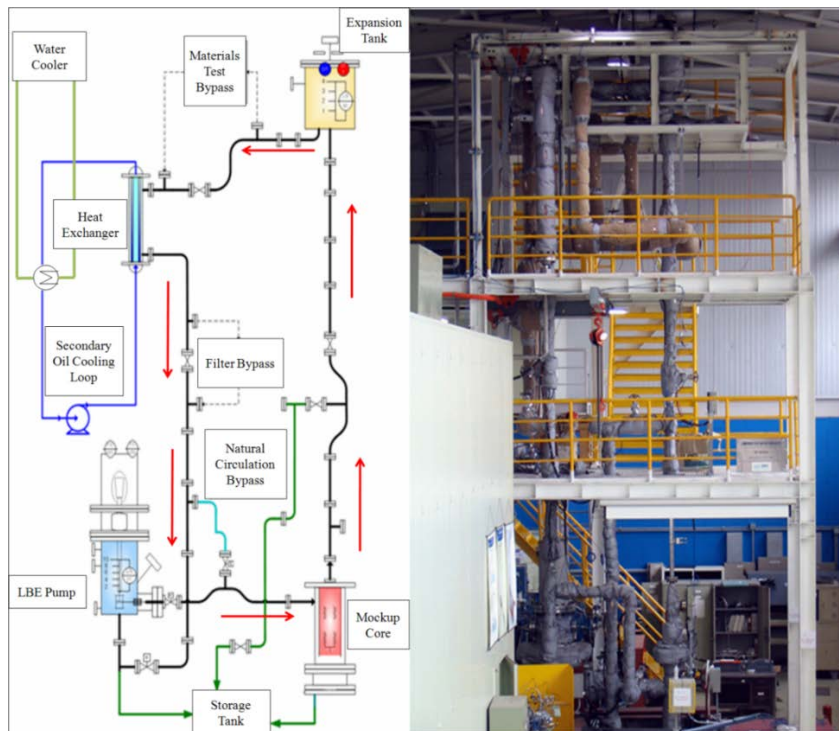
2. Benchmark specifications

2.1 The HELIOS facility

2.1.1 Facility description

The heavy eutectic liquid metal loop for integral test of operability and safety (HELIOS) of the proliferation-resistant, environment-friendly, accident-tolerant, continual and economical reactor (PEACER) is a down-scale loop-type test facility of a prototype, PEACER-300 reactor, which is a lead-bismuth eutectic (LBE) cooled nuclear waste transmutation reactor [1]. With the thermal power ratio of 5 000:1 and height ratio of 1:1, it was designed for the validation of the operation capability and safety characteristics of the prototypic reactor under either forced or natural circulation (NC) modes [2, 3]. The loop has capabilities for both thermal-hydraulic experiments and materials corrosion test. The schematic diagram and picture of the loop are depicted as Figure 2.1 [4].

Figure 2.1 – Schematic (left) and photograph (right) of HELIOS [4].



HELIOS basically consists of two closed loops that simulate the primary and secondary sides of the prototypic reactor. Components on the loop such as pipes, tanks and others are mostly made of Type 316 L stainless steel. Working fluids are LBE for the primary loop and a single-phase, high flashing-point heat transfer oil for the secondary side (Dowtherm® RP oil). HELIOS adopted it to exclude pressurisation and complex designs on the heat exchanger and the secondary loop, although pressurised water and saturated steam are used for

the actual reactor. This fluid can be operated without boiling in atmospheric pressure due to its high boiling point (360°C at 0.1 MPa) compared to water. Table 2.1 provides the thermophysical properties of Dowtherm® RP fluid [5].

Table 2.1 – Thermophysical properties of Dowtherm® RP thermal fluid [5].

Temperature (°C)	Specific heat (kJ/kg K)	Density (kg/m ³)	Thermal conductivity (W/m K)	Viscosity (mPa s)
50	1.710	1008.3	0.1275	10.05
60	1.739	1001.3	0.1262	7.19
70	1.769	994.2	0.1249	5.39
80	1.799	987.2	0.1236	4.20
90	1.829	980.1	0.1223	3.37
100	1.858	973.0	0.1210	2.77
110	1.888	965.9	0.1197	2.32
120	1.918	958.8	0.1184	1.98
130	1.948	951.7	0.1171	1.71
140	1.978	944.5	0.1158	1.49
150	2.007	937.3	0.1145	1.32
160	2.037	930.1	0.1132	1.18
170	2.067	922.9	0.1119	1.06
180	2.097	915.6	0.1106	0.96
190	2.126	908.3	0.1093	0.87
200	2.156	901.0	0.1080	0.80
210	2.186	893.7	0.1067	0.73
220	2.216	886.3	0.1054	0.68

The primary loop is comprised of a mock-up core, an expansion tank, a mechanical pump, a heat exchanger (shell side), straight piping with 49.5 mm (ANSI SCH 80 2" pipes) inner diameter, and other hydrodynamic elements such as tee-junctions, gate valves and elbows. In accordance with general concepts on hot leg and cold leg of a nuclear reactor, the primary loop can be divided into hot leg and cold leg by the mock-up core and heat exchanger: hot leg from the mock-up core outlet to the heat exchanger inlet, and cold leg from the heat exchanger outlet to the mock-up core inlet.

The mock-up core is an assembled component for core inlet pipe, downcomer, lower plenum and active core region, which contains four electric heating rods working as heat source with 60.0 kW maximum power. The expansion tank is located on the highest point of hot leg and it is necessary for the accommodation of LBE volume change accompanied with varying liquid temperature. The heat exchanger is connected after the expansion tank outlet. LBE flows downward in the shell side, while the secondary fluid flows upward in the tube side. There are two passages between the heat exchanger and the mock-up core, and they can be selected according to the purpose of test campaign. For a forced convection case, LBE passes through a passage connected to the mechanical pump, which is a centrifugal sump type having 14 m LBE head and 14 kg/s maximum flow rate. Under an NC test condition, the fluid flows through a bypass directly from the heat exchanger outlet to the mock-up core inlet.

A LBE storage tank is located beside, at the bottom of the loop. When not operated, all of LBE is stored and frozen in the tank. If a test campaign is planned, then surface heaters on the tank are turned on and hydrogen gas (4% hydrogen with argon balance) is purged until operation condition is met to get rid of oxygen that may be dissolved in LBE.

The main loop of HELIOS is enclosed by thermal insulation to reduce the amount of heat loss from the system to ambient. However, there are several local surface heaters on the outermost surface of components to compensate heat dissipation. With the activation of these heaters, adiabatic test conditions can be achieved. Meanwhile, these surface heaters function at increased temperature in order to avoid freezing the loop in LBE filling stage.

2.1.2 Change in loop configuration

Phase II of the benchmark is devoted to natural circulation studies so that, in order to conduct the proper natural circulation experiments on HELIOS loop, the mechanical pump has been completely isolated from the circuit, avoiding flow of the LBE through the loop seal and then improving the natural circulation performance. The layout of HELIOS facility for natural circulation experiments is shown in Figure 2.2. It should be noted that, apart from the pump region replaced by the bypass piping, the configuration of the rest of the loop is the same as that already studied in Phase I of the benchmark.

Figure 2.2 – Natural circulation flow path in the HELIOS: (a) Bird’s-eye view from top, (b) natural circulation bypass in detail

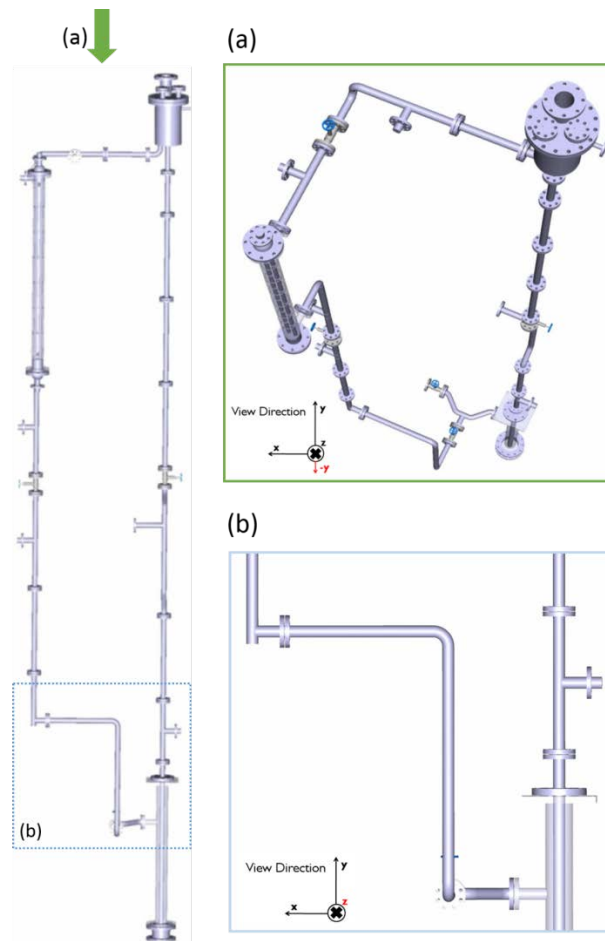


Figure 2.3 shows component division and number of each component, as well as actual flow paths with yellow boxes; Table 2.2 provides detailed data and dimensions in the primary loop. Component numbers are the same as the ones given in Figure 2.3 and dimensions are given in millimetres. Additional blueprints or three-dimensional plans of the components can be found respectively in Appendix A and Appendix B of the Phase I report. Note that component No. 8, which includes orifice, is exchanged with component No. 19 to move orifice flow meter from hot leg to cold leg, compared to the geometry reported in the former phase. With this change, the component numbers are not consecutive, but the loop still remains the same total height and flow path length (accumulated length) because two components have the same total component lengths of 1 000 mm.

Figure 2.3 – Component map of the HELIOS primary loop in natural circulation test campaigns

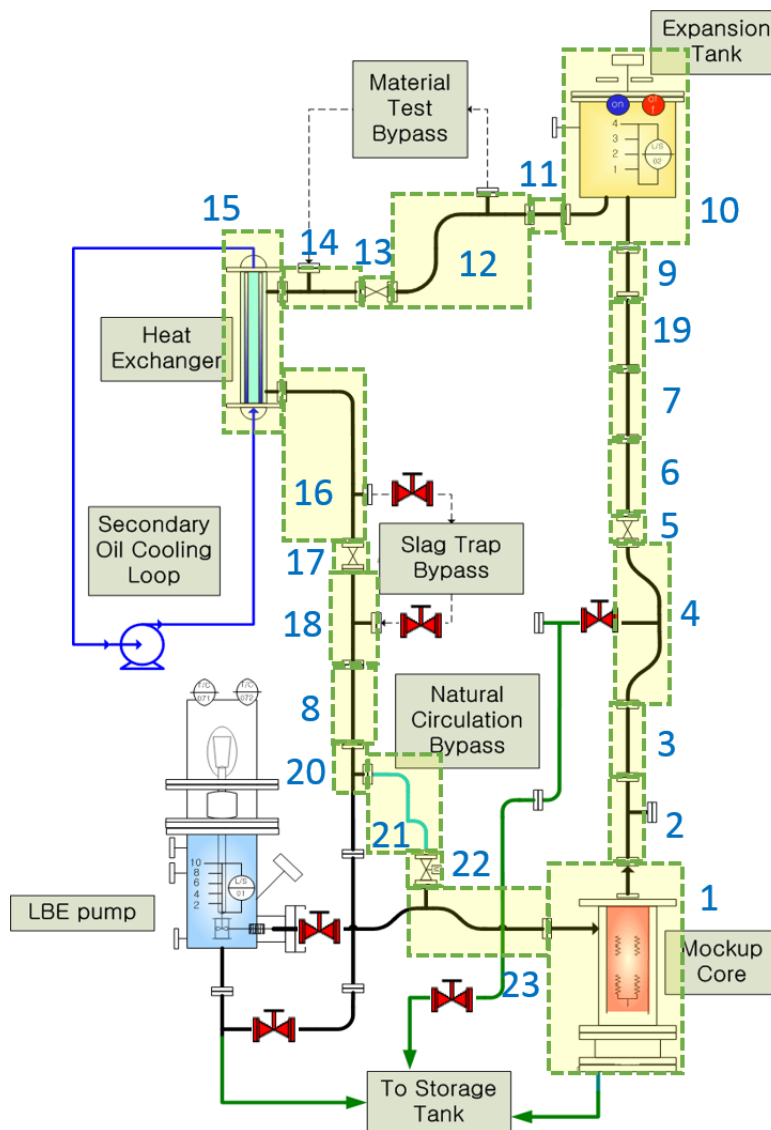


Table 2.2 – List of components and parts of the HELIOS primary loop in natural circulation test campaigns

Component number	Part name	Reference length [mm]	Component 3D plan (Appendix A in Phase I report)	Part drawings/data (Appendix B in Phase I report)
1	Core Vessel	3633.1	A-1	B-1
	Barrel			B-2
	Rod			B-3
	Bottom			B-4
	Gasket [Between Flanges]	4.5		B-34
2	Pipe [One Side Flange]	300	A-2	B-16
	Tee	127		B-27
	Pipe [One Side Flange]	300		B-16
	Gasket [Between Flanges]	4.5		B-34
3	Pipe [Both Side Flange]	1000	-	B-24
	Gasket [Between Flanges]	4.5		B-34
4	45 Degree Elbow [One Side Flange]	82.5	A-4	B-29
	Pipe	180.68		B-11
	45 Degree Elbow	60		B-28
	Pipe	718.86		B-21
	Tee	127		B-27
	Pipe	171.11		B-10
	45 Degree Elbow	60		B-28
	Pipe	180.68		B-11
	45 Degree Elbow [One Side Flange]	82.5		B-29
5	Gasket [Between Flanges]	4.5		B-34
	Glove Valve	216	-	B-31
6	Pipe [Both Side Flange]	1000	-	B-24
	Gasket [Between Flanges]	4.5		B-34
7	Pipe [Both Side Flange]	1000	-	B-24
	Gasket [Between Flanges]	4.5		B-34
19	Pipe [Both Side Flange]	1000	-	B-24
	Gasket [Between Flanges]	4.5		B-34
9	Pipe [Both Side Flange]	500	-	B-20
	Gasket [Between Flanges]	4.5		B-34
10	Expansion Tank	872.7	-	B-5
	Gasket [Between Flanges]	4.5		B-34
11	Pipe [Both Side Flange]	500	-	B-20
	Gasket [Between Flanges]	4.5		B-34
12	Pipe [One Side Flange]	300	A-12	B-16
	Tee	127		B-27
	Pipe	305.41		B-17
	90 Degree Elbow	120		B-30
	90 Degree Elbow	120		B-30
	Pipe [One Side Flange]	200		B-12
	Gasket [Between Flanges]	4.5		B-34

13	Glove Valve	216	-	B-31
	Gasket [Between Flanges]	4.5		B-34
14	Pipe [One Side Flange]	200	A-14	B-12
	Tee	127		B-27
	Pipe [One Side Flange]	382.32		B-18
	Gasket [Between Flanges]	4.5		B-34
15	Heat Exchanger Vessel	2415.5	A-15	B-6
	Heat Exchanger 2 nd Line	-		B-7
	Gasket [Between Flanges]	4.5		B-34
16	Pipe [One Side Flange]	219.75	A-16	B-14
	90 Degree Elbow	120		B-30
	Pipe	785.5		B-23
	Tee	127		B-27
	Pipe [One Side Flange]	500		B-19
	Gasket [Between Flanges]	4.5		B-34
17	Glove Valve	225	-	B-31
	Gasket [Between Flanges]	4.5		B-34
18	Pipe [One Side Flange]	500	A-18	B-19
	Tee	127		B-27
	Pipe [One Side Flange]	500		B-19
	Gasket [Between Flanges]	4.5		B-34
8	Pipe [One Side Flange]	200	-	B-12
	Orifice	600		B-32, B-33
	Pipe [One Side Flange]	200	-	B-12
	Gasket [Between Flanges]	4.5		B-34
20	Pipe [One Side Flange]	500	A-20	B-19
	Tee	127		B-27
	Pipe [One Side Flange]	100		B-9
	Gasket [Between Flanges]	4.5		B-34
21	Pipe [One Side Flange]	757.12	A-21	B-22
	90 Degree Elbow	120		B-30
	Pipe	1204.62		B-26
	90 Degree Elbow	120		B-30
	Pipe [One Side Flange]	276.25		B-15
	Gasket [Between Flanges]	4.5		B-34
22	Glove Valve	216	-	B-31
	Gasket [Between Flanges]	4.5		B-34
23	Pipe [One Side Flange]	100	A-23	B-9
	Tee	127		B-27
	45 Degree Elbow	60		B-28
	Pipe	180.68		B-11
	45 Degree Elbow [One Side Flange]	82.5		B-29
	Gasket [Between Flanges]	4.5		B-34

2.2 The NACIE facility

2.2.1 Facility description

The NATural Circulation Experiment (NACIE) facility, cooled by lead-bismuth eutectic (LBE), was designed and built up in Brasimone Research Centre of the National Agency for New Technologies, Energy and Sustainable Economic Development (ENEA) in Italy with the purpose of qualifying components and procedures to be implemented in other integral facilities. In addition, the facility is useful for the characterisation of natural circulation and gas enhanced circulation (GEC) flow regimes as well as for obtaining experimental data on heat transfer coefficient in a rod bundle assembly.

NACIE is an LBE-cooled loop that basically consists of two vertical pipes (O.D. 2.5") working as riser and downcomer, connected by means of two horizontal branches (O.D. 2.5"), as shown in Figure 2.4. The adopted material is stainless steel (AISI 304) and the total inventory of LBE is about 1 000 kg. The design temperature and pressure are 550 °C and 10 bar respectively. The general layout of the loop and a picture are shown in Figure 2.4, while the main geometrical data that characterise the NACIE facility are summarised in Table 2.3. A more detailed scheme of the whole loop can be found in Appendix A, NACIE General View.

Figure 2.4 – NACIE Loop Layout

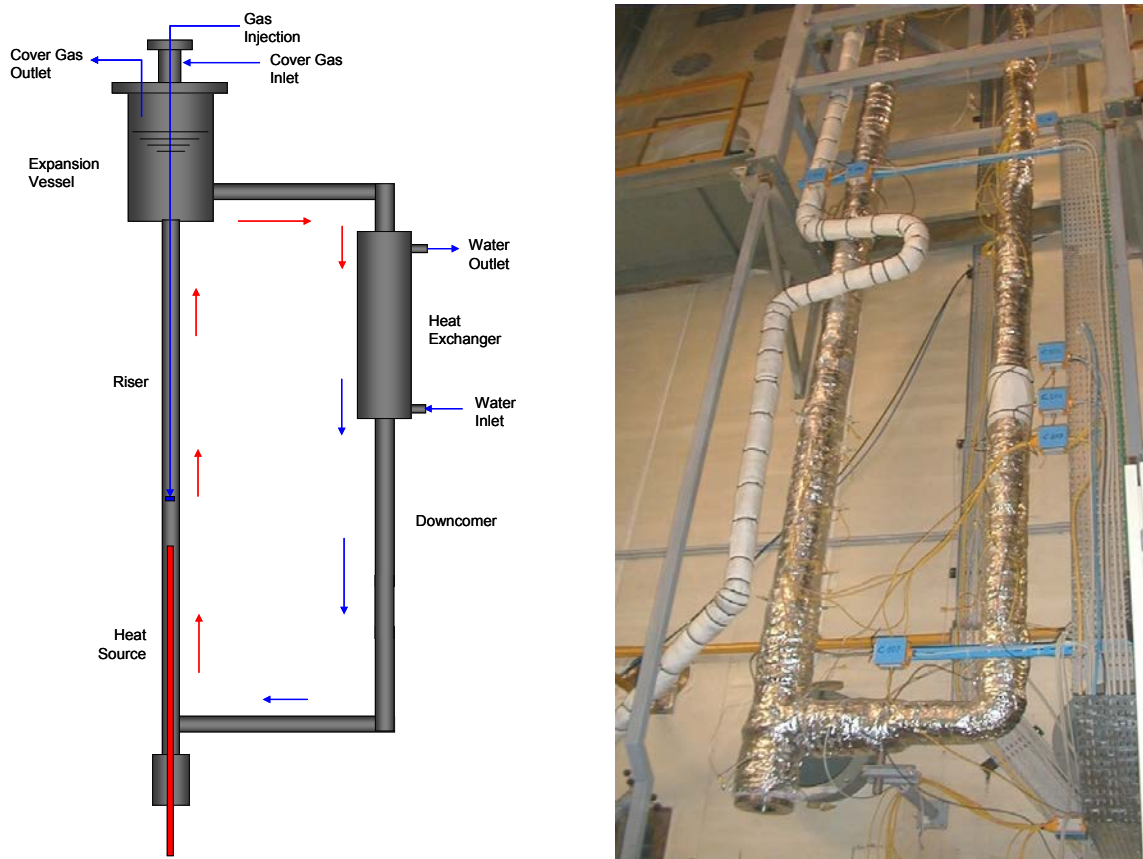


Table 2.3 – NACIE Main Geometrical Data

Total Vertical Length	9231	[mm]
Horizontal Length	1000	[mm]
Pipe Inner Diameter	62.7	[mm]
Pipe Thickness	5.16	[mm]
Expansion Vessel Height	765	[mm]
Expansion Vessel Inner Diameter	254.5	[mm]
Heat Exchanger Length	1500	[mm]
Heat Source Active Length	854	[mm]

In the bottom part of the riser of NACIE, a heat source is installed through an appropriate flange, while the upper part of the downcomer is connected to a heat exchanger.

The elevation difference between the midplanes of the heat source and heat sink was fixed to 4.5 m. The driving force available during the enhanced circulation flow regime by gas lifting was reported to be about 400 mbar with an average void fraction in the riser of about 10%. The loop is completed by an expansion vessel located on the top part of the loop, coaxially to the riser. A more detailed scheme of the expansion vessel can be found in Appendix A, NACIE Expansion Vessel.

NACIE loop is prepared to house different kinds of fuel bundles, characterised by different geometries, pin heat flux and power density. The NACIE bundle consists of two high thermal performance electrical pins and two dummy pins to support the bundle itself. The characteristics of the active pins are described in Table 2.4.

Table 2.4 – NACIE Bundle Characteristics

Number of Active Pins	2	
Diameter	8.2	[mm]
Active Length	854	[mm]
Total Length	1400	[mm]
Maximum Heat Flux	100	[W/cm ²]
Flux Axial Distribution	Uniform	
Maximum Thermal Power	45	[kW]
Number of Dummy Pins	2	
Diameter	8.2	[mm]

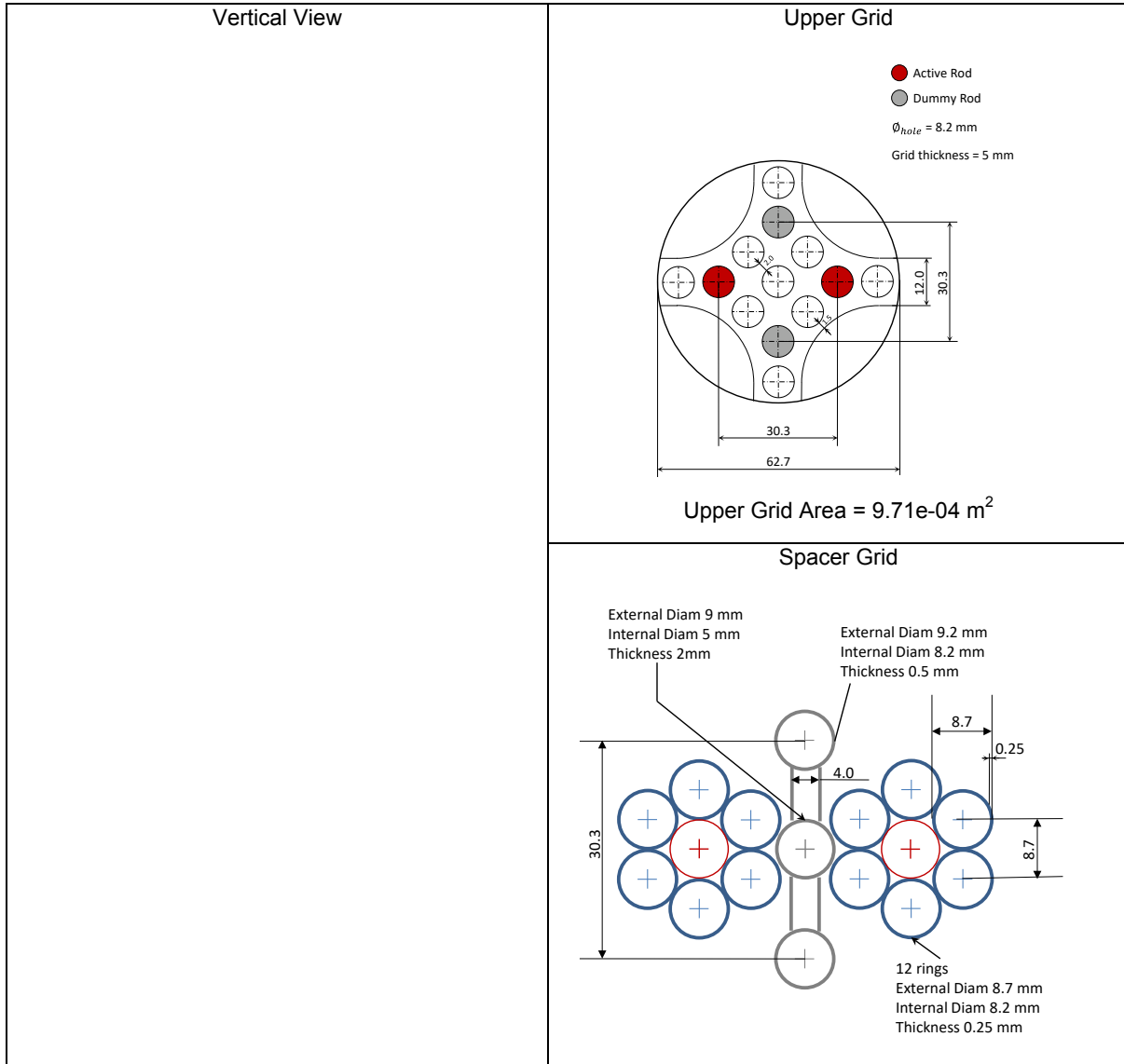
The total installed power is about 45 kW, even if during the tests only one pin is active. In Figure 2.5, some design drawing and schemes are reported. In the vertical view, it can be seen that the positions of the intermediate and upper spacer grids are installed to allow the thermal expansion of the pins, keeping constant the flow area of the subchannel which could be affected by the bowing of the pins itself. The active rods length of the head terminations is 36 mm and the active length measures 854 mm, according to Thermocoax[®] specifications.

In Figure 2.5, the schemes and main dimensions characteristic of the intermediate and upper grids are also shown. Since the geometry of the grids is not provided in design projects because they were constructed in situ, some computer aided design (CAD) graphs (reported in Appendix A) have been prepared starting from the dimensions in the figure, in order to evaluate the area occupied by the grids. The grid areas are also reported in Figure 2.5.

In Figure 2.6, a picture of the intermediate spacer grid is reported showing the spacer grid, the active and dummy pins, as well as the thermocouples installed close to the grid on the pin cladding. The wires that drive the TC signals have a diameter of 1 mm. The roughness of the electrically heated rods is $3.2e-5$ m.

The bundle pictures taken after the dismantling of the facility to which the present test campaign refers are included in Appendix A. NACIE is now being rebuilt with new advanced components, becoming NACIE-UP facility.

Figure 2.5 – Vertical section of the NACIE Bundle and grids



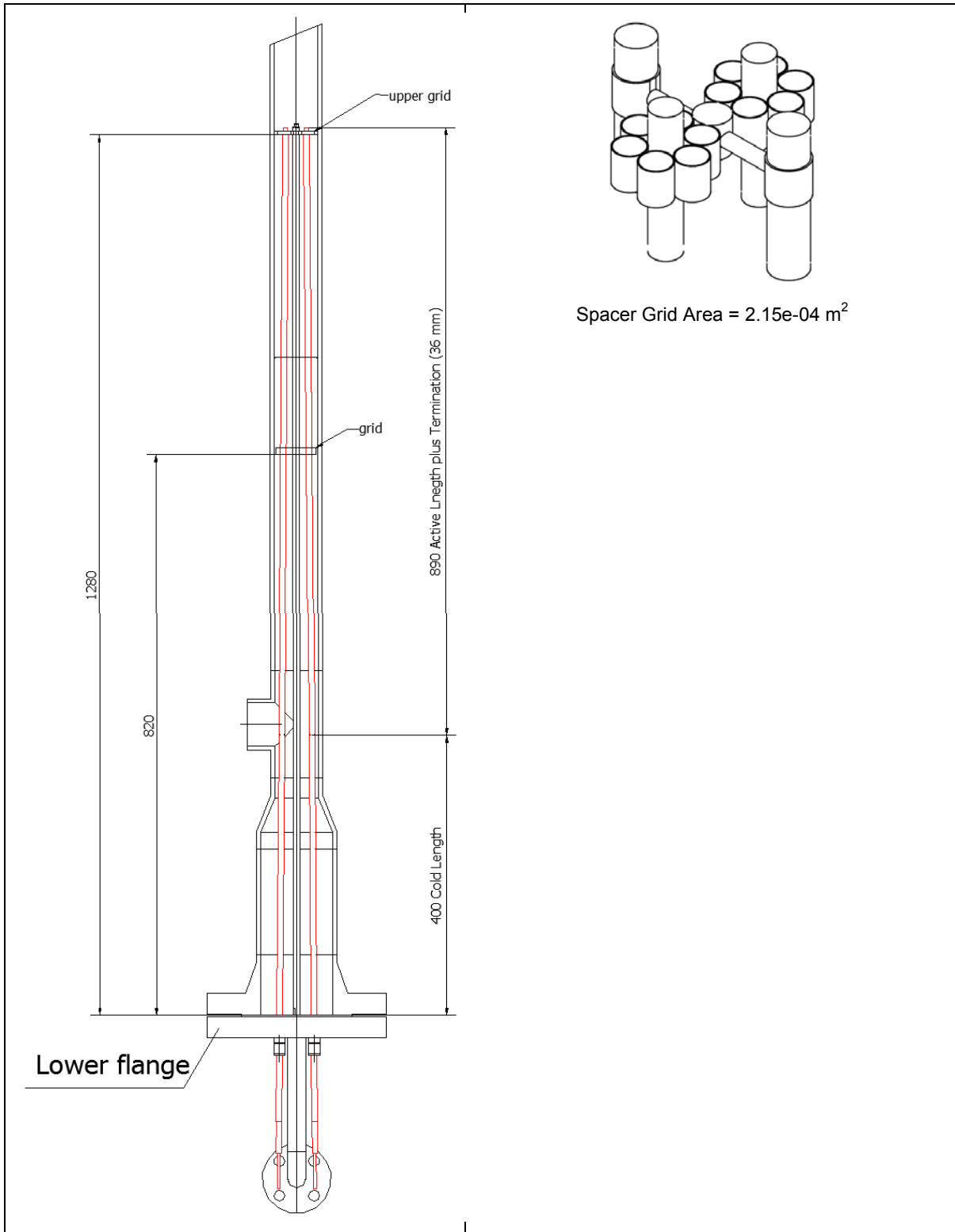


Figure 2.6 – Picture of the NACIE spacer grid (before operation)



For each active pin, seven thermocouples have been installed, in order to monitor the trend of the cladding temperature during the test in different positions. Table 2.5, starting from the bottom of the active length, reports the height as well as the azimuthal position, of the thermocouples installed on each active pin. Each TC is connected to the data acquisition system by wires of 1 mm in diameter that penetrate the lower flange. As can be noted, the TCs installed allow to make a rough evaluation of the hot spot factor on the pins due to the spacer grid installation, as well as to draw the axial temperature profile along the active pin.

Table 2.5 – Height and azimuthal position of the TCs installed along the active length of the pins

TC	Active Pin n. 1	Active Pin n. 2
1	+50 mm (0°)	+50 mm (0°)
2	+390 mm (0°)	+390 mm (0°)
3	+420 mm (0°)	+420 mm (0°)
4	+420 mm (120°)	+420 mm (120°)
5	+420 mm (240°)	+420 mm (240°)
6	+450 mm (0°)	+450 mm (0°)
7	+790 mm (0°)	+790 mm (0°)

To promote the LBE circulation in the loop, a gas lift technique has been adopted [6-9]. A pipe with an inner diameter of 10 mm is housed inside the riser, connected through the top flange of the expansion tank to the argon feeding system. On the other end of the pipe, the injection nozzle is mounted, located just downstream from the heating section. The gas is injected in the riser through the nozzle enhancing the liquid metal circulation. In the expansion tank, the separation between the phases takes place. In this way, the possibility of having a two-phase mixture flowing through the heat source is avoided. The gas injection system is able to supply argon flow rate in the range 1÷75 NI/min with a maximum injection pressure of 5.5 bar.

The heat exchanger (HX) designed for the NACIE loop is a “tube in tube” countercurrent flow type, where the secondary fluid is water at low pressure (about 1.5 bar) for a maximum thermal power of 30 kW. The HX is made by three coaxial tubes with different thickness, whose characteristics are reported in Table 2.6. A more detailed scheme of the heat exchanger can be found in Appendix A, NACIE HX View.

Figure 2.7 – Scheme of the HX and view of the expansion joint

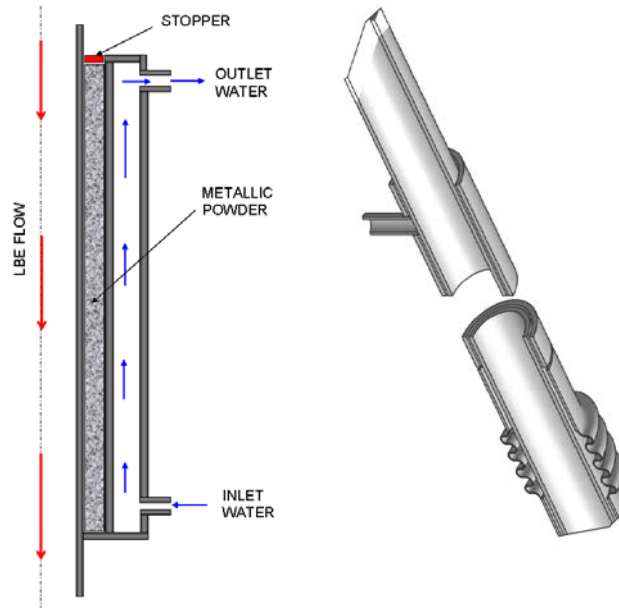


Table 2.6 – NACIE HX Pipes Dimension

[mm]	Internal Pipe	Middle Pipe	External Pipe
Inner Diameter	62.68	84.9	102.3
Outer Diameter	73	88.9	114.3
Thickness	5.16	2.0	6.02
Length	1500	1500	1500
Material	AISI 304	AISI 304	AISI 304

LBE flows downward into the internal pipe, while water flows upwards into the annulus between the middle and the external pipes (see Figure 2.7). The annulus created by the internal and middle pipe is filled by stainless steel powder that aim to guarantee the thermal flux towards water (good thermal conductivity) mitigating the thermal stresses on the pipes due to the differential thermal expansion along the axis during the operation. In fact, the three pipes are welded together in the lower part by a plate, while in the upper part only the middle and external pipe are constrained together. In this way, the internal pipe has no axial constraints with the HX secondary side.

The annulus containing the powder is closed on the top by a “stopper” made of graphite, in order to avoid the powder leakage. Finally, on the external pipe an axial expansion joint is installed to compensate the different axial expansion between the middle and external pipe. Moreover, the powder gap allows reducing the thermal gradient through the thickness of the pipes; in fact, its thermal resistance is about the 30-50% of the overall resistance.

In order to avoid any possible misunderstanding and to solve some uncertainties that arose during the development of the models for system code, in the following Figure 2.8, the scheme of the effective position of the active heating section inside the riser channel is depicted. In Figure 2.9, the scheme of the NACIE loop is shown with the lengths (or elevations) of the main subsections in which the facility can be divided. Table 2.7 can help the model developers to “close” the NACIE loop.

Figure 2.8 – Scheme of heating section position in the loop

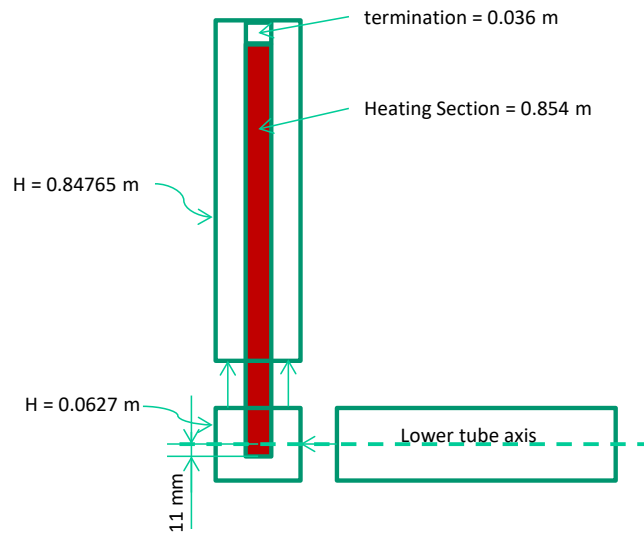


Figure 2.9 – Scheme of NACIE with section lengths

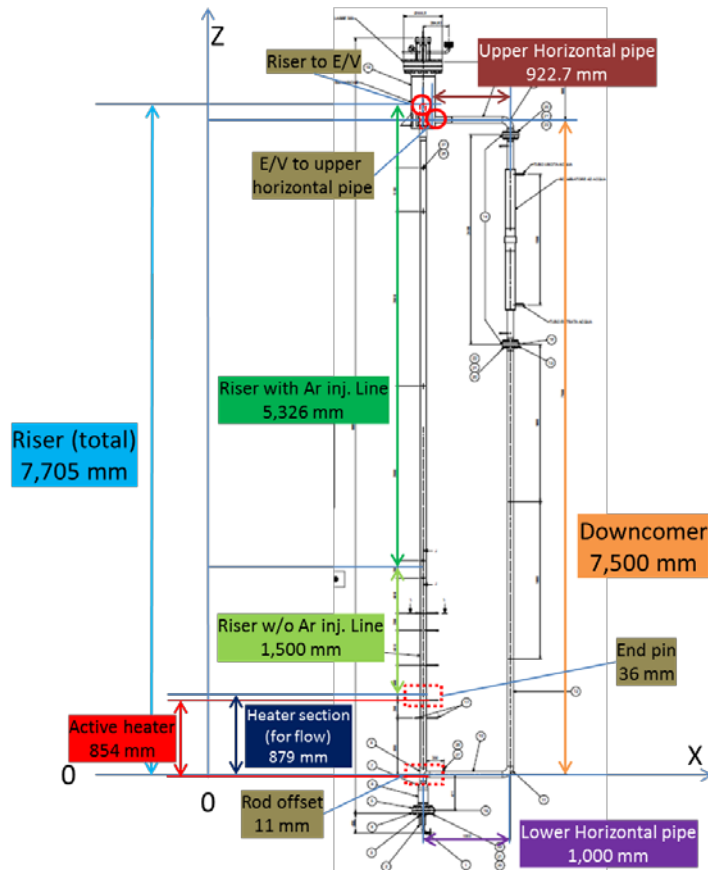


Table 2.7 – Main section lengths

Rod offset	-0.011	m
Heating+termination	+0.890	m
Riser w/o Ar injection	+1.500	m
Riser w Ar injection	+5.326	m
TOTAL «RISER»	7.705	m
E/V to upper horizontal	-0.205	m
Downcomer	-7.500	m
TOTAL «DOWNCOMER»	-7.705	m

2.3 Guidelines for pressure loss coefficient evaluation and comparison

In a natural circulation system, pressure loss, especially total pressure loss, is of importance because mass flow rate can be restricted by the amount of hydraulic resistance. In general, most of the one-dimensional system's thermal-hydraulics codes calculate pressure loss with user-defined pressure loss coefficients due to its complex nature with varying geometry and flow conditions such as flow velocity and surface roughness. In this regard, it is necessary to compare pressure loss calculation results given by different users to clarify the benchmark results not only on code-to-experiment comparison but also code-to-code comparison. There are various experimental activities on the evaluation of pressure loss coefficients of different hydrodynamic components so far and one can utilise the results from open literature. Recently, the coefficients can also be derived with three-dimensional computational fluid dynamics simulations.

2.3.1 Definition of pressure loss coefficients

The pressure drop given by a component, ΔP_i , can be defined as:

$$\Delta P_i = \frac{1}{2} \rho v_i^2 \left(f \frac{l}{d_h} + K \right)_i,$$

where i component number, ρ fluid density, v (average) flow velocity in the component, f Darcy-Weisbach friction factor, l length of the component, d_h hydraulic diameter of the component, and K form loss coefficient. The total pressure drop can be calculated by adding all the pressure losses given in a system such as:

$$\Delta P_{total} = \sum_i \Delta P_i = \sum_i \frac{1}{2} \rho v_i^2 \left(f \frac{l}{d_h} + K \right)_i.$$

2.3.2 Guideline on the selection of pressure loss

In this phase, each participant of the benchmark had agreed to evaluate pressure loss coefficients by following the best-estimate guideline given in the phase I [4]. For HELIOS simulation, all of the coefficients can be designated by referring to the report. Meanwhile, there is some degree of freedom on the pressure loss coefficient selection on NACIE simulation because not all of the correlations in the guideline are suitable for NACIE due to some prototypical flow disturbances given to straight flow such as bends, expansion and restriction, grids and so on. For the evaluation of friction losses on both systems, root-mean-square surface roughness values are provided.

2.3.3 Report formats for pressure loss coefficients under non-isothermal natural convection conditions in HELIOS

Based on the guideline described in the previous section, evaluated pressure loss coefficients of each component of HELIOS are requested to be summarised using formats as provided in Appendix B.

References

- [1] I.S. Hwang (2006), "A Sustainable Regional Waste Transmutation System: P E A C E R", Plenary Invited Paper, ICAPP '06, Reno, NV, United States, June 4-6 2006.
- [2] Jeong, S. H., C. B. Bahn, S. H. Chang, Y. J. Oh, W. C. Nam, K. H. Ryu, H. O. Nam, J. Lim, N. Y. Lee and I. S. Hwang (2006), "Operation Experience of LBE loop: HELIOS", Paper #6284, Proceedings of ICAPP '06, Reno, NV, United States, June 4-6, 2006.
- [3] J. Lim, S. H. Jeong, Y. J. Oh, H. O. Nam, C. B. Bahn, S. H. Chang, W. C. Nam, K. H. Ryu, T. H. Lee, S. G. Lee, N. Y. Lee and I. S. Hwang (2007), "Progresses in the Operation of Large Scale LBE Loop : HELIOS", Paper #7536, Proceedings of ICAPP 2007, Nice, France, May 13-18, 2007.
- [4] NEA (2012), *Benchmarking of thermal-hydraulic loop models for lead-alloy-cooled advanced nuclear energy systems – Phase I: Isothermal forced convection case*, OECD, Paris.
- [5] Dow Chemical Company (1996), DOWTHER RP Heat Transfer Fluid, *Product Technical Data*, Nov 1996.
- [6] W. Ambrosini, G. Forasassi, N. Forgione, F. Oriolo, and M. Tarantino (2005), "Experimental study on combined natural and gas -injection enhanced circulation," *Nuclear Engineering and Design*, vol. 235, pp. 1179–1188.
- [7] W. Ambrosini, G. Forasassi, N. Forgione, F. Oriolo, and M. Tarantino (2003), "Natural and Gas-injection Enhanced Circulation in a Loop with Variable Friction," International Conference on Global Environment and Advanced Nuclear Power Plants, GENES4/ANP2003, Kyoto Research Park, Kyoto, Japan, September 15-19 2003.
- [8] G. Benamati, C. Foletti, N. Forgione, F. Oriolo, G. Scaddozzo, and M. Tarantino (2007), "Experimental study on gas-injection enhanced circulation performed with the CIRCE facility," *Nuclear Engineering and Design*, vol. 237, pp. 768-777.
- [9] M. Tarantino (2007), "Gas Enhanced Circulation Experiments On Heavy Liquid Metal System," Report ENEA HS-F-R-001.

3. Method of the benchmark

3.1 Approach

In this phase, non-isothermal natural circulation test data were produced using the heavy eutectic liquid metal loop for integral test of operability and safety (HELIOS) facility at Seoul National University (SNU), Korea, and the NATural Circulation Experiment (NACIE) facility at the National Agency for New Technologies, Energy and Sustainable Economic Development (ENEA) Brasimone Research Centre, Italy. These data were provided by test performers to all participants as benchmark specifications. Information on the geometric and thermal-hydraulic configuration of HELIOS was encouraged to refer to the Appendices in the former phase report [1] and that of NACIE was also distributed to participants along with benchmark specifications so that base input decks can be generated.

With these inputs, the participants were asked to model the loop tests with their own system analysis codes. The calculation results obtained by the participants were compared one against the other and with the produced experimental data sets as well.

3.2 RSE, Italy

“Lego Plant Simulation Tools” (LegoPST) is an integrated software environment designed for the real time dynamic simulation of power plants. It is a multipurpose scalable system that is suitable for analysis of integrated processes, the check of control and automation systems, the analysis of operational transients and the training of the plant operators.

LegoPST was successfully used to build power plant dynamic simulators based on various processes and technologies such as combined cycles, coal gasification, desalination stations and light water reactor (LWR) nuclear power plants [2-7].

In the last few years, LegoPST modelling capability has been extended to the simulation of the thermal-hydraulic loops employing liquid metal. The physical properties of liquid sodium, liquid lead and liquid lead-bismuth have been embedded in the LegoPST libraries of the fluid physical properties, and the models of the plant components (drums pipes, pumps, valves, etc.) have been updated.

The participation in benchmarking the thermal-hydraulic loop models for Lead-Alloy-Cooled Advanced Nuclear Energy Systems (LACANES) is relevant for the validation of the LegoPST update.

3.2.1 *Lego plant simulation tools*

LegoPST suite consists of: 1) a master solver for non-linear differential and algebraic equation systems; 2) an expandable library of mathematical models of plant components; 3) integrated tools covering all plant simulator building steps, from design to final simulator, including debugging, monitoring and configuration. In particular, Lego Process CAD (LegoPC) is useful for developing and testing process models; Lego Automation CAD (LegoAC) allows full graphic editing of automation schemes. LegoHMI is specific for Plant Display and Operating Window building and configuration; Lego Simulation Manager (LegoSM) runs the whole simulator, managing multiple links among processes, automation and human machine interface (HMI) models.

The models library consists of an expandable set of mathematical models of the plant components (valves, pipes, etc.) and physical properties of various fluids (water, gases, liquid metals, etc.). All the mathematical models are based on the mass, momentum and energy conservation equations, developed with a lumped parameter approach and in one-dimensional geometry. The related equation system is closed by coupling

material properties correlations and fluid state equations. A short description of the LegoPST tools is reported in [1]. To model HELIOS and NACIE facilities and carry out the benchmark simulations, only the LegoPC tool is required. It runs both under Linux and Windows operating systems.

3.2.2 LegoPC model of HELIOS

Figure 3.1 shows the graphic representation of the model of the HELIOS natural circulation path in the LegoPC environment. The modelling details of the heat exchanger and the core mock-up are highlighted in Figure 3.2 and Figure 3.3. The correlations of the Lead-Bismuth physical properties and the state equations come from the *Handbook on Lead-bismuth Eutectic Alloy and Lead Properties, Materials Compatibility, Thermal-hydraulics and Technologies* [8] , while [9] is the reference for the properties of the diathermic oil. The pressure loss coefficients are calculated according to the recommendations worked out in the LACANES phase I [1].

Figure 3.1 – Graphical description of the HELIOS model in the LegoPST environment

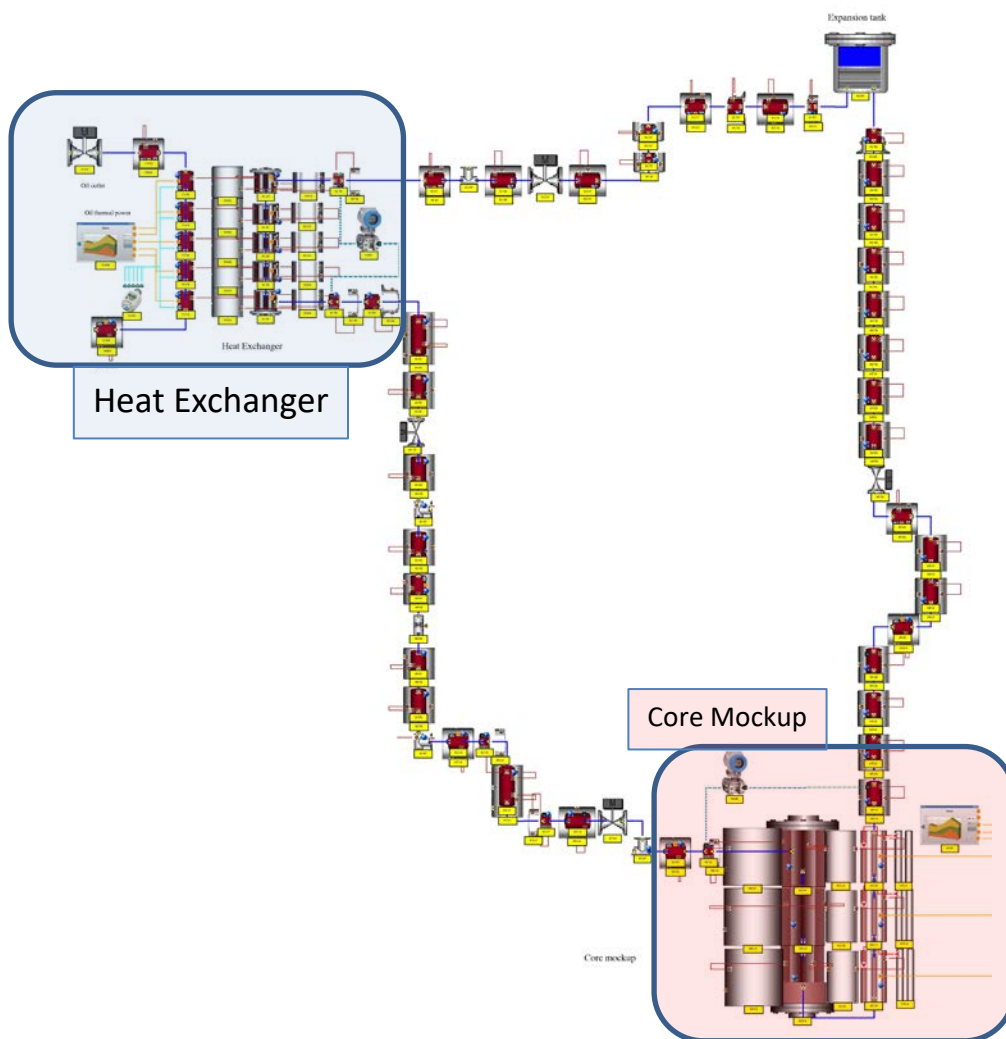


Figure 3.2 – Graphical representation of the model of HELIOS heat exchanger in LegoPC environment

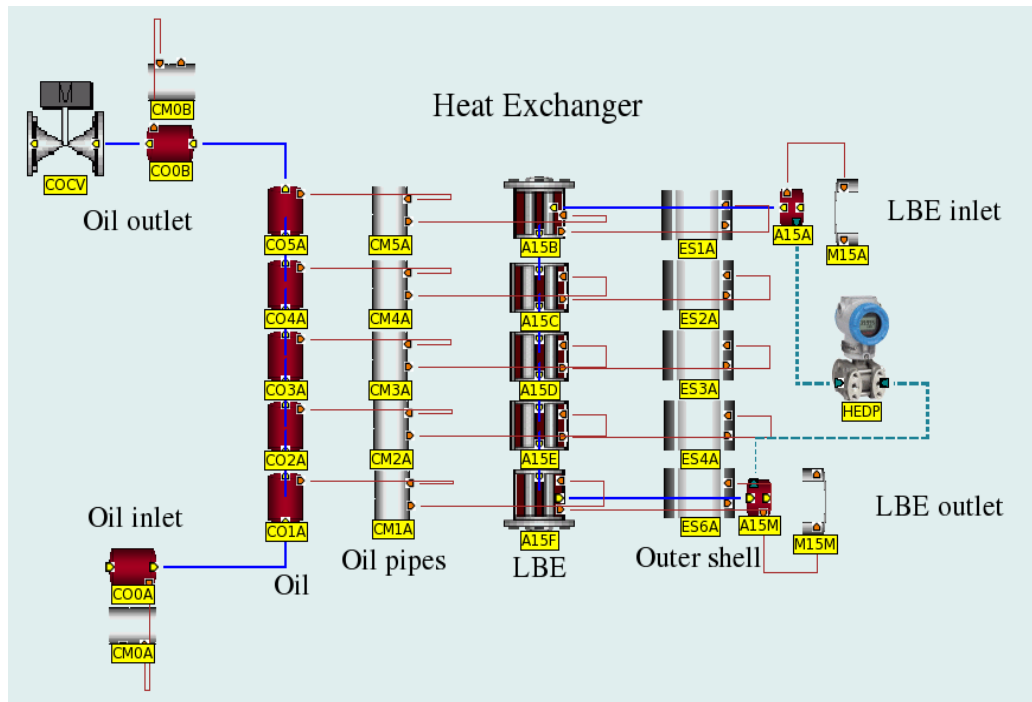
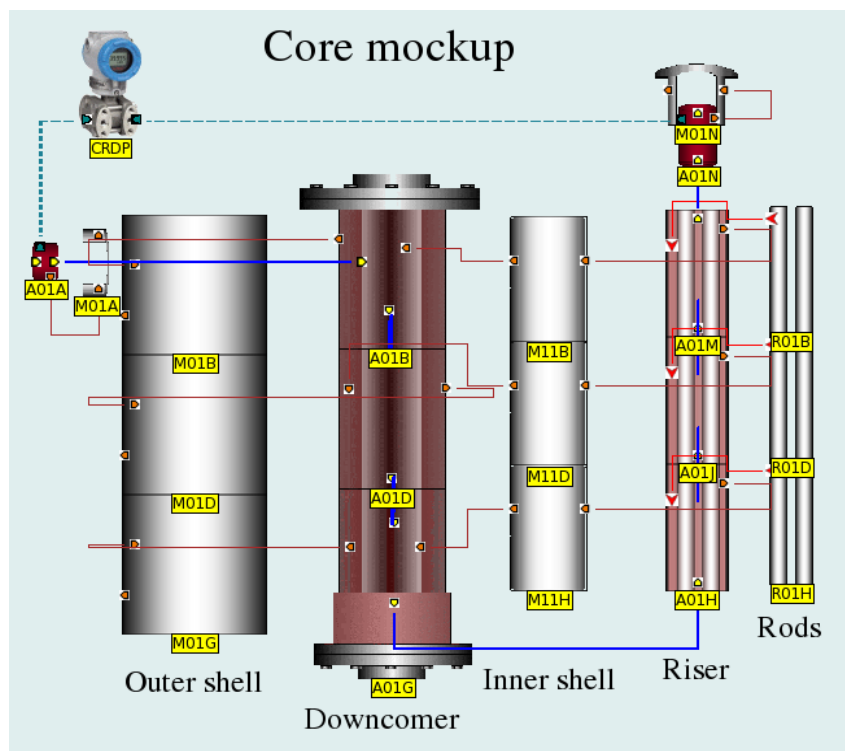


Figure 3.3 – Graphical representation of the model of HELIOS core mock-up in LegoPC environment



The length of each volume of integration can be assigned by the user. The values assigned to the HELIOS model are in the range of 5 cm to 15 cm. All the metal of the pipes' wall is taken into account as well as the heat transfer between pipe and fluid. Table 3.1 summarises the physical properties assigned to the metal of the pipes. A set of heat transfer correlations is available in the LegoPC libraries, Seban-Shimazaki ($Nu=5.+0.025 \cdot Pe^{0.8}$) and Sieder-Tate ($Nu=0.027 \cdot Re^{0.8} Pr^{0.33} (\mu/\mu_w)^{0.14}, \mu/\mu_w=1$) have been selected, respectively, for lead-bismuth eutectic (LBE) and oil.

Table 3.1 – Reference physical properties of AISI316L, AISI304 [10]

AISI 316 L, AISI 304	
T-Temperature [K], Tc-Thermal conductivity [$W \cdot m^{-1} \cdot K^{-1}$]	$T_c = 9.2 + 0.0175 \cdot T - 2.0 \cdot 10^{-6} \cdot T^2$
T-Temperature [K], Cp-Specific heat [$J \cdot kg^{-1} \cdot K^{-1}$]	$C_p = 472.0 + 0.136 \cdot T - 2.82 \cdot 10^{-6} \cdot T^2$
Ro-Density [$kg \cdot m^{-3}$]	Ro = 7900

Concerning the interaction with the environment, all of the loop is considered perfectly insulated. The boundary conditions required to work out a simulation are the oil inlet conditions (pressure, temperature and mass flow rate) and the power supplied to the rods. As mentioned before, the problem solving method of LegoPC is briefly described in the report about LACANES phase I [1], as well as the correlations for calculating the pressure loss across pipes, bends, tee, orifice, etc. In LACANES Phase II, the recommended ones in phase I are used, except for pipe connections and valves. Pressure loss due to gasket between flanges are neglected and valves are modelled by the standard sizing equation of the manufacturers [11, 12], which also takes into account the pressure loss of the valve fitting to the pipe (Figure 3.4). The valve sizing equation for incompressible fluids can be written, in generalised form, as

$$\Delta P = f(\theta) \cdot A_v^* \frac{w^2}{2\rho},$$

where $f(\theta)$ is a characteristic function of the valve actuator θ ($f(\theta)=1$. valve fully open), A_v^* is the flow coefficient whose value depends on the system of measurement, w is the mass flow rate of the fluid and ρ its specific mass. To characterise the valves of HELIOS for Phase II, the value of A_v^* has been identified on the basis of the measurement of the pressure loss at the gate valve reported in phase I (Figure 3.5).

Figure 3.4 – Standard test set up for valve sizing

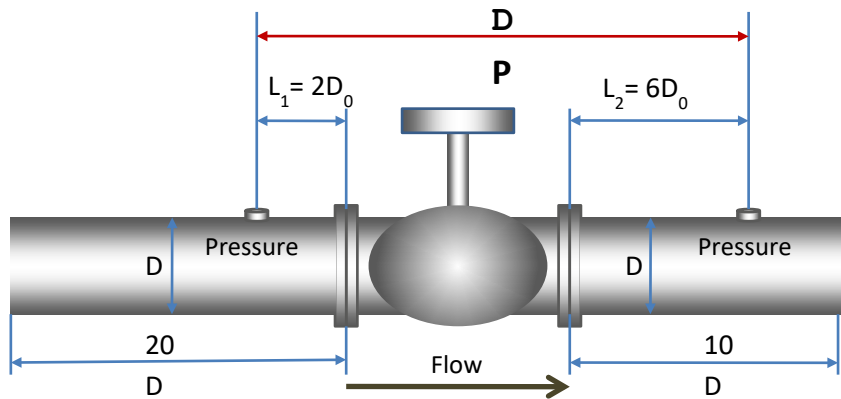
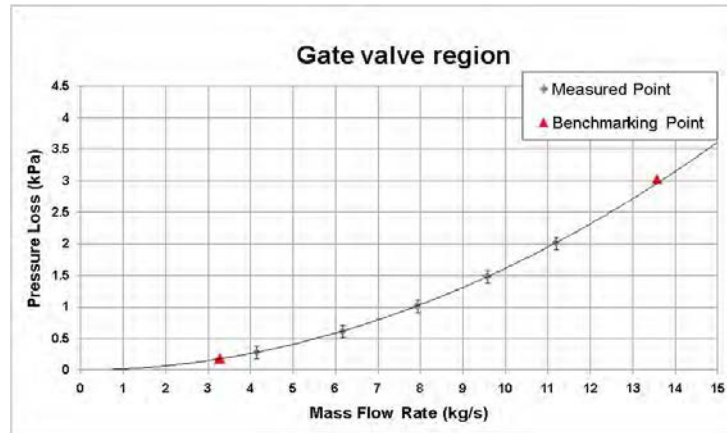


Figure 3.5 – LACANES phase I – Pressure loss at gate valve



The constraints of consistency with the Darcy pressure loss equation, which defines the pressure loss coefficients, allows us to set up the identity:

$$\Delta P = A_v^* \frac{w^2}{2\rho} = \frac{1}{2} \rho \left(f \frac{L}{D} + K \right) V^2$$

V =fluid velocity, $f \frac{L}{D}$ = friction factor, K = form pressure loss coefficient, which is verified for fully open valve. If we identify as S_0 the flow section, we can write mass flow rate as $W = \rho S_0 V$, so:

$$A_v^* \frac{\rho^2 S_0^2 V^2}{2\rho} = \frac{1}{2} \rho \left(f \frac{L}{D} + K \right) V^2$$

and, simplifying:

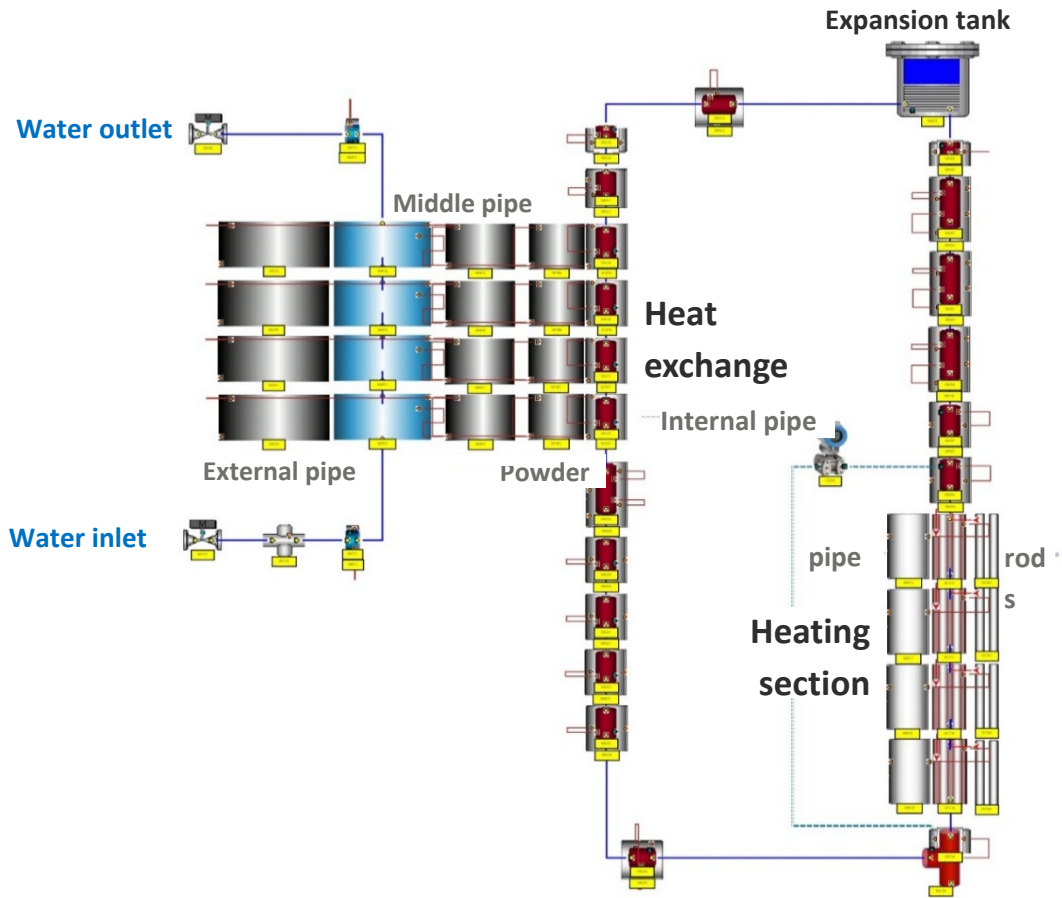
$$A_v^* S_0^2 = \left(f \frac{L}{D} + K \right)$$

we define the equivalent global pressure loss coefficient.

3.2.3 LegoPC model of NACIE

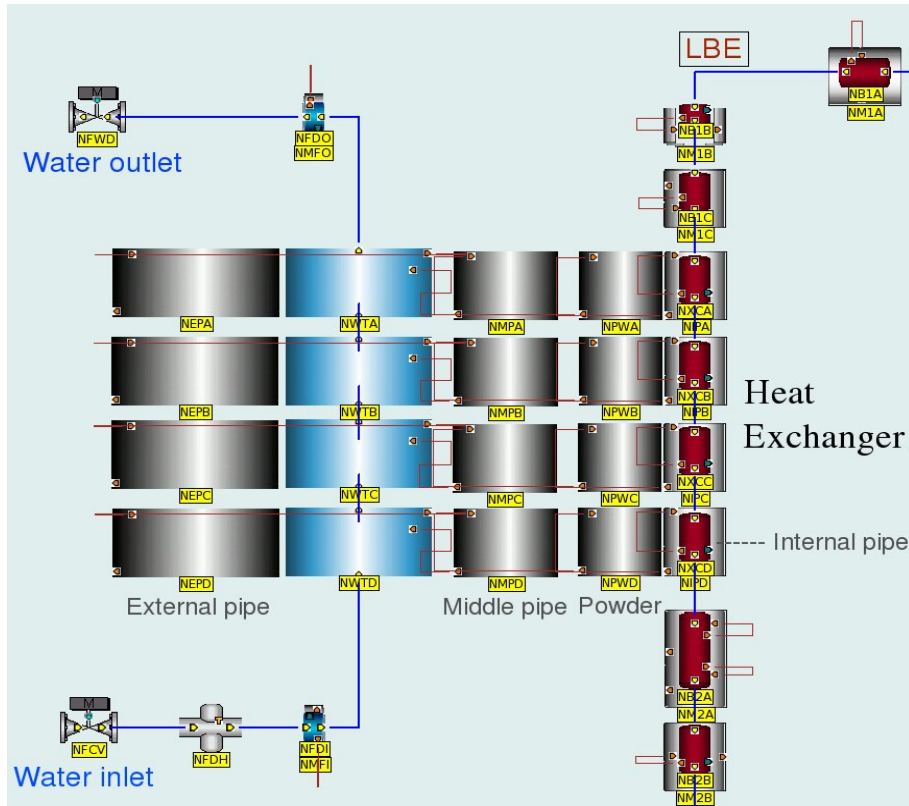
Graphical representation of the NACIE model in the LegoPST environment is drawn in Figure 3.6. The system is considered perfectly insulated. The length of the integration volume differs from one section to the other; the nodes of the heating section have a length of 5 cm, the heat exchanger has nodes 7.5 cm in length, while the downcomer and riser are partitioned into nodes 20 cm in length. As for the HELIOS model, all the metal of the pipes and the heating rods is taken into account. The reference physical properties of the metal are reported in Table 3.1. The thermal conductivity of the steel powder layer in the heat exchanger requires a specific hypothesis. Actually, it has been identified on the basis of the experimental data of test 301.

Figure 3.6 – Graphical description of the NACIE model in the LegoPST environment



The methodology for tuning the steel powder thermal conductivity consists in setting up the open loop model of the heat exchanger (Figure 3.7) and assigning the inlet condition of LBE and water measured in the test as boundary conditions. Finally, the thermal conductivity of the powder is tuned to get the output conditions of LBE and water closest to the output conditions measured in test 301. The method has worked out a value of $2.575 \text{ Wm}^{-1}\text{K}^{-1}$ of the powder thermal conductivity, with a deviation of the outlet temperature of LBE and water, respectively of $\Delta T_{LBE} = -0.03\%$ and $\Delta T_{water} = -1.71\%$. The value of the thermal conductivity of the steel powder accounts for about 14% of the thermal conductivity of AISI 316 at 310°C . This value is of the same order of magnitude reported on the NACIE benchmark specification (10%), and it is consistent with the studies of O. Biceroglu et al. [13], and B.D. Turland et al. [14].

Figure 3.7 – NACIE heat exchanger open loop model – graphical representation in LegoPC environment



The heat power transferred to water can be explained by the Dittus-Boelter correlation ($Nu=0.027Re^{0.8}Pr^{0.4}$), while the Seban-Shimazaki correlation is kept to evaluate the heat power exchanged by LBE. Figure 3.8 points out the main pressure losses calculated by the model of the entire loop (Figure 3.6). Friction factors are evaluated according to the flow regime; in laminar flow by the Darcy formula ($f=64/Re$, $[0 \leq Re \leq 2000]$); in turbulent flow by solving the Colebrook interpolation formula:

$$\left(\frac{1}{f^{1/2}} = -2.0 \log_{10} \left(\frac{\varepsilon/d}{3.7} + \frac{2.51}{f^{1/2} Re} \right), [Re > 2000] \right)$$

via the Newton-Raphson iterative method. The form loss coefficients are calculated in accordance with the recommendation of LACANES phase I [1], except for the upper grid whose value is suggested by Ansaldo as best practice. To evaluate the pressure loss across the expansion tank, two changes of flow have been taken into account: discharge into the tank and exit from the tank. The former is can be explained by a sudden expansion, while the latter as entrance into a tube. Table 3.2 reports the values of the calculated form loss coefficient and their references.

Figure 3.8 – Main pressure losses calculated using the Lego PC model of the NACIE facility

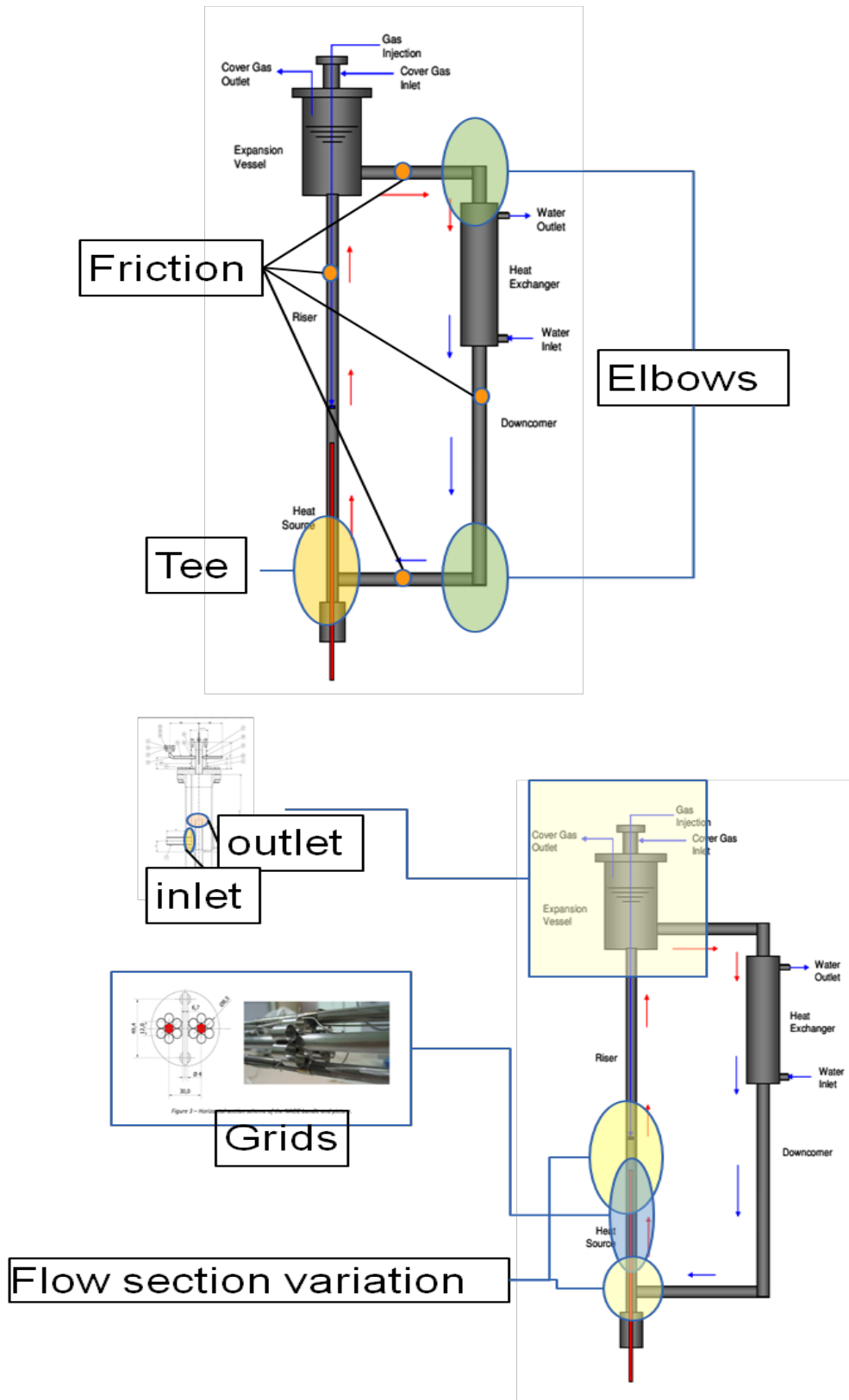


Table 3.2 – Form loss coefficient calculated by the LegoPC model of NACIE

Form	Correlation	K	Reference
Elbows (90°)	$K_{sb}=K_{Re} \cdot A \cdot B$ $K_{Re} \sim 1.44, A=1, B \sim 0.17$	0.2435	[8, 15]
Tee	$K = \text{const.}$	1.29	[8]
Sudden Expansion	$K = (1 - F_0/F_1)^2$ $F_0 \sim 0.0029 \text{ [m}^2\text{]}, F_1 \sim 0.051 \text{ [m}^2\text{]}$	0.89	[8, 15]
Sudden Contraction	$K = 0.5(1 - F_0/F_1)^{3/4}$ $F_0 \sim 0.003 \text{ [m}^2\text{]}, F_1 \sim 0.0031 \text{ [m}^2\text{]}$	0.072	[15]
Entrance into a tube	$K = \text{Tabulation}$	0.5	[8, 15]
Spacer grid	$K = C_v(A_s/A_v)^2, C_v = -7.65 \log_{10} Re + 49$ $A_s = 0.000199 \text{ [m}^2\text{]}, A_v = 0.0029 \text{ [m}^2\text{]}, Re = 41729$	0.0653	[8]
Upper grid	$K = \xi(1 - F_0/F_1) + (1 - F_0/F_2)^2 + \tau(1 - F_0/F_1)^{1/2}(1 - F_0/F_2) + \xi_{fr}$ $\xi = 0.5, \tau = 1.35, \xi_{fr} = 0.0129, F_0 \sim 0.0029 \text{ [m}^2\text{]}, F_1 \sim 0.0017 \text{ [m}^2\text{]}, F_2 \sim 0.0031 \text{ [m}^2\text{]}$	0.697	[15]

3.3 ENEA, Italy

ENEA participation in the benchmark aims to assess the RELAP5 code specifically modified for treating heavy metal cooling fluids. The RELAP5 Mod3.3 code is the ENEA's reference tool for transient and accident analyses in heavy liquid metal (HLM) cooled systems. Within the first phase of the benchmark, the code used an old version of the fluids thermodynamic properties coming from a Monte-Carlo based Soft-Sphere model [16]. In the present phase, the code has been provided with new thermodynamic properties taken from the Handbook 2007 [8].

3.3.1 RELAP5 code version for HLM

The RELAP5 code was developed for LWR LOCA analysis, extensively validated and used worldwide as a best-estimate code for LWRs. The thermo-hydraulic system code is based on a 6-equation 2-fluid model describing mass, momentum and energy balances of separated steam and liquid phases. This code [17] was chosen in the framework of the Italian research programme on accelerator-driven systems (TRASCO) as the reference code for the thermal-hydraulics analysis of lead and lead-bismuth cooled systems.

This original version was modified generating the physical and thermodynamic properties for Pb, Pb-Bi (soft-sphere model) and for diathermic oil and updating several original routines in order to implement new correlations dedicated to heavy liquid metals (HLMs). Moreover, specific heat transfer correlations were added: convective heat transfer for HLMs evaluated according to Seban-Shimazaky (pipe) or Subbotin-Ushakov (tube bundle), and for oil helical path (Gnielinsky).

The previous modifications that concern Pb and Pb-Bi physical properties and thermal exchange correlations have been validated against experimental data. The qualification was mainly based on an experimental program carried out at the ENEA Research Centre of Brasimone (Italy) in support of eXperimental Accelerator-Driven System (XADS) design and Megawatt Pilot Experiment (MEGAPIE) experiment:

- ability to simulate a two-component, two-phase mixture of liquid lead-bismuth and steam successfully assessed using the EGTAR-3 experiment (Ansaldo);
- ability to simulate LBE natural circulation in a loop successfully assessed on CHEOPE experimental facility (Brasimone, Italy) [18];
- ability to simulate a two-component, two-phase mixture of liquid lead-bismuth and gas successfully assessed using the CIRCE gas-lifting tests (Brasimone, Italy) [19];
- validation of thermal exchange correlations against MEGAPIE single-pin tests (Brasimone, Italy) and integral tests (Paul Scherrer Institute, Switzerland) [20].

In the last few years, the old implementation was also used for benchmark activity on CIRCE pool facility [21], and to support the design safety assessment of the European Facility for Industrial Transmutation (EFIT) reactor [22, 23], the European Lead SYstem (ELSY) reactor [24] and the Advanced Lead Fast Reactor European Demonstrator (ALFRED) lead-cooled reactor [25]. The new thermodynamic properties implementation is benchmarked for the first time in the present activity, where significant improvements on simulation results are expected with a high degree of confidence.

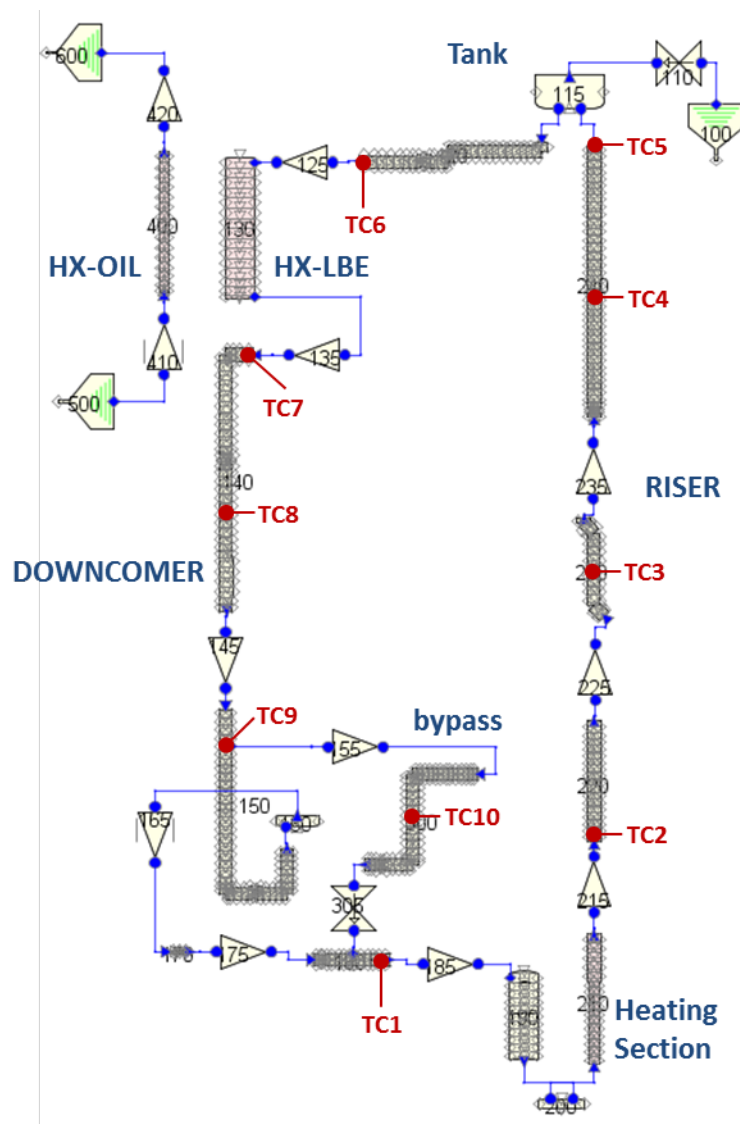
The objective of ENEA's participation in the LACANES benchmark is to assess both the code used for transient analysis and the procedure followed to build the code model of the heavy metal-cooled system to be analysed. For this reason, the nodalisations of the HELIOS and NACIE loops have been developed with the simulation detail adopted in the reactor applications; moreover, the models for the computation of the singular pressure drops have been drawn from Idelchik's hydraulic handbook, usually used as a reference [26].

3.3.2 HELIOS model for RELAP5

The nodalisation scheme of HELIOS for the RELAP5 is reported in Figure 3.9. It represents a complete one-dimension description of the flow path of the HELIOS loop. The 250 hydraulic meshes range between 0.05 m and 0.15 m in order to combine sufficient detail in the description with an acceptable computation time. That

implies an error in calculating the punctual value of the parameters like pressure and temperature due to the averaging process in the mesh.

Figure 3.9 – HELIOS nodalisation for RELAP5 (ENEA)



The main structure of the model comes from that developed in Phase I of the LACANES benchmark, where isothermal forced convection tests have been simulated, hence only the hydraulic path had been modelled. Actually, the model has been improved with the addition of the thermal structures for:

- the 4-rod core bundle (in the pipe 200 of the model in Figure 3.9);
- the LBE/oil heat exchanger (between pipes 130 and 400);
- all the connecting piping in AISI 316 surrounded by a layer of glass wool.

The secondary side cooled by oil (Dowtherm® RP [9]) is explicitly described for what regards the heat exchanger (HX) part while it is driven by boundary conditions to set the pressure, inlet temperature and mass flow rate.

The correlations used to calculate the Nusselt number and the convective heat transfer coefficient are the default Seban-Shimazaki correlation for the LBE side flowing in the shell:

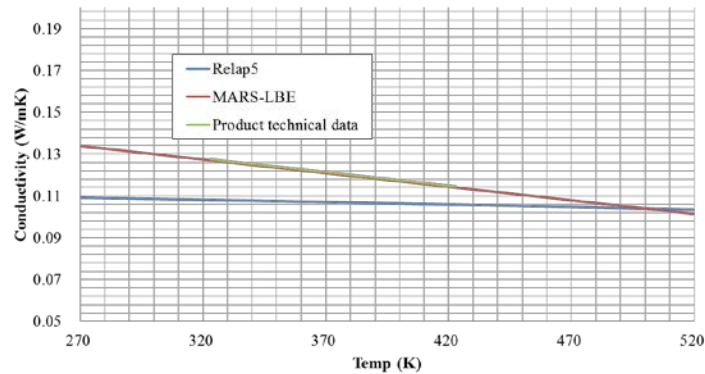
$$Nu = 5.0 + 0.025Pe^{0.8}$$

and Dittus-Boelter standard RELAP5 correlation for the oil side flowing in a couple of parallel tubes:

$$Nu = 0.023Re^{0.8} Pr^{0.4}$$

The thermodynamic properties of the oil implemented in RELAP5 are those provided by the TetraHydroThiophen (THT) oil, a type of oil with slightly different properties from the Dowtherm® RP employed in HELIOS. Differences between the two oils were found in the thermal conductivity as shown Figure 3.10 in which the Dowtherm® RP versus the conductivities implemented in MARS-LBE code of SNU and RELAP5 are compared.

Figure 3.10 – Comparison of the thermal conductivity (ENEA)

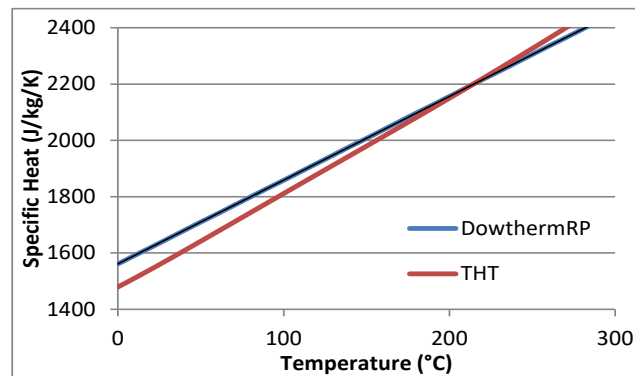


Thanks to the fact that the modification of the conductivity subroutine of the source code is relatively simple in RELAP5, the conductivity has been changed with the introduction of the correlation used by SNU to better fit the real property:

$$\lambda(T) = 0.169 - 0.00013T$$

The same treatment cannot be pursued for other properties, such as the heat capacity in Figure 3.11, because it would have involved an extensive modification of the oil library. Despite the heat capacity being slightly lower in RELAP5 in the temperature range of interest, the calibration of the secondary side is not considered in the following simulations.

Figure 3.11 – Comparison of the heat capacity (ENEA)



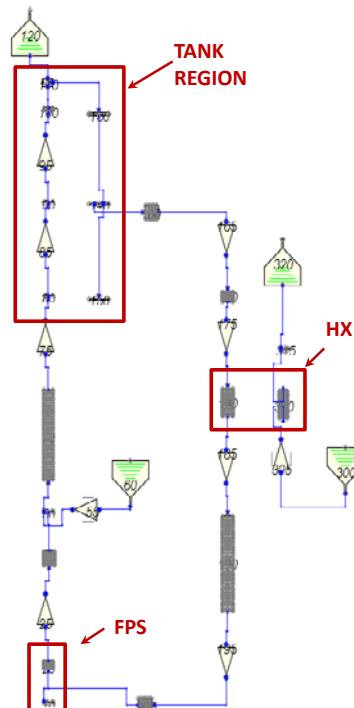
Since phase 2 of the benchmark is dedicated to the simulation of natural circulation tests in steady-state conditions, the time-dependent junction that was previously used for the pump modelling (165) has been set to zero mass flow rate, and the bypass line (300) has been introduced.

The pressure drops coefficients are those calculated using literature correlations [26] in Phase I of the benchmark [1] and then slightly tuned with the help of the HELIOS forced convection tests. The friction losses are calculated by the RELAP5 code.

3.3.3 NACIE model for RELAP5

The nodalisation scheme of the RELAP5 model adopted for NACIE simulations is reported in Figure 3.12. The complete natural circulation flow path of NACIE is modelled with one-dimensional elements. The model consists of about 250 hydraulic meshes with lengths that range from 5 to 10 cm in order to have a detailed description and acceptable computation time.

Figure 3.12 – NACIE nodalisation for RELAP5 (ENEA)



The thermal structures are completely simulated: pipes, heat exchanger (HX), tank and Fuel Pin Simulator (FPS), constituted by two electrically heated rods (only one active during the tests) and two dummy rods. The explicit description of the secondary side is limited to the HX cooled by water driven by boundary condition to impose the inlet temperature (300), mass flow rate (305) and pressure (320).

In the first approximation, the piping is considered adiabatic and in line with the experimental data. The convective heat transfer in the LBE pipe is simulated using the Seban-Shimazaki correlation (equation (1) below) while the standard Dittus-Boelter is used for the secondary side circulating in the external annular region of the HX (equation (2) below), where Nu= Nusselt number, Pe= Peclet number, Re= Reynolds number, Pr=Prandtl number.

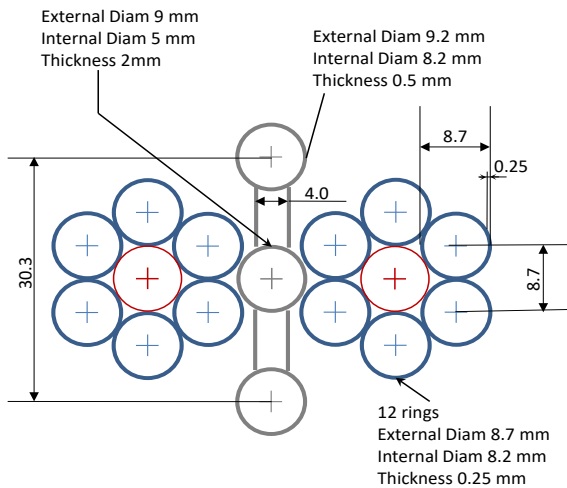
$$Nu = 5.0 + 0.025Pe^{0.8} \quad (1)$$

$$Nu = 0.023 Re^{0.8} Pr^{0.4} \quad (2)$$

The thermal conductivity of the steel powder gap between the LBE and water side is calibrated to 12.5% of the AISI 304 stainless steel.

The friction loss coefficients are calculated using the code, while the form loss coefficients are evaluated using the Idelchik correlations, in particular:

▪ **Spacer grid**



Area undisturbed (A_v) ($A_{ch}-A_{4rod}-A_{10wire}$)	2.8666E-03	m ²
Grid Area (A_s)	1.9935E-04	m ²
Ref. Re (core)	35000	

The Rehme correlation [27] is used to evaluate the spacer grid pressure drop:

$$K = C_v \left(\frac{A_s}{A_v} \right)^2, \quad C_v = -7.65 \log_{10} Re + 49.0$$

Resulting in: $k_{spacer} = 0.06887$.

▪ **Upper grid**

In this case, the considerations made by Ansaldo have been taken into account as a good practice (see section 3.5.4). The k-value adopted in this case is: $k_{grid} = 0.697$.

▪ **90° elbow**

The resistance coefficient of the two 90° elbows at the downcomer inlet and outlet have been evaluated with Idelchik's diagram 6.1. For both: $k_{elbow} = 0.3134$.

▪ *Tank to horizontal pipe*

In this case, the entrance into a straight tube of cross section (Idelchik Diag. 3.1) combined with various inlet with facing baffle (Idelchik Diag. 3.8) are used with the following values:

δ_1	5.16	mm	δ_1/Dh	0.082
Dh	62.7	mm	b/Dh	0.8
b	50	mm	h/Dh	0.64
h	40	mm	σ_1	0.12

$$k = k' + \frac{\sigma_1}{n^2}$$

With $k' = 0.5$ from Diag 3.1 and $n = 1$ results in: $k_{\text{tank}} = 0.62$

▪ *Sudden change in flow area*

The common formulations for sudden contraction and expansion are used for several concentrated pressure coefficients' evaluation:

$$k_{\text{contraction}} = 0.5 \times \left(1 - \frac{A_0}{A_1} \right)$$

$$k_{\text{expansion}} = \left(1 - \frac{A_0}{A_1} \right)^2$$

where A_0 is always the smallest area and A_1 is always the biggest one.

- Expansion from riser to tank

$$A_0 = 0.002854655 \text{ m}^2$$

$$A_1 = 0.050726591 \text{ m}^2$$

$$k = 0.8906$$

- Area contraction due to gas injection line

$$A_0 = 0.002854655 \text{ m}^2$$

$$A_1 = 0.003085658 \text{ m}^2$$

$$k = 0.374$$

- Contraction in the tee at the core inlet (to be added at k_{tee} calculated using the Idelchik correlation)

$$A_0 = 0.002863422 \text{ m}^2$$

$$A_1 = 0.003085658 \text{ m}^2$$

$$k = 0.036$$

▪ Tee

The elbow sharp corner with recess component and rough walls of Idelchik’s handbook (Diag. 6.7) is adopted. The formulation is:

$$k = 1.2 \times k_{\Delta} \times k_{Re} \times C_1 \times A \times k_{loc}$$

Where the coefficient 1.2 refers to the presence of recess, and the other coefficients are:

k_{Δ}	1.255264837
k_{Re}	1.108419573
C1	1
A	1.2
k_{loc}	0.99

This results in a k_{rec} of 1.984, and by adding the sudden contraction in the corresponding section a total coefficient: of $k_{rec} = 2.02$ is found.

3.4 SNU, Korea

3.4.1 Code characteristics of MARS-LBE

The MARS (Multi-dimensional Analysis Reactor Safety) code was developed by KAERI (Korea Atomic Energy Research Institute) by unifying widely used codes for LWR analysis, such as the RELAP5 code, which aims system safety analysis, and the COBRA-TF code, which targets subchannel analysis [28]. The RELAP5 is based on one-dimensional, transient, two-fluid flow model given by 2-fluid, 6-equation system considering phase transition between water and steam, and mass, momentum, and energy conservation of each phase. The COBRA-TF is a three-field, three-dimensional thermal-hydraulic analysis code and is also able to handle two-phase flow with reflood heat structure (HS) model on flexible nodalisation schemes. In the MARS structure, two codes are coupled implicitly. The code also includes other features such as the point kinetics model with versatile and robust features by coupling.

Fulfilling the necessity of system analysis for the Generation-IV type reactor developments, the MARS has been improved by implementing various fluid properties such as sodium (Na), helium (He), carbon dioxide (CO₂) and LBE. Currently used MARS-LBE version 3.11 is a revision of MARS version 3.1 by updating hydraulic relations and heat transfer correlations suitable for HLM modelling. This code has been used from the Phase I.

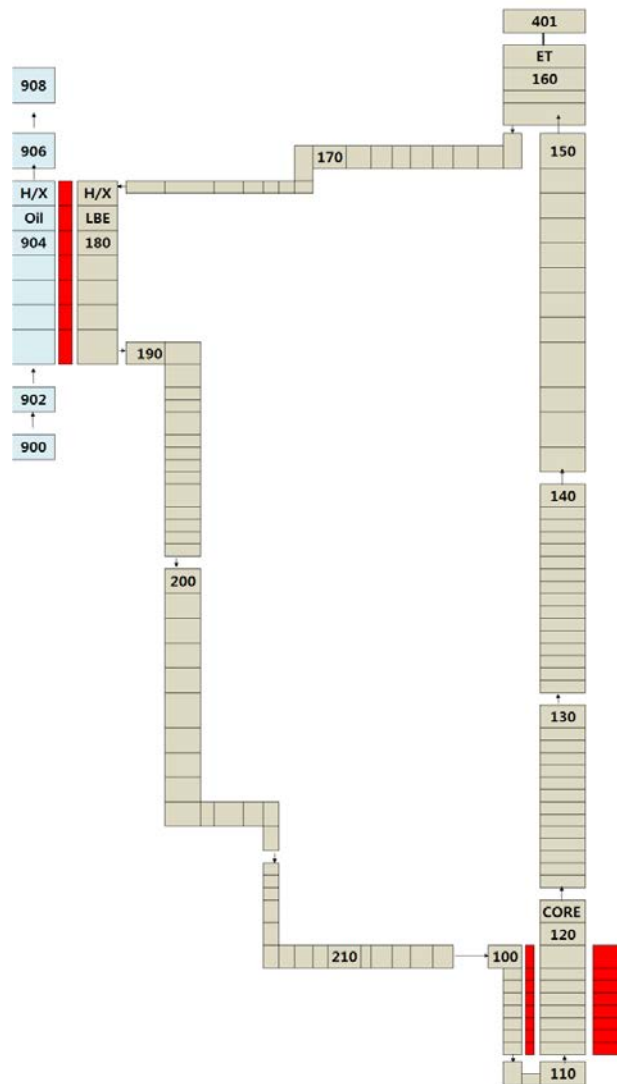
For interpreting a real system into a calculation model, the MARS-LBE requires nodalisation process, which stands for dividing whole system into small segments and explaining relationships between these segments. In a broad perspective, the MARS-LBE have two components, VOLUME and JUNCTION models, for hydrodynamic calculation. For easier input generation, some VOLUMES and JUNCTIONs can join to simulate piping (PIPE component), an annular channel (ANNULUS component), and so on. Some components such as pump (PUMP component), accumulator (ACCUM component), pressuriser (PRIZER component), valve (VALVE component), etc., are prepared to simulate their special functions and behaviours. For initialisation of a calculation system, initial conditions should be assigned for every component described in the input. Hence, basically, a VOLUME component requires temperature and pressure and a JUNCTION component needs mass flow rate. Moreover, other physical parameters would be additionally necessary if some options are used. There are also unsteady models, time-dependent volume (TMDPVOL component) and time-dependent junction (TMDPJUN component) to assign boundary conditions with varying time. In the modelling of HELIOS and NACIE, most of components are interpreted with PIPE components, JUNCTION components, unsteady boundary conditions (TMDPVOL and TMDPJUN components) because these facilities do not have other kinds of components.

Moreover, to include heat transfer modelling among components in a system, HS models are utilised. They permit heat transfer across solid bodies in which thermophysical properties are asked to be supplied. In the modelling of two facilities, heat sources and heat sinks such as heater rods and heat exchangers are modelled with heat structures.

3.4.2 HELIOS model for MARS-LBE

The layout and components used for MARS-LBE model in the current phase is slightly changed from the one used in the former phase; regions that accompany heat transfer such as heater rods and heat exchanger tubes are also included in the model and natural circulation bypass is considered because flow no longer passes through the pump. Applying those changes, HELIOS nodalisation on natural circulation test campaign prepared for MARS-LBE input is depicted as Figure 3.13. Two hydrodynamic systems, the primary (LBE) and secondary (Dowtherm® RP thermal oil) loops are modelled with 13 PIPE components, 2 single volume (SNGLVOL) components, 16 single junction (SNGLJUN) components, 3 time-dependent volume (TMDPVOL) components and 1 time-dependent junction (TMDPJUN) component.

Figure 3.13 – HELIOS nodalisation prepared for MARS-LBE simulation



Moreover, three heat structures are involved for the model; heater rods, wall between the downcomer and active core inside the core mock-up, and heat exchanger tube walls. The power given to the heater rods is simulated by heat transfer rate vs. time, and the uniform heat transfer rate is guessed using the same power condition with respect to time advancement. Thermophysical properties of solid wall, stainless steel 316L are given as a function of temperature, as described in Table 3.3 [10]. It should be noted that only thermal conductivity and volumetric heat capacity are required for a solid on the code calculation.

Table 3.3 – Thermophysical properties of stainless steel 316L included in MARS-LBE simulations [10]

Temperature (°C)	Thermal conductivity (W/m K)	Volumetric heat capacity (J/m ³ K)
20	14.2	3.78E+06
94	15.3	3.93E+06
205	17.1	4.09E+06
316	18.8	4.21E+06
427	20.5	4.31E+06
538	22.1	4.41E+06
649	23.6	4.50E+06
760	25.1	4.58E+06
871	26.6	4.66E+06
1205	30.7	4.90E+06

The MARS codes simulate convective heat transfer by calculating convective heat transfer coefficient from Nusselt number, which is generally given by Reynolds number and Prandtl number (also Peclet number, which can be calculated from the product of two nondimensional numbers) of a fluid in a component. To calculate the coefficients of LBE and secondary side oil at a given condition, the Seban-Shimazaki correlation is applied to any kind of pipe flow conditions on LBE:

$$Nu = 5.0 + 0.025Pe^{0.8},$$

and Sieder-Tate correlation is used for the oil, which is also recommended by the manufacturer [9]:

$$Nu = 0.027 Re^{0.8} Pr^{0.33} \left(\frac{\mu}{\mu_w} \right)^{0.14}.$$

In this case, the viscosity term in the equation above (μ/μ_w) is assumed to be negligible so the modified equation below is actually used:

$$Nu = 0.027 Re^{0.8} Pr^{0.33}.$$

Considering the fact that flow velocity (mass flow rate) under natural circulation is strongly coupled with power, height and total pressure loss, it is important to impose proper hydraulic resistance coefficients to the components where pressure loss happens. As a result of activities performed in the former phase, the HELIOS facility already has best practice guidelines for the prediction of pressure drop coefficients in every component and the results are to be utilised in this phase, especially on the form loss calculations. Friction losses along

flow path will be calculated by the internal subroutine of the MARS-LBE code. For the calculation of it, the code requires pipe roughness and it is given as and assumed to be $2.53\mu\text{m}$, as already measured in the phase I [1].

3.4.3 NACIE model for MARS-LBE

For the MARS-LBE simulation of natural circulation, test #301, the NACIE is nodalised as shown in Figure 3.14 by following benchmark specifications as described in section 4.2.4. In this phase, only two different hydraulic systems, LBE side and water side, without argon gas injection system, are considered because gas enhanced circulation (GEC) is out of the benchmark scopes. In the hydrodynamic model, there are 9 PIPE components, 2 ANNULUS components, 2 single volume (SINGLVOL) components, 14 single junction (SINGLJUN) components, 3 time-dependent volume (TMDPVOL) components, 1 time-dependent junction (TMDPJUN) component. To differentiate the use of PIPE components and ANNULUS components in Figure 3.14, ANNULUS components are expressed with dashed lines inside the series of rectangles.

Similar to the HELIOS input, three heat structures are contained; a heating rod, wall inside the expansion vessel and layers in the heat exchanger outer wall. In fact, there are two heater rods in the heating section so flow area is reduced by the cross-sectional areas of two rods, but only one heating rod is active in the Test #301. Hence, 21.5kW of electric power is given to a single heating element. It is implemented with a power table that defines time-varying heat source, and the source is designated to exert same power over time. For the expansion tank, a part of riser that goes through inside the tank is simulated also as an HS. However, the amount of heat dissipation between the small part of riser inside the tank and a bulk inside the tank itself is negligible so that this model is found to be redundant. As shown in Figure 3.14, three different layers are engaged to simulate the heat transfer region in the heat exchanger. The three layers model stainless steel powder between two stainless steel pipes, respectively.

For heat transfer calculation, thermophysical properties such as thermal conductivity and volumetric heat capacity of AISI stainless steel 304 are implemented in terms of varying temperature because most of the constituent elements are made of it. However, these properties cannot be used for the stainless steel powder layer inside the heat exchanger. Moreover, such properties of the powder were not provided nor measured so that a simple assumption that the powder has 13% of thermal conductivity and volumetric heat capacity in a given temperature was imposed to avoid complexity of calculation and use of other heat transfer models. The properties of stainless steel 304 and the powder used in calculation are described in Table 3.4.

Figure 3.14 – NACIE nodalisation prepared for MARS-LBE simulation

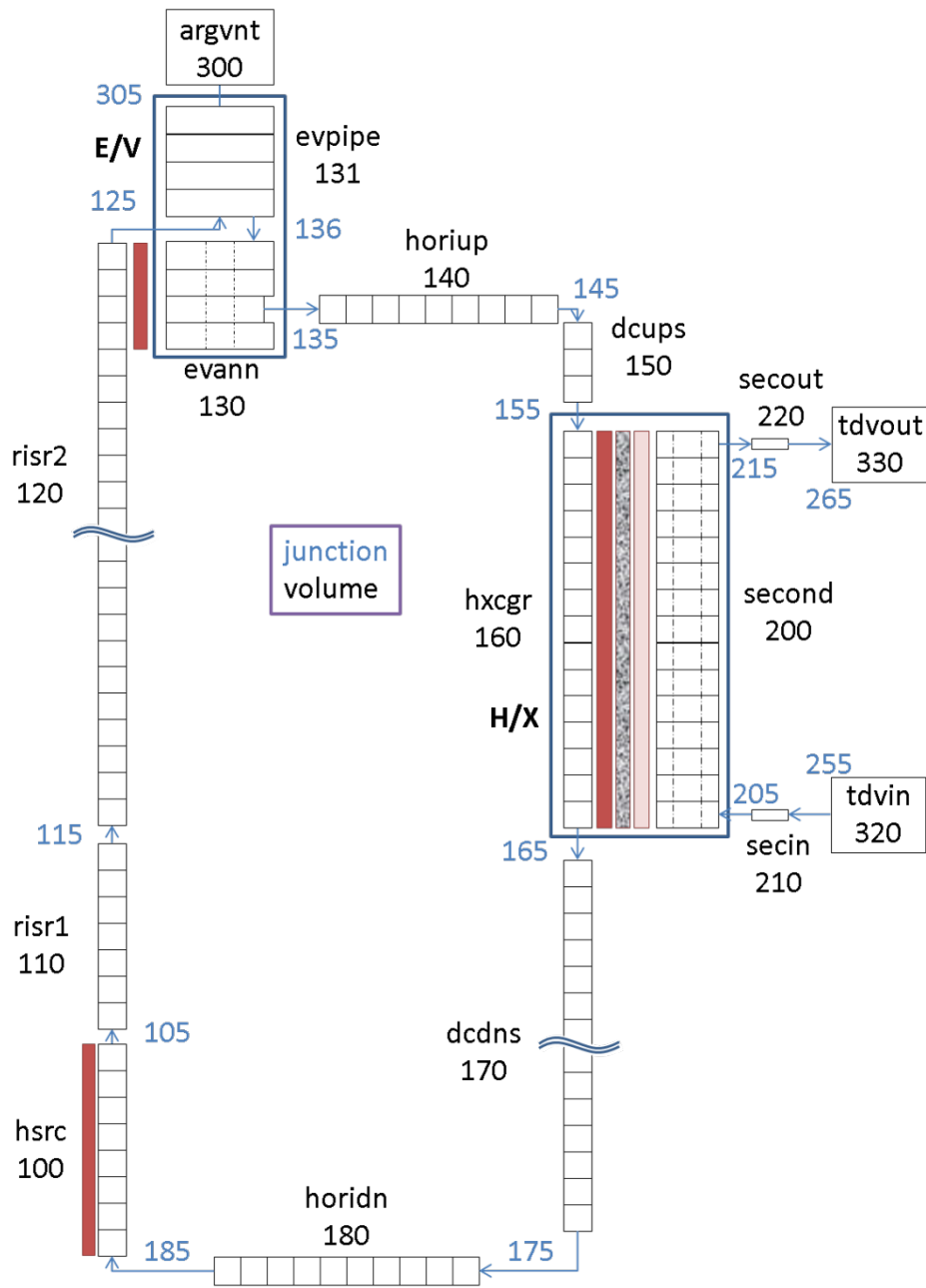


Table 3.4 – Thermophysical properties of stainless steel 304 and stainless steel powder used for MARS-LBE input for NACIE

Temperature (°C)	Thermal conductivity (W/m K)		Volumetric heat capacity (J/m ³ K)	
	AISI stainless steel 304	304 powder*	AISI stainless steel 304	304 powder*
293	14.76	1.919	3.81E+06	4.96E+05
300	14.89	1.936	3.83E+06	4.98E+05
350	15.79	2.053	3.95E+06	5.13E+05
400	16.61	2.159	4.05E+06	5.27E+05
500	18.28	2.376	4.23E+06	5.50E+05
600	19.77	2.570	4.39E+06	5.71E+05
700	21.21	2.757	4.53E+06	5.88E+05
800	22.59	2.937	4.65E+06	6.04E+05
900	23.99	3.119	4.76E+06	6.19E+05
1000	25.33	3.293	4.87E+06	6.33E+05
1100	26.58	3.455	4.97E+06	6.46E+05
1200	27.81	3.615	5.06E+06	6.58E+05
1300	29.18	3.793	5.15E+06	6.69E+05
1400	30.34	3.944	5.23E+06	6.80E+05
1500	31.55	4.102	5.32E+06	6.91E+05
1600	32.70	4.251	5.39E+06	7.01E+05
1672	33.53	4.359	5.45E+06	7.08E+05
1727	28.15	3.660	5.49E+06	7.14E+05
1800	28.90	3.757	5.54E+06	7.21E+05

* The thermophysical properties of 304 powder are assumed to be 13% of the original steel.

Considering the solving process of the MARS-LBE code, convective heat transfer must be properly imposed. As in the HELIOS case, the coefficients of LBE follow Seban-Shimazaki correlation, in any kind of pipe flow aspects:

$$Nu = 5.0 + 0.025Pe^{0.8},$$

and the well-known, widely used Dittus-Boelter correlation is used for the water side:

$$Nu = 0.027 Re^{0.8} Pr^{0.4}.$$

Although the NACIE is in a rather simple geometry compared to the HELIOS, hydraulic resistance coefficients for some components must be carefully imposed due to the absence of pressure loss measurement in the NACIE. By following the best practice guidelines given in the former phase some components can be dealt with. Others can be estimated by referring to the hydraulic loss handbook [15] and use of computational fluid dynamics (CFD) calculation.

Hydraulic loss coefficients used for the NACIE simulation are designated as in the following:

- 90° elbows

There are two 90° elbows in the primary side. One is in the inlet side of the downcomer, and the other one is connecting the downcomer outlet and lower horizontal pipe. In the MARS-LBE input, they are simulated with single junction (SNGLJUN) components and in this case the pressure loss over these components is evaluated by designating the value of form loss coefficients. As the HELIOS has 90° elbows, a best practice guideline on them is also given in Table 6.1 in the phase I report. By referring to this, for both elbows, $K_{elbow} = 0.3109$ is used.

- Tee (branch) in the heating region

The tee is connecting the lower horizontal pipe and the heating section. It is a branch-type tee because of its upstream and downstream being not on the same axis. With the same reason for 90° elbows, the hydraulic loss coefficient can be found in Table 6.1 in the former report and the value K_{tee} can be obtained as $K_{tee} = 1.29$.

- Entrance from expansion vessel into the upper horizontal pipe

This type of hydraulic loss happens in the expansion vessel outlet region. A part of the upper horizontal pipe penetrates into the expansion vessel and flow goes out through the penetration. By following the guidelines, the form loss coefficient in this geometry $K_{entrance}$ is evaluated as $K_{entrance} = 0.5$.

- (Lower) grid spacer

Generally, grid spacers are widely used over nuclear reactors and thermal-hydraulic test facilities to keep nuclear fuel rods or heating rods as first arranged. For the same reason, the spacers were adopted in the HELIOS mock-up core and their hydraulic losses were measured. In the former phase, a formula was suggested with test data and CFD calculation results by modifying a coefficient given in Rehme correlation of form loss coefficient for grid spacers, due to their different geometries from Rehme’s study [27]. In the case of the NACIE grid spacer, the formula is used because all participants agreed to follow the best practice guideline given in the phase I where it is applicable at the beginning of the NACIE benchmark.

The modified Rehme correlation is given as:

$$K_{grid} = C_v \left(\frac{A_s}{A_v} \right)^2, \quad C_v = -7.65 \log_{10} Re + 49.0,$$

where A_s is the projected area of spacer grid and A_v is the undisturbed area, which is defined as flow area in the upstream region. With the design of the spacer given in Figure 2.5, the form loss coefficient of the spacer grid is calculated in Table 3.5.

Table 3.5 – Projected area, undisturbed area and form loss coefficient of the NACIE spacer grid

Item	Value/unit
Grid spacer projected area (A_s)	1.993e-04 m ²
Undisturbed area (A_v)	2.877e-03 m ²
Reference Reynolds no. (Re)	3.561e+04
Grid spacer form loss coefficient (K_{grid})	6.805e-02

- Upper grid

At first, being considered as another grid spacer, the modified Rehme's correlation was adopted to the upper grid. Nevertheless, the calculated value turned out to be quite different from Ansaldo's CFD calculations and all participants agreed to implement their results, as described in section 3.5.4. The form loss coefficient is given by: $K_{grid} = 0.697$.

- Abrupt area change and friction loss

Abrupt area changes, both expansion and contraction, and friction loss are evaluated inherently by subroutines in the MARS-LBE. Hence, in the NACIE input prepared for MARS-LBE, form loss coefficients for discharge from riser to expansion vessel, area change due to the gas injection line in riser and other general area changes are not implemented but calculated automatically. For calculation of friction loss, the code needs pipe roughness and it is measured to be 32 μm .

3.5 Ansaldo, Italy

The activities conducted by Ansaldo within the benchmark LACANES are to be considered as a part of the objectives of the master thesis reported in [29].

In the following the description of the RELAP5 model set for the simulation of the natural circulation Test 301 is provided, as well as the main assumptions adopted.

3.5.1 NACIE RELAP5 thermal-hydraulic model description

In RELAP5, the hydraulic description of the circuit is performed by means of hydrodynamic elements such as pipes, annuli, single volumes and time-dependent volumes, connected to each other with junctions. The wall heat transfer, instead, is described through HS components, which simulate the metal surface through which the heat is exchanged between the fluids on the opposite sides. The HS model makes it possible to take into account, also, the potential of the power generation inside the structure itself.

The NACIE RELAP5 model has the following main characteristics:

- two systems: the LBE loop and the HX water loop;
- an HS simulating the HX tube walls on which the thermal heat exchange occurs between the hot LBE and the cold water;
- an HS simulating the heating rods that provide for the generation of the nominal loop power of 21.5 kW.

Additional inputs to the model consist in the specification of the reference volume associated with the reference height of each simulated system, and, of course the fluid present in that dominion (RELAP5 input card 120). To account for the presence of non-condensable species (i.e. Argon in our case) transported with the system fluid, the RELAP5 input card 110 is set ([30], vol. 2, p. A2-11).

The description of the NACIE RELAP5 model set for Test 301 simulation is provided in the following using the sketch reported in Figure 3.15.

The LBE loop (nodes number 10X, and time-dependent volume 300) consists of:

- **Vertical downcomer** – The vertical downward oriented downcomer is represented by P 102, P 104 and P 106. Here, there are junctions SJ 101 and SJ 107, which represent 90° bends, while SJ 109 is the tee branch at the bottom of the riser.
- **Horizontal portions of the facility** – Represented by two pipes: upper P 100 and lower P 108.
- **HX LBE side** – P 104 simulates the inner pipe of the HX. Note that P 104 is thermally connected to the heat structure (HS) 1041 that represents the composite wall (inox-steel powder-inox) of the heat exchanger through which the LBE power is transferred to the cold water side.

- **Riser** – The vertical upward oriented riser is represented by P 110, P 112 and A 114; P 110 is correspondent to the heaters active length, while A 114 is correspondent to the part of the riser in which is housed the argon inlet pipe of 3/8". Note that the cross section of P 112 is different compared to P 110 and A 114, because of the presence of the two heater pins and the two dummy pins in P110, and the presence of argon inlet pipe in A114 (see Figure 3.16). Note that junctions SJ 113 and IJ 11008 simulate the two spacer grids in the NACIE heating section. Note also that P 110 is thermally connected to the HS 1121 representing the power generated by the heating rods.
- **Expansion vessel** – The expansion vessel at the top of the riser is represented by the use of two hydrodynamic elements. The first is A 116, which is the part of the vessel above A 114 outlet, and is filled partially with LBE, and partially with argon; in particular, as initial configuration, six parts out of ten are filled with LBE, setting in the card 1200 of the element to the flag 003, while the remaining are filled with the Ar, setting in the same card the flag 004 for dry incondensable. Component A 116 is connected through junction SJ 117 to A 118, which is the annulus surrounding the final riser portion of A 116, filled completely with LBE. Consequently, a level of about 0.412 m is set in the expansion vessel (see also Figure 3.17 for the detail of the expansion vessel model). Note also that SJ 115 connects A 114 to A 116; as the flow area changes abruptly, the opportune flag of abrupt area change is set in the card 1101 of the junction. The same is for SJ 119, which connects the expansion vessel to the pipe P 100 that leads to the downcomer.
- **LBE system pressure boundary condition** – The atmospheric pressure is set by means of TDV 300 which represents the argon outlet from the circuit.

The HX secondary side water loop (nodes number 20X) consists of the HX driven by boundary conditions. The very simple model is shown in the blue portion of Figure 3.15; it is characterised by the annulus A 200 that represents the outer tubes of the HX; it is connected by two junctions – SJ 203 and TDJ 201 – to time-dependent volumes TDV 202 and TDV 204. TDV 202 set the inlet temperature of water/pressure in the heat exchanger at 35.1°C/1 bar and the time-dependent TDJ 201 set the water flow rate to the required 0.47 m³/h, according to the following Table 4.7.

Figure 3.15 – RELAP5 geometrical configuration scheme (Ansaldo)

NACIE - Test 301

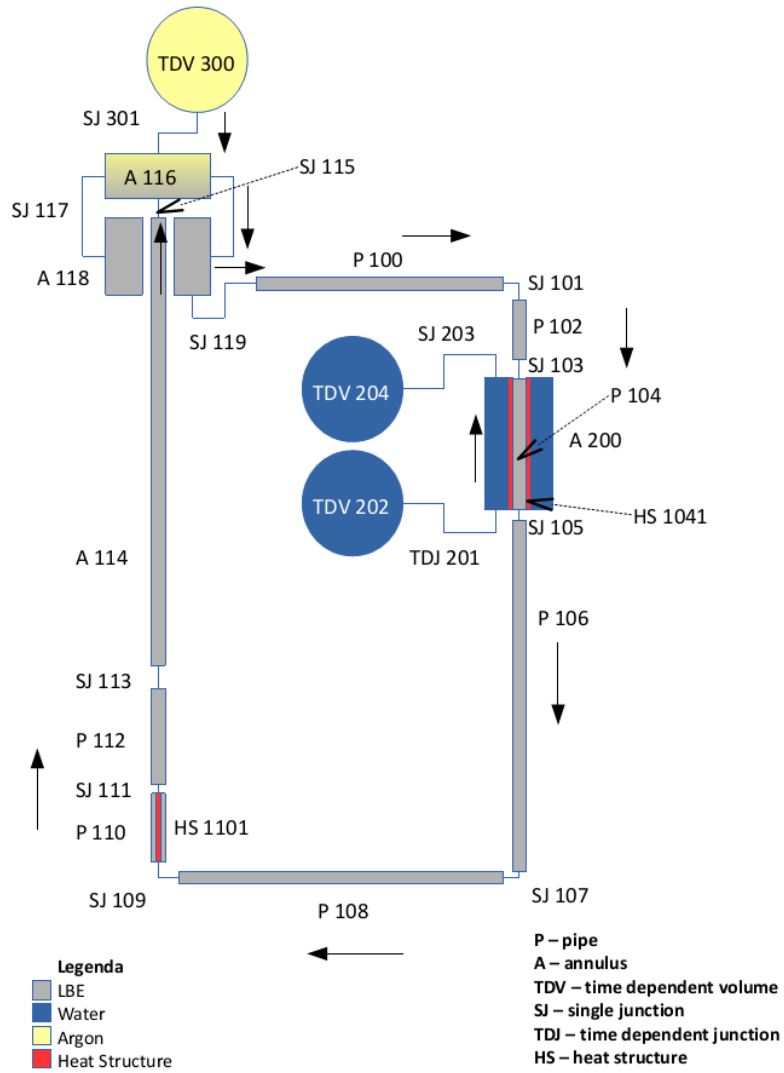


Figure 3.16 – Sections of the elements in the riser (Ansaldo).

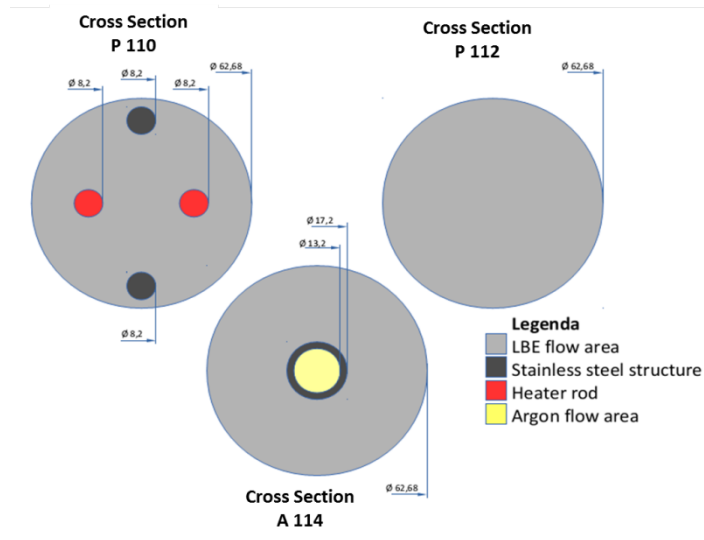
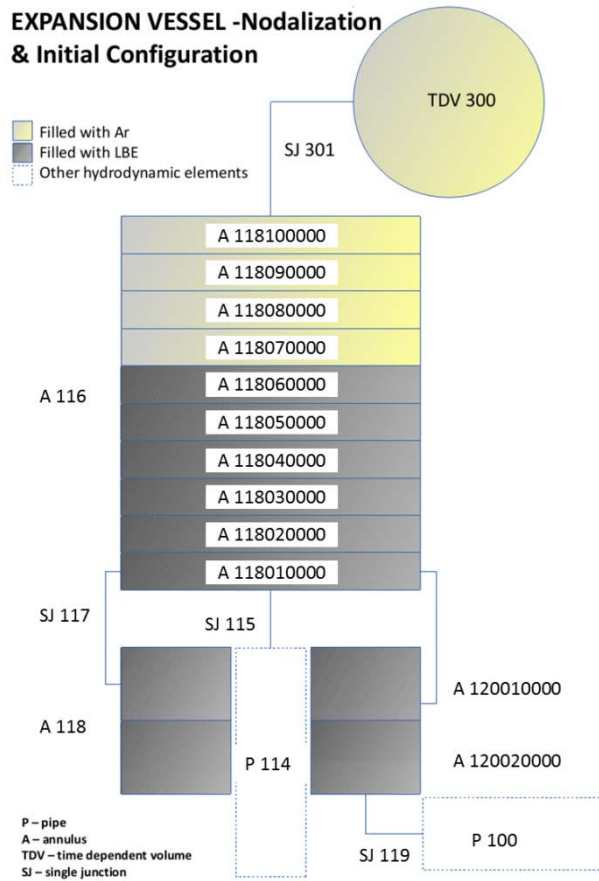


Figure 3.17 – Details of expansion vessel nodalisation and initial configuration



3.5.2 Main assumptions

It is worth to say that some assumptions are made in these first simulations, because of some inconsistency/incompleteness in the data contained in the benchmark specifications. They are listed in the following:

- Heating rods active length – an active length of 850 mm is assumed, even though, as a result of direct inspection, an active length of 854 mm (Figure 2.9) has been determined (note that 850 mm corresponds to the length assigned to pipe P110 in the RELAP5 model).
- Heating section cross section (Appendix A, NACIE General View) – shows that the heating section includes three heaters, but the preliminary bundle represented in the drawing has been changed during the facility commissioning phase. As such, two heaters and two dummies are assumed and the heating section LBE cross flow area has been calculated accordingly to the benchmark specification.
- Conductivity of the steel powder filling the gap between inner and middle HX tube – the thermal properties (in particular thermal conductivity) of the steel powder set in the HX between the primary and secondary side are not well-known but a magnitude of about 10% is suggested; in any case they should be tuned to agree with the experimental data.
- Argon Injection pipe – the dimension assumed for the argon injection pipe is 3/8" (i.e. 17.2 mm of external diameter and 13.2 mm of inner diameter).
- Heat Losses – as suggested by the benchmark specification, heat losses are omitted due to the good loop insulation.
- LBE level in the expansion tank – no information is given about the LBE level in the expansion vessel, so that the LBE level in the expansion tank has been assumed to be 6/10 of the volume above the riser pipe termination.
- Pipe roughness – no roughness values were given in the first benchmark specifications received, hence, different values are used to perform a sensitivity of the predicted flow rate on the distributed pressure losses value.
- 90° Bend radius – the 90° bend curvature radius is not provided in the specifications; it is assumed to be 1.5 times the diameter.
- Spacer grids pressure loss coefficient – a sensitivity is performed, taking into account two different values for concentrated pressure loss coefficients, as provided by correlations from literature (i.e. Rehme [27] and the Idelchik correlation [31]).
- Thermocouple cables – the obstruction caused by the heating rods thermocouple cables in the riser is considered to be negligible.

3.5.3 Heat structures model

As already stated, in Test 301 the heating section provides a power of 21.5 kW to the LBE, which is rejected to the HX (H₂O cooled) located in the upper region of the vertical downcomer. The differential density between the riser (where the power is generated by means of the heating rods) and the downcomer determines the natural circulation of the LBE in the loop.

The generated power is simulated by means of HS 1121, while the composite walls (intermediate tube wall + steel powder + inner tube wall) of the HX tubes are simulated by means of HS 1041.

- The HS 1041 model is summarised below:

In the HS 1041 left boundary (HX LBE side, volume P 104), a convective condition is set (by setting word 3 of card 501 equal to one). RELAP5 will therefore calculate a heat transfer coefficient, on the LBE side, by using the Subbotin correlation for the Nusselt number, according to the subroutine modification mentioned in ref. [32]:

On the right boundary (HX H₂O side, volume A 200), a convective condition is set (word 3 of card 601 equal to one); the code will use the heat transfer coefficient (for the case of forced convection valid for the water circuit) of the well-known Dittus-Boelter correlation to find the Nusselt number.

Properties of HS 1041 are set in order to follow the geometry of the HX reported in the specifications (Appendix A, NACIE heat exchanger view): since there are different materials and each of those has a different thickness, the HS is divided in three different parts, with suitable intervals, by the use of card 101.

Materials thermal properties (i.e. the thermal conductivity and heat capacity as a function of the temperature ([30], vol. 2, pp. A10-1 – A10-2)) are fixed in the dedicated tables (material tables are specified by input card 201XXX0000): the number XXX equal to 001 identifies the stainless steel, while number 004 identifies stainless steel powder. Stainless steel powder thermal conductivity used in the run is assumed to be equal to 10.0% of that of stainless steel, as suggested in the benchmark specification. Heat structure (HS) features are reported in Table 3.6.

Table 3.6 – HS 1041 characteristics.

Inter.	Left volume and boundary condition	Right volume and boundary condition	Left coord. [m]	Right coord. [m]	Material	Card in HS ([30], vol. 2, pp. A8-1 – A8-14)	Left coord. thermal diam. [m]	Right coord. thermal diam. [m]	Surface area or factor
1	P 104 Wall-fluid heat transfer	A 200 Wall-fluid heat transfer	0.031335	0.036515	AISI304 Material Table 001	201	0.06268	0.0287	Element Length
2									
3									
4									
5									
6									
7				0.04234	AISI304 Steel powder Material Table 004	202			
8									
9									
10									
11									
12									
13				0.04445	AISI304 Material Table 001	203			
14									
15									
16									

- The HS 1121 is used to simulate the heat source in the riser. It is set as a single full cylindrical pin: left co-ordinate is set to 0, as well as word 1 of card 501 (left boundary conditions card in [30] (vol. 2, pp. A8-1 – A8-14)), in order to have no elements connected to this boundary. In card 601 (right boundary conditions card in [30] (vol. 2, pp. A8-1 – A8-14)) is specified the right boundary and the connection to all the volumes of P 112. In general table 202 ([30], vol. 2, pp. A11-1 – A11-2), the power generated in the HS is set to the nominal value of 21500 W when the time counter is still set to zero. This value is identified by the general table number 100, which is recalled in card 701 of HS 1121.
 - Initial LBE temperature is set to 300°C coherently with the specifications. HS main features are reported in Table 3.7. It must be remarked that heater rod material, right co-ordinate geometry and thermal diameter are not reproducing any real data, because there is no interest in the

determination of the temperature distribution in the heater rod: since the power is a fixed parameter, fluid temperature depends only on the power input and not on heat transfer coefficient, nor geometry.

Table 3.7 – HS 1121 characteristics

Inter.	Left volume and boundary condition	Right volume and boundary condition	Left coord. [m]	Right coord. [m]	Material	Card in HS ([30], vol. 2, pp. A8-1 – A8-14)	Left coord. thermal diam. [m]	Right coord. thermal diam. [m]	Surface area or factor
1	Power input from general Table 100	P 110 Wall-fluid heat transfer	0	0.005798	AlSi304 Material Table 001	201	-	0.0383	Element length
2									
3									
4									
5									
6									

3.5.4 Concentrated pressure drops evaluation

The last step before launching the analysis is to evaluate the concentrated pressure drop on the junctions SJ 101, SJ 107, SJ 109, IJ 11008, SJ 111.

For the concentrated hydraulic loss coefficients calculation are used literature correlations, mainly from [31]: it must be remarked that these correlations are obtained mainly for water, and their application to cases involving a LBE flow may not bring to realistic results. Anyway, another experience, reported in [33], has assessed that, in the design of a Venturi nozzle, by using the same correlations for water, the results obtained for LBE were in good agreement with that of water, giving some confidence on the validity of the literature correlations mentioned above for LBE case.

In order to make the concentrated pressure drops evaluation, Reynolds number and other hydraulic properties of the fluid are to be determined for the following specific conditions, and assumed the same. As the specifications say for Test 301, a referring temperature is taken between 300 and 350°C (see Table 4.6), meaning a LBE density of about 10300 kg/m³, and dynamic viscosity of 1.5932e-3 Pa s. The hydraulic diameters were calculated, while, for fluid velocity, the value of 0.15m/s is taken from the experimental results of specifications (see Table 4.7). The resulting Reynolds is of about 60700, which means turbulent flow. With these parameters the evaluation of pressure drop is possible.

- SJ 101 and SJ 107 are two 90° elbow bends. The pressure drop evaluation is made by calculating the resistance coefficient as a sum of two other coefficients representing respectively the local (concentrated) and friction (distributed) components ([31], Diagram 6.1)

$$\zeta = k_{Re} k_{\Delta} \zeta_{loc} + \zeta_{fr}$$

The distributed resistance coefficient can be evaluated as:

$$\zeta_{fr} = \pi \frac{\delta(^{\circ})}{180^{\circ}} \frac{R_0}{D_h} \lambda = 0.0175 \frac{R_0}{D_h} \delta(^{\circ}) \lambda$$

where:

δ curvature angle (°) in this case of 90°, R_0/D_h curvature radius over hydraulic diameter in this case 1.5, λ friction factor.

The local resistance coefficient can be evaluated as a product of three factors, as suggested by Abramovich formula ([31], pp. 268-269)

$$\zeta_{loc} = ABC$$

where

$$A=1.0 \text{ for } \delta=90^\circ \quad A=0.9\sin \delta \text{ for } \delta<70^\circ \quad A=0.7+0.35\frac{\delta}{90} \text{ for } \delta>100^\circ \quad (\text{Nekrasov})$$

$$B=\frac{0.21}{(R_0/D_0)^{0.25}} \text{ for } \frac{R_0}{D_0}<1.0 \quad B=\frac{0.21}{\sqrt{R_0/D_0}} \text{ for } \frac{R_0}{D_0}\geq 1.0$$

and D_0 pipe diameter, C is a parameter that in a circular section is equal to 1 ([31], Diagram 6-1, p. 260).

$\zeta_{loc}=1.7146$ correlation coefficient obtained by Abramovich correlation used before;

ζ_{fr} correlation coefficient for distributed pressure drop;

$k_{Re}=64f \approx 1.4$ Reynolds correction coefficient where f is the friction factor

$k_d=2$ relative roughness correction coefficient.

For the roughness of 32 μm the resistance coefficient is 0.3192.

- SJ 109 is a tee. The hydraulic loss was estimated by a superposition of effects correlated to the flow change of direction and the obstacles represented by the rods encountered by the flow coming from the lower horizontal pipe. The following configuration is considered: a first heater rod near the horizontal branch, two decentralised dummies in the middle and the last heater rod in the most distant position to the horizontal branch.
 - The correlations used for evaluating the simple tee branch pressure losses may be incorrect, because it is extrapolated for a configuration in which the branch flow cross section is the biggest area in consideration. This fact would imply some modifications in the geometry that are not considered in the handbook, so that the composition of the two pressure losses may require that the limit case of equal cross sections should be considered in the correlation. The correlation of [31] (Diagram 7-4, p. 347) should give the following hydraulic resistance coefficient:

$$\zeta = 0.6 \left(1 + \left(\frac{A_{branch}}{A_{pipe}} \right)^2 \right) = 0.6(1+1) = 1.2$$

- Another contribution may be represented by the flow area contraction, which can be seen as:

$$\zeta = 0.5 \left(1 + \frac{A_{pipe}}{A_{branch}} \right)^{3/4} \left(\frac{A_{branch}}{A_{pipe}} \right)^2$$

- The contribution computed is 0.0711, reported to the branch flow cross section. The other contribution to the dissipation is given by the obstacles to the flow coming from the horizontal pipe. The way to account the contribution of obstacles is considering only the heater rods near to the branch pipe, as, for the others, the flow is deviated in a direction parallel to the riser axis, and the collision with the obstacles may be not so effective.
- The correlation hydraulic loss coefficient is again that of [31] (Diagram 10-1 and 10-2, pp. 477-478).

$$\zeta = 1.15C_x \frac{S_m / A_{branch}}{(1 - \tau S_m / A_{branch})^3}$$

$C_x=1.08$ from the diagram of the cylinder drag coefficient: Reynolds' number referred to the diameter of the obstacle is 7490;

$S_m / A_{branch}=0.1667$ obstacle flow area occupation over flow cross section

$\tau=0.625$ parameter referred to the obstacle edge, which is not sharp.

The hydraulic resistance coefficient referred only to the first obstacle is computed, and it is 0.2878. In synthesis, the hydraulic resistance coefficients given by correlations considered for the simulations is 1.488.

- SJ 113 consists in a contraction of flow area due to the passage from a pipe to an annulus of reduced hydraulic diameter because of the presence of the argon injection pipe. It will be described as a pipe that abruptly contracts to a smaller section. Correlations are found in literature ([31], p. 151).

$$\zeta_{loc} = 0.5(1 - A_{min} / A_{max})^{3/4}$$

The resistance coefficient found is very small and it is of about 0.072.

- SJ 115, SJ 119 consist, respectively in an expansion in the tank above the riser pipe, and in a contraction of the flow area.

The sudden expansion resistance coefficient of SJ 115 was evaluated, referring to the inlet area velocity, by the Borda-Carnot formula ([31], p. 145)

$$\zeta_{loc} = \left(1 - \frac{A_{inlet}}{A_{outlet}}\right)^2$$

that gives a resistance coefficient of 0.889.

The flow U turn is still to be taken into consideration, together with the fact that the upward flow expansion may not take place in the whole expansion vessel cross section: indeed, the turning of the fluid requires that part of the expansion vessel cross section is interested by downward flow.

The P 100 intake is a quite hard configuration to be characterised by a handbook. First of all is important to evaluate the contribution of the horizontal pipe penetration in the expansion vessel downcomer. In the diagram in [31] (Diagram 3-1, p. 122) this contribution depends on the tube thickness over the hydraulic diameter (of the horizontal pipe) and on the length of the penetration over the hydraulic diameter. The penetration is 50 mm long (Appendix A, NACIE – expansion vessel view), meaning a ratio over hydraulic diameter of 0.798. From the same sketch the tube thickness can be obtained, and is of 5.17 mm: its ratio over the hydraulic diameter is of 0.0824. From the diagram mentioned above the hydraulic resistance coefficient should be equal to 0.50.

As the inlet velocity may be low enough to be considered 0, this problem is treated as the case of an entrance from infinite space, and the diagram in [31] (Diagram 3-2, p. 123) is considered, from which a coefficient of 0.5 can be found for this specific situation. This result similar to that computed before, suggests that the tube penetration is not giving contribution to the pressure drop.

Another way is to treat the problem as a diverging side branch: referring to the P 100 velocity, the correlation that can be used is the following ([31], Diagram 7-15, p. 361):

$$\zeta_{loc} = A' \left(1 + \left(\frac{Q_{outlet} A_{inlet}}{Q_{inlet} A_{outlet}} \right)^2 \right) \left(\frac{A_{outlet}}{A_{inlet}} \right)^2$$

valid for $\alpha=90^\circ$ and $h_s/h_c=0.365 \leq 2/3$

$$A' = 0.85 \text{ for } \frac{A_{outlet}}{A_{inlet}} = 0.0677 < 0.35 \text{ and } \frac{Q_{outlet}}{Q_{inlet}} = 1 > 0.4$$

It gives a resistance coefficient of 0.854, higher than the one computed by RELAP5. As the lower part of the expansion vessel is closed, the reader is induced to think that this is a better model for the problem, because the bottom of expansion vessel should see a local pressurisation of the stagnant fluid that makes the flow deviate to the upper horizontal pipe.

CFD calculations have been performed to determine which way of treating the problem is better.

- SJ 111 and IJ 11008 represents the upper grid and the spacer grid of the rod bundle. The computation of the pressure drop is performed as suggested in the handbook [31] (p. 152), in which the reference velocity is taken as that of the restricted area:

$$\zeta = \left(\zeta' \left(1 - \frac{A_{restricted}}{A_{inlet}} \right) + \left(1 - \frac{A_{restricted}}{A_{outlet}} \right)^2 + \tau \sqrt{1 - \frac{A_{restricted}}{A_{inlet}} \left(1 - \frac{A_{restricted}}{A_{outlet}} \right)} + \zeta_{dist} \right)$$

$\zeta' = 0.5$ shape coefficient of the orifice plate: in this case the orifice plate is sharp edged, $\tau=1.08$ coefficient representing the wall thickness effect and the inlet opening shape. It is function of the ratio of the orifice thickness over the hydraulic diameter.

From calculations come out different resistance coefficients by varying the value of surface roughness: the dependence from this parameter is in the distributed pressure losses ascribed to the orifice. All coefficients are around 0.7, and, in particular, the one for a roughness of 100 μm is 0.699 and for 50 μm is 0.697 for the upper grid. A value of 0.05 is obtained for the spacer grid.

The same hydraulic loss coefficient is computed according to Rehme correlation,

Rehme correlation use a modified drag coefficient multiplied by the squared ratio of the projection of the blockage area on the flow area [27]. The reference flow area is the constricted area.

$$\zeta_{loc} = C_v \epsilon^2$$

$\epsilon = A_{blockage}/A_{flow}$ is the ratio of projected blockage area over the flow area

$C_v = 3.5 + 74.14/\text{Re}^{0.264} + 2.79\text{E}+10/\text{Re}^{2.79}$ is the modified drag coefficient correlation giving a resistance coefficient ascribed to the constricted section of 1.179.

The CFD calculations were performed to investigate phenomenology which is, *a priori*, not known, so that the choice of a more suitable correlation (if any) maybe done for the evaluation of the concentrated pressure loss coefficients. In particular CFD calculations can help understand:

- the different dissipation mechanisms when they come up together (as the case of the converging tee);
- the three-dimensional aspects of geometry, that can be taken in consideration in the dissipative phenomena.

In the present work, CFD calculations are used to evaluate the validity of the literature correlations used. In Table 3.8 are resumed the coefficients obtained by correlation that better resemble the results found with CFD.

Table 3.8 – Concentrated hydraulic loss coefficients overview

	Coefficient from correlation	Coefficient from CFD calculation
Converging tee (referred to the inlet velocity)	1.488	1.438
Spacer grid (referred to the constricted area velocity)	0.05	0.0408
Upper grid (referred to the constricted area velocity)	0.6965	0.5349
Area change due to the gas injection line	0.0719	-
Riser to Expansion Vessel (referred to the inlet velocity)	0.889	0.6426
Expansion Vessel to horizontal pipe (referred to the outlet velocity)	0.854	0.747
90° elbow	0.3192	-

3.6 INEST, China

3.6.1 RELAP5 MOD4.0 code modification for HLM

The original RELAP5 code was developed to model small-break loss-of-coolant accidents (SBLOCAs) for pressurised water reactors (PWRs), widely used as a best-estimate code for PWRs.

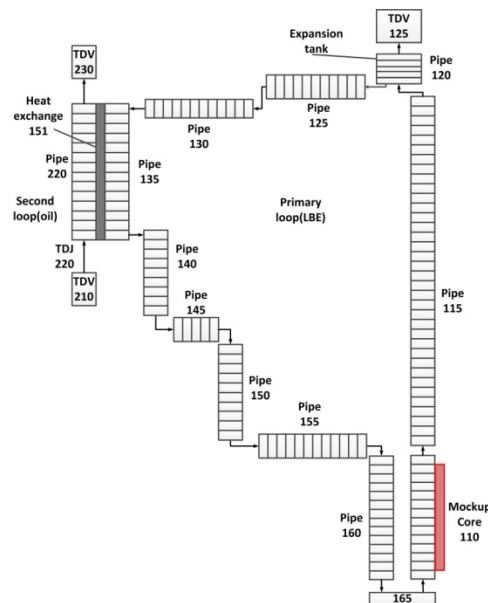
The RELAP5 MOD4.0 version was modified based on the original RELAP5 code, adding a lot of physical and thermodynamic properties, such as Pb, Pb-Bi, Na, Li-Pb. Therefore, the RELAP5 MOD4.0 version can be used for liquid heavy metal reactor safety analysis.

In the second part of the benchmark, the oil and convective heat transfer correlations were added by adding several oil subroutines by INEST as well as the Pb-Bi heat transfer correlations based on the LACANES phase I activities.

3.6.2 HELIOS model for RELAP5

The natural circulation flow of HELIOS NC loop was simulated by 1D with RELAP5 code. The RELAP5 nodalisation model of HELIOS NC loop is shown in Figure 3.18.

Figure 3.18 – RELAP5 nodalisation model of HELIOS NC loop



Core rod bundle and heat exchanger were simulated by heat structures. Friction loss coefficient were calculated by RELAP5 using the recommended correlation. K-factor coefficients were calculated using the recommended correlations obtained in phase I (forced circulation tests). The HX secondary side was driven by boundary conditions. Second loop pump was simulated with time-dependent junctions.

1) Pb-Bi correlations

Pb-Bi dynamic viscosity correlation was modified in RELAP5 MOD4.0 code [8]. Korea Institute of Machinery and Materials (KIMM) dynamic viscosity correlation is used.

Table 3.9 – Pb-Bi property correlations

Item	Correlation	Reference
Density	$R_o = 11096 - 1.3236 \cdot T$ for 398 - 1073 K	Handbook on Lead-bismuth Eutectic Alloy and Lead Properties
Specific heat	$C_p = 159 - 2.72E-02 \cdot T + 7.12E-06 \cdot T \cdot T$ for 398 - 1073 K	
Thermal conductivity	$k = 3.61 + 1.517E-02 \cdot T - 1.741E-06 \cdot T \cdot T$ for 398 - 1073 K	
Dynamic viscosity	$\mu = 4.94 \times 10^{-4} \cdot e^{754.1/T}$ for 400 - 1100 K	

Seban-Shimazaki LBE heat transfer correlation was used in RELAP5 MOD4.0 code:

$$Nu = 5. + 0.025 \cdot Pe^{0.8}$$

2) Oil correlations

Oil property correlations were added to RELAP5 MOD4.0 code. The oil thermodynamic properties refer to THT oil (Correlation from RSE and KIMM).

Table 3.10 – Oil property correlations [9]

Item	Correlation
Density	$R_o = -0.00025 \cdot (T+273.15)^2 - 0.65272 \cdot (T+273.15) + 1044.88319$ for 273 - 773 K
Specific heat	$C_p = 1563.77195 + 2.99957845 \cdot T$ for 273 - 773 K
Thermal conductivity	$k = -0.000127384847 \cdot T + 0.168491405$ for 273 - 773 K
Dynamic viscosity	$\mu = 1.4926 \cdot 10^{13} \cdot T^{-6.0975}$ for 323 - 493 K

Oil heat transfer correlation was added to RELAP5 MOD4.0 code:

$$Nu = 0.027 \cdot Re^{0.8} \cdot Pr^{0.33} \cdot (\mu/\mu_w)^{0.14}$$

The adjustment factor is $(\mu/\mu_w)^{0.14}$, which can adjust the Nusselt number. The results reported in this document are based on the assignment $(\mu/\mu_w)^{0.14} = 1$.

3) Friction losses

The friction losses are calculated directly by the RELAP5 code. To perform the calculation of friction factor for the friction loss inside the loop, the code utilises the different correlations in table 2 at different flow

regimes. In detail, it uses correlations for laminar flow regime, for turbulent flow regime and for transition flow regime from laminar to turbulent.

The laminar friction factor is calculated as

$$\lambda_L = \frac{64}{Re\Phi_S} \text{ for } 0 \leq Re \leq 2,200$$

where Re is the Reynolds number and Φ_S is a user-input shape factor for noncircular flow channels (Φ_S is 1.0 for circular channels).

The friction factor in the transition region between laminar and turbulent flows is computed by reciprocal interpolation as

$$\lambda_{L,T} = \left(3.75 - \frac{8,250}{Re}\right)(\lambda_{T,3000} - \lambda_{L,2200}) + \lambda_{L,2200} \quad \text{for } 2,200 < Re < 3,000$$

where $\lambda_{L,2200}$ is the laminar factor at a Reynolds number of 2,200, $\lambda_{T,3000}$ is the turbulent friction factor at a Reynolds number of 3,000, and the interpolation factor is defined to lie between zero and one.

The turbulent friction factor is given by the Zigrang-Sylvester approximation to the Colebrook-White correlation, which is

$$\frac{1}{\sqrt{\lambda_T}} = -2 \log_{10} \left\{ \frac{\epsilon}{3.7D} + \frac{2.51}{Re} \left[1.14 - 2 \log_{10} \left(\frac{\epsilon}{D} + \frac{21.25}{Re^{0.9}} \right) \right] \right\} \quad \text{for } 3,000 \leq Re$$

where ϵ is the surface roughness, and the other variables have been defined previously.

Wall roughness 2.53 μ m was used in the NACIE loop simulation.


4) Form losses

The flow area variation as well as elbows, orifices and grids are taken into account in the RELAP5 model by means of concentrated pressure drops. The pressure losses coefficients are calculated by means of correlations mainly drawn by Idelchik’s handbook and introduced in the corresponding junctions of the RELAP5 nodalisation [26]. The following correlations are briefly described:

a. Spacer grid

The heat exchanger and core grids loss coefficients correlations are shown in Table 3.11.

Table 3.11 – The grids loss coefficients correlation

Spacer		$K = C_V \left(\frac{A_s}{A_v} \right)^2 \quad C_V = -7.65 \log_{10} Re + 49.0$	<p>Idelchik, I.E., Determination of the resistance coefficients during discharge through orifices, Gidrotekh. Stroit., no. 5, 31-36, 1953</p>
--------	---	--	---

Core grids loss coefficients

The core grids loss coefficients are shown in Table 3.12.

Table 3.12 – The core grids loss coefficients correlation

Loop power	9.8kW	15kW
A_v	0.001924	0.001924
A_s	0.000743	0.000743
Ref. Re(core)	34301	34418
C_v	14.305	14.294
K	2.134	2.132

Heat exchanger grids loss coefficients

The heat exchanger grids loss coefficients are shown in Table 3.13.

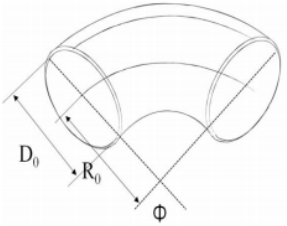
Table 3.13 – The heat exchanger grids loss coefficients correlation

Loop power	9.8kW	15kW
A_v	0.012588	0.012588
A_s	0.003422	0.003422
Ref. Re(HX)	10229	12882
C_v	18.325	17.559
K	1.354	1.297

b. Bend loss correlations

The bend loss coefficients are shown in Table 3.14.

Table 3.14 – The bend loss coefficients correlation

<p>45°, 90° elbow</p> 	$K = K_{Re} \cdot K_{loc} + K_{fr}$ $K_{fr} = 0.0175 \cdot \frac{R_0}{D_0} \cdot \phi \cdot \lambda$ $K_{loc} = A_1 \cdot B_1$	<p>Nippert, H., Über den Stromungsverlust in gekrümmten Kanälen, Forschungsarb. Geb. Ingenieurwes, no. 320, VDI, 1922, 85pp</p>																																																																																																																											
	<table border="1" style="width: 100%; text-align: center;"> <tr> <td>δ</td> <td>20.0</td> <td>30.0</td> <td>45.0</td> <td>60.0</td> <td>75.0</td> </tr> <tr> <td>A_1</td> <td>0.31</td> <td>0.45</td> <td>0.60</td> <td>0.78</td> <td>0.90</td> </tr> <tr> <td>δ</td> <td>90.0</td> <td>110.0</td> <td>130.0</td> <td>150.0</td> <td>180.0</td> </tr> <tr> <td>A_1</td> <td>1.00</td> <td>1.13</td> <td>1.20</td> <td>1.28</td> <td>1.40</td> </tr> </table> <table border="1" style="width: 100%; text-align: center;"> <tr> <td>R_0/D_0</td> <td>0.50</td> <td>0.60</td> <td>0.70</td> <td>0.80</td> <td>0.90</td> </tr> <tr> <td>B_1</td> <td>1.18</td> <td>0.77</td> <td>0.51</td> <td>0.37</td> <td>0.28</td> </tr> <tr> <td>R_0/D_0</td> <td>1.00</td> <td>1.25</td> <td>0.50</td> <td>2.00</td> <td>4.00</td> </tr> <tr> <td>B_1</td> <td>0.21</td> <td>0.19</td> <td>0.17</td> <td>0.15</td> <td>0.11</td> </tr> </table> <table border="1" style="width: 100%; text-align: center;"> <tr> <td colspan="7">Values of k_{Re}</td> </tr> <tr> <td rowspan="2">R_0/D_0</td> <td colspan="6">$Re \times 10^{-5}$</td> </tr> <tr> <td>0.1</td> <td>0.14</td> <td>0.2</td> <td>0.3</td> <td>0.4</td> <td>0.6</td> </tr> <tr> <td>0.5-0.55</td> <td>1.40</td> <td>1.33</td> <td>1.26</td> <td>1.19</td> <td>1.14</td> <td>1.09</td> </tr> <tr> <td>>0.55-0.70</td> <td>1.67</td> <td>1.58</td> <td>1.49</td> <td>1.40</td> <td>1.34</td> <td>1.26</td> </tr> <tr> <td>>0.70</td> <td>2.00</td> <td>1.89</td> <td>1.77</td> <td>1.64</td> <td>1.56</td> <td>1.46</td> </tr> <tr> <td rowspan="2">R_0/D_0</td> <td colspan="6">$Re \times 10^{-5}$</td> </tr> <tr> <td>0.8</td> <td>1.0</td> <td>1.4</td> <td>2.0</td> <td>3.0</td> <td>4.0</td> </tr> <tr> <td>0.5-0.55</td> <td>1.06</td> <td>1.04</td> <td>1.0</td> <td>1.0</td> <td>1.0</td> <td>1.0</td> </tr> <tr> <td>>0.55-0.70</td> <td>1.21</td> <td>1.19</td> <td>1.17</td> <td>1.14</td> <td>1.06</td> <td>1.0</td> </tr> <tr> <td>>0.70</td> <td>1.38</td> <td>1.30</td> <td>1.15</td> <td>1.02</td> <td>1.0</td> <td>1.0</td> </tr> </table>	δ	20.0	30.0	45.0	60.0	75.0	A_1	0.31	0.45	0.60	0.78	0.90	δ	90.0	110.0	130.0	150.0	180.0	A_1	1.00	1.13	1.20	1.28	1.40	R_0/D_0	0.50	0.60	0.70	0.80	0.90	B_1	1.18	0.77	0.51	0.37	0.28	R_0/D_0	1.00	1.25	0.50	2.00	4.00	B_1	0.21	0.19	0.17	0.15	0.11	Values of k_{Re}							R_0/D_0	$Re \times 10^{-5}$						0.1	0.14	0.2	0.3	0.4	0.6	0.5-0.55	1.40	1.33	1.26	1.19	1.14	1.09	>0.55-0.70	1.67	1.58	1.49	1.40	1.34	1.26	>0.70	2.00	1.89	1.77	1.64	1.56	1.46	R_0/D_0	$Re \times 10^{-5}$						0.8	1.0	1.4	2.0	3.0	4.0	0.5-0.55	1.06	1.04	1.0	1.0	1.0	1.0	>0.55-0.70	1.21	1.19	1.17	1.14	1.06	1.0	>0.70	1.38	1.30	1.15	1.02	1.0	1.0	
δ	20.0	30.0	45.0	60.0	75.0																																																																																																																								
A_1	0.31	0.45	0.60	0.78	0.90																																																																																																																								
δ	90.0	110.0	130.0	150.0	180.0																																																																																																																								
A_1	1.00	1.13	1.20	1.28	1.40																																																																																																																								
R_0/D_0	0.50	0.60	0.70	0.80	0.90																																																																																																																								
B_1	1.18	0.77	0.51	0.37	0.28																																																																																																																								
R_0/D_0	1.00	1.25	0.50	2.00	4.00																																																																																																																								
B_1	0.21	0.19	0.17	0.15	0.11																																																																																																																								
Values of k_{Re}																																																																																																																													
R_0/D_0	$Re \times 10^{-5}$																																																																																																																												
	0.1	0.14	0.2	0.3	0.4	0.6																																																																																																																							
0.5-0.55	1.40	1.33	1.26	1.19	1.14	1.09																																																																																																																							
>0.55-0.70	1.67	1.58	1.49	1.40	1.34	1.26																																																																																																																							
>0.70	2.00	1.89	1.77	1.64	1.56	1.46																																																																																																																							
R_0/D_0	$Re \times 10^{-5}$																																																																																																																												
	0.8	1.0	1.4	2.0	3.0	4.0																																																																																																																							
0.5-0.55	1.06	1.04	1.0	1.0	1.0	1.0																																																																																																																							
>0.55-0.70	1.21	1.19	1.17	1.14	1.06	1.0																																																																																																																							
>0.70	1.38	1.30	1.15	1.02	1.0	1.0																																																																																																																							
		<table border="1" style="width: 100%; text-align: center;"> <tr> <td colspan="10">Value of λ</td> </tr> <tr> <td rowspan="2">$\frac{\Delta}{D_h}$</td> <td colspan="9">Re</td> </tr> <tr> <td>3×10^3</td> <td>4×10^3</td> <td>6×10^3</td> <td>10^4</td> <td>2×10^4</td> <td>4×10^4</td> <td>6×10^4</td> <td>10^5</td> <td>2×10^5</td> </tr> <tr> <td>0.0008</td> <td>0.043</td> <td>0.040</td> <td>0.036</td> <td>0.032</td> <td>0.027</td> <td>0.024</td> <td>0.023</td> <td>0.022</td> <td>0.020</td> </tr> <tr> <td>0.0006</td> <td>0.046</td> <td>0.040</td> <td>0.036</td> <td>0.032</td> <td>0.027</td> <td>0.023</td> <td>0.022</td> <td>0.021</td> <td>0.018</td> </tr> <tr> <td>0.0004</td> <td>0.036</td> <td>0.040</td> <td>0.036</td> <td>0.032</td> <td>0.027</td> <td>0.023</td> <td>0.022</td> <td>0.020</td> <td>0.018</td> </tr> <tr> <td>0.0002</td> <td>0.036</td> <td>0.040</td> <td>0.036</td> <td>0.032</td> <td>0.027</td> <td>0.022</td> <td>0.021</td> <td>0.019</td> <td>0.017</td> </tr> <tr> <td>0.0001</td> <td>0.036</td> <td>0.040</td> <td>0.036</td> <td>0.032</td> <td>0.027</td> <td>0.022</td> <td>0.021</td> <td>0.019</td> <td>0.017</td> </tr> <tr> <td>0.00005</td> <td>0.036</td> <td>0.040</td> <td>0.036</td> <td>0.032</td> <td>0.027</td> <td>0.022</td> <td>0.021</td> <td>0.019</td> <td>0.016</td> </tr> <tr> <td>0.00001</td> <td>0.036</td> <td>0.040</td> <td>0.036</td> <td>0.032</td> <td>0.027</td> <td>0.022</td> <td>0.021</td> <td>0.019</td> <td>0.016</td> </tr> <tr> <td>0.000005</td> <td>0.036</td> <td>0.040</td> <td>0.036</td> <td>0.032</td> <td>0.027</td> <td>0.022</td> <td>0.021</td> <td>0.019</td> <td>0.016</td> </tr> </table>	Value of λ										$\frac{\Delta}{D_h}$	Re									3×10^3	4×10^3	6×10^3	10^4	2×10^4	4×10^4	6×10^4	10^5	2×10^5	0.0008	0.043	0.040	0.036	0.032	0.027	0.024	0.023	0.022	0.020	0.0006	0.046	0.040	0.036	0.032	0.027	0.023	0.022	0.021	0.018	0.0004	0.036	0.040	0.036	0.032	0.027	0.023	0.022	0.020	0.018	0.0002	0.036	0.040	0.036	0.032	0.027	0.022	0.021	0.019	0.017	0.0001	0.036	0.040	0.036	0.032	0.027	0.022	0.021	0.019	0.017	0.00005	0.036	0.040	0.036	0.032	0.027	0.022	0.021	0.019	0.016	0.00001	0.036	0.040	0.036	0.032	0.027	0.022	0.021	0.019	0.016	0.000005	0.036	0.040	0.036	0.032	0.027	0.022	0.021	0.019	0.016														
Value of λ																																																																																																																													
$\frac{\Delta}{D_h}$	Re																																																																																																																												
	3×10^3	4×10^3	6×10^3	10^4	2×10^4	4×10^4	6×10^4	10^5	2×10^5																																																																																																																				
0.0008	0.043	0.040	0.036	0.032	0.027	0.024	0.023	0.022	0.020																																																																																																																				
0.0006	0.046	0.040	0.036	0.032	0.027	0.023	0.022	0.021	0.018																																																																																																																				
0.0004	0.036	0.040	0.036	0.032	0.027	0.023	0.022	0.020	0.018																																																																																																																				
0.0002	0.036	0.040	0.036	0.032	0.027	0.022	0.021	0.019	0.017																																																																																																																				
0.0001	0.036	0.040	0.036	0.032	0.027	0.022	0.021	0.019	0.017																																																																																																																				
0.00005	0.036	0.040	0.036	0.032	0.027	0.022	0.021	0.019	0.016																																																																																																																				
0.00001	0.036	0.040	0.036	0.032	0.027	0.022	0.021	0.019	0.016																																																																																																																				
0.000005	0.036	0.040	0.036	0.032	0.027	0.022	0.021	0.019	0.016																																																																																																																				

▪ **90° elbow**

The resistance coefficients of the 90° elbows in the loop have been evaluated according to the bend loss coefficients correlation.

Table 3.15 – The 90° elbows loss coefficients correlation values

Loop power	9.8kW	15kW
K_{Re}	1.64	1.56
K_{loc}	0.16	0.17
K_{fr}	0.00093	0.00093
K	0.263	0.266

▪ 45° elbow

The resistance coefficients of the 45° elbows in the loop have been evaluated according to the bend loss coefficients correlation.

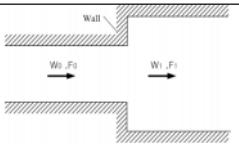
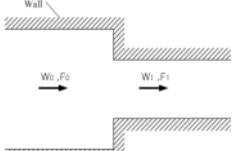
Table 3.16 – The 45° elbows loss coefficients correlation values

Loop power	9.8kW	15kW
K_{Re}	1.64	1.56
K_{loc}	0.16	0.17
K_{fr}	0.00093	0.00093
K	0.263	0.266

c. Sudden change in flow area

The area change loss coefficients relations in Table 3.17 had been used for all concerned flow situations:

Table 3.17 – The area change loss coefficients correlation

Sudden changes		$K_{SE} = \left(1 - \frac{F_0}{F_1}\right)^2$	Idelchik I.E., - Handbook of Hydraulic Resistance, 2nd edition, Hemisphere Pub. Corp., -1986
		$K_{SC} = 0.5 - 0.7 \cdot \left(\frac{F_1}{F_0}\right) + 0.2 \cdot \left(\frac{F_1}{F_0}\right)^2$	B.S.Massey, Mechanics of Fluids, D.Van Nostrand Co., New York, 1968, pp.217-219

where F_0 is always the inlet area and F_1 is always the outlet one.

The area change loss coefficients are used in several particular cases:

- Lower Plenum inlet

$$F_0 = 0.03885305 \text{ m}^2$$

$$F_1 = 0.032461205 \text{ m}^2$$

$$k = 0.038772$$

- Lower Plenum outlet

$$F_0 = 0.032461205 \text{ m}^2$$

$$F_1 = 0.000749812 \text{ m}^2$$

$$k = 0.483937$$

- Expansion Tank inlet

$$F_0 = 0.001924 \text{ m}^2$$

$$F_1 = 0.073301 \text{ m}^2$$

$$k = 0.948182$$

- Expansion Tank outlet

$$F_0 = 0.073301 \text{ m}^2$$

$$F_1 = 0.001924 \text{ m}^2$$

$$k = 0.481760$$

- Heat exchanger outlet

$$F_0 = 0.012588016 \text{ m}^2$$

$$F_1 = 0.001924422 \text{ m}^2$$

$$k = 0.397660$$

- Valve

Valve inlet:

$$F_0 = 0.002123717 \text{ m}^2$$

$$F_1 = 0.001075210 \text{ m}^2$$

$$k = 0.196864$$

Valve outlet:

$$F_0 = 0.001075 \text{ m}^2$$

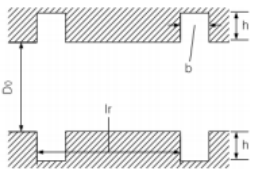
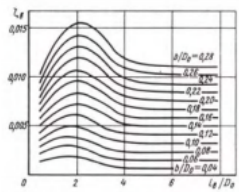
$$F_1 = 0.002124 \text{ m}^2$$

$$k = 0.243753$$

d. Gasket

The gasket loss coefficients are shown in Table 3.18.

Table 3.18 – The gasket loss coefficients correlation

<p>Gasket</p>		$l_r / D_0 \geq 4, K = 0.046 \frac{b}{D_0}$ $l_r / D_0 = 2, K = 0.059 \frac{b}{D_0}$ $l_r / D_0 \leq 4, K = f \left(\frac{b}{D_o}, \frac{l_r}{D_o} \right)$		<p>Trubenok, V.D., Determination of the coefficient of local resistances in tubes with rectangular annular recesses, in Applied Aerodynamics, pp.3-6, Kiev, 1980</p>
---------------	---	--	--	--

l_r : large enough

$$D_0 = 0.0495 \text{ m}^2$$

$$b = 0.0045 \text{ m}^2$$

$$K = 0.004182$$

e. Orifice

The orifice loss coefficients are shown in Table 3.19.

Table 3.19 – The orifice loss coefficients correlation

Orifice		$K = \left(1 + 0.707 \sqrt{1 - \frac{F_0}{F_1} - \frac{F_0}{F_1}} \right)^2 \left(\frac{F_1}{F_0} \right)^2$ $Re > 10^5$	Idelchik, I.E., Determination of the resistance coefficients during discharge through orifices, Gidrotekh. Stroit., no. 5, 31-36, 1953
---------	--	--	---

$F_0 = 0.000828 \text{ m}^2$

$F_1 = 0.001044 \text{ m}^2$

$k = 0.446016$

f. Tee

The tee loss coefficients are shown in Table 3.20.

Table 3.20 – The tee loss coefficients correlation

Tee- straight		Approximated as straight pipe																	
Tee- elbow		<table border="1"> <tr> <td>Wa/Wz</td> <td>0.0</td> <td>0.2</td> <td>0.4</td> </tr> <tr> <td>K</td> <td>0.98</td> <td>0.87</td> <td>0.90</td> </tr> <tr> <td>Wa/Wz</td> <td>0.6</td> <td>0.8</td> <td>1.0</td> </tr> <tr> <td>K</td> <td>0.98</td> <td>1.12</td> <td>1.29</td> </tr> </table>	Wa/Wz	0.0	0.2	0.4	K	0.98	0.87	0.90	Wa/Wz	0.6	0.8	1.0	K	0.98	1.12	1.29	Verein Deutscher Ingenieure, VDI- Wärmeatlas 3.0, Springer Verlag, Berlin Heidelberg, 2006
Wa/Wz	0.0	0.2	0.4																
K	0.98	0.87	0.90																
Wa/Wz	0.6	0.8	1.0																
K	0.98	1.12	1.29																

Where **W** is flow rate (m³/s), F is flow area (m²), D is diameter (m), R is radius (m), Φ is angle (degree), and Re is Reynolds number.

For core inlet, heat exchange inlet and outlet:

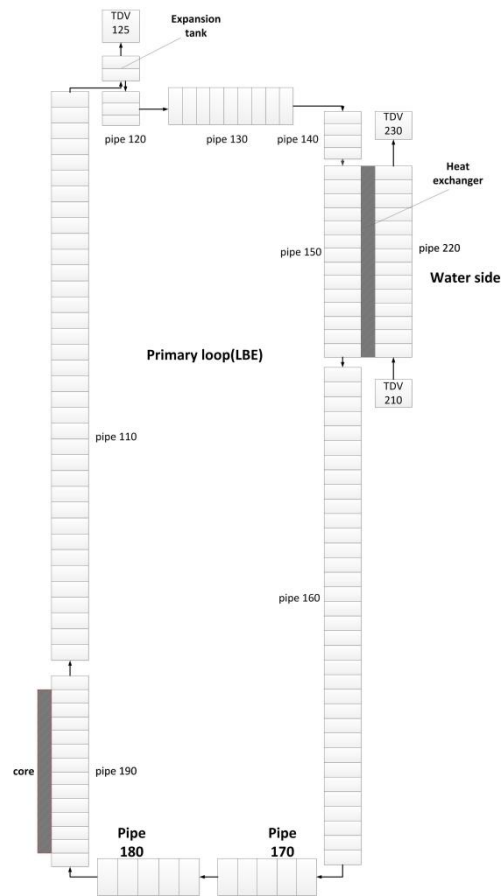
$W_a/W_z=1.0$

$K=1.29$

3.6.3 NACIE model for RELAP5

The natural circulation flow of NACIE NC loop was simulated by 1D with RELAP5 code. The RELAP5 nodalisation model of NACIE NC loop is shown in Figure 3.19.

Figure 3.19 – RELAP5 nodalisation model of NACIE NC loop



Core rod bundle and heat exchanger were simulated by heat structures. Friction loss coefficient were calculated by RELAP5 using the recommended correlation, which were shown in HELIOS model section 3.6.2. K-factor coefficients were calculated using the recommended correlations obtained in phase I on forced circulation tests. The HX secondary side was driven by boundary conditions. The second loop pump was simulated with time-dependent junctions. Seban-Shimazaki LBE heat transfer correlation was used as well.

Dittus-Boelter water heat transfer correlation was used in RELAP5 MOD4.0 code:

$$Nu=0.027*Re^{0.8}*Pr^{0.33}*(\mu/\mu_w)^{0.14}$$

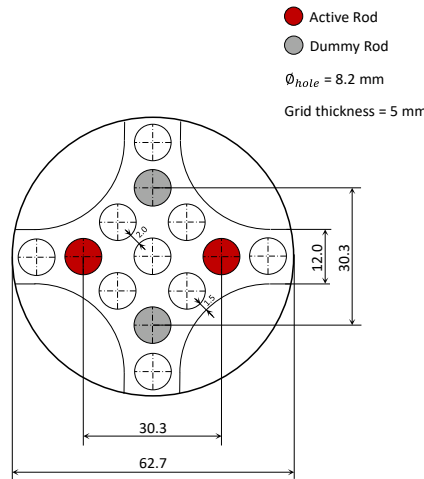
The thermal conductivity of the steel powder gap between the LBE and water side was set to 10% of AISI 304 metal thermal property. AISI 304 metal thermal properties are shown in Table 3.21.

Table 3.21 – AISI 304 thermal property table

Temp (K)	Th. Cond. (W/m-K)	Vol. heat cap. (J/m ³ -K)
293	15.16	3.5800E+6
373	16.37	3.8600E+6
473	17.31	4.1100E+6
573	19.2	4.3000E+6
673	20.5	4.4400E+6
773	21.77	4.5600E+6
873	22.95	4.6800E+6
973	24.12	4.8200E+6
1073	25.25	5.0300E+6
1573	30.8	7.5600E+6

The form loss coefficients are evaluated with Idelchik’s handbook correlations [26], in particular:

a. Spacer grid



The Rehme correlation [27] is used to evaluate the spacer grid pressure drop:

$$K = C_v \left(\frac{A_s}{A_v} \right)^2, \quad C_v = -7.65 \log_{10} Re + 49.0 \quad (3.6-7)$$

The k-value adopted in this case is: $k_{spacer} = 0.0681$.

b. Upper grid

In this case, the considerations made by Ansaldo has been taken into account as a good practice (see section 3.5.4). The k-value adopted in this case is: $k_{grid} = 0.697$.

c. 90° elbow

The resistance coefficients of the two 90° elbows at the downcomer inlet and outlet have been evaluated with Idelchik’s diagram 6.1 [26]. For both: $k_{elbow} = 0.3125$.

d. Tank to horizontal pipe

In this case, the entrance into a straight tube of cross section (Diag. 3.1 in [26]) combined with various inlet with facing baffle (Diag. 3.8 in [26]) are used: $k_{tank} = 0.5$.

e. *Sudden change in flow area*

The common formulations for sudden contraction and expansion are used for several concentrated pressure coefficients evaluation. The area change loss coefficients are used according to Table 3.17 in the section 0.

Area change due to the gas injection line: $k_{injection} = 0.0719$.

Area change from riser to E/V: $k_{injection} = 0.8909$.

f. *Tee*

The tee loss coefficients are used according to Table 3.20 in the section 0. $K=1.29$ is used.

References

- [1] NEA (2012), *Benchmarking of thermal-hydraulic loop models for lead-alloy-cooled advanced nuclear energy systems – Phase I: Isothermal forced convection case*, OECD, Paris.
- [2] S. Spelta (1981) – “Confrontation du model LEGO-REP 900 MW CP2 avec l’essai d’ilotage de St. Laurent B1 du 22/7/81”, SEPTEN (EDF), Internal Report TH-85-09 A (DF07).
- [3] S. Spelta (1985), *An application of the LEGO Packages to PWR Power Plant Modelling, Proc. of the Fifth International Conference on Mathematical Modelling*, Berkeley, California..
- [4] G. Garbossa, R. Mosca, S. Spelta, R. Cori, P. Cento (1989), “A model of Alto Lazio boiling water reactor using the Lego code: Nuclear Steam Supply System Simulation”, Seventh Power Plant Dynamics, Control and Testing Symposium, Knoxville, Tenn. (USA), May 15-17, 1989.
- [5] S. Spelta, G. Garbossa, P. Cento, L. Ferrari (1989), “A model of Alto Lazio boiling water reactor using the Lego code: Balance of Plant Simulation”, Seventh Power Plant Dynamics, Control and Testing Symposium, Knoxville, Tenn. (USA), May 15-17, 1989.
- [6] R. Cori, G. Migliavacca, S. Spelta (1997),– “A new approach to LEGO steady state calculation for power plants dynamic models”, 15th IMACS World Congress on Scientific Computation Modeling Applied Mathematics, Berlin, August 1997.
- [7] V. Casamassima, G. Garbossa, and G. Migliavacca (2002), “A Modular Approach to Desalination Plants Modeling – Modeling, Identification and Control (MIC 2002)”, Innsbruck, Austria, February 2002.
- [8] NEA (2007), *Handbook on Lead-bismuth Eutectic Alloy and Lead Properties, Materials Compatibility, Thermal-hydraulics and Technologies*, OECD, Paris.
- [9] Dow Chemical Company (1996), “DOWTHERM® RP Heat Transfer Fluid”, *Product Technical Data*, Nov 1996.
- [10] K.C. Mills, Yuku Su, Zushu Li, R. F. Brooks (2004), Equations for the calculation of the thermo-physical properties of stainless steel, ISIJ international, vol. 44 (2004), N° 10, pp. 1661-1668.
- [11] EMERSON – FISHER (2005), *Control Valve Handbook*, 4th edition, 2005.
- [12] ISA-75.01.01-2007 (IEC 60534-2-1 Mod), Flow Equations for Sizing Control Valves, 2007.
- [13] O. Biceroglu, A. S. Mujumdar, et al. (1976), Thermal conductivity of sintered metal powders at room temperature, Letters in heat and mass transfer, vol. 3, pp.183-192, 1976.
- [14] B.D. Turland, G. P. Dobson, E. J. Allen et al. (1999), “Models for melt-vessel interactions”, Report produced for the Health and Safety Executive and European Commission DG XII AEA Technology (UK), AEAT-4544, November 1999.
- [15] Idelchik I.E, Malyavskaya G.R., Martynenko O.G., Fried, E. (1986), – *Handbook of Hydraulic Resistance*, 2nd edition, Hemisphere Pub. Corp.

- [16] D. A. Young (1977), "A Soft Sphere Model for Liquid Metals," Lawrence Livermore Laboratory, UCRL-52352, November 8.
- [17] P. Meloni et al. (2001), "Implementation and Preliminary Verification of the RELAP5/PARCS Code for Pb-Bi Cooled Subcritical System", Proc. of the International Conference on Accelerator, Applications AccApp01, Nuclear American Society, Reno, United States.
- [18] P. Meloni et al. (2002), "Natural circulation of Lead-Bismuth in a one-dimensional loop: experiments and code predictions", Proc. of the International Conference ICONE-10, Arlington, United States.
- [19] P. Meloni et al. (2004), "Investigation of RELAP5 Capability to simulate the LBE Cooling System Thermal-Hydraulic", Proc. of the 8th Information Exchange Meeting on Transmutation and Partitioning (IEMTP), Las Vegas, United States.
- [20] P. Meloni et al. (2008), "Verification of the RELAP5 Code against the MEGAIE Irradiation Experiment", presented at the 10th Information Exchange Meeting on Transmutation and Partitioning (IEMTP), 6-10 October 2008, Mito, Japan.
- [21] G. Bandini, M. Polidori, P. Meloni, M. Tarantino, I. Di Piazza (2015), "RELAP5 and SIMMER-III code assessment on CIRCE decay heat removal experiments", Nuclear Engineering and Design 281 (2015) 39–50. DOI:10.1016/j.nucengdes.2014.11.005, 2015. ISSN: 0029-5493.
- [22] G. Bandini, P. Meloni, M. Polidori (2007), "T/H and transient analyses to confirm EFIT preliminary design", Journal of Nuclear Materials, 376 (2008), 405-408. Proceeding of IV International Workshop on Materials for HLM Cooled Reactors and Related Technologies Rome, May 21-23, 2007. DOI:10.1016/j.jnucmat.2008.02.081. ISSN: 0022-3115.
- [23] G. Bandini, P. Meloni, M. Polidori, M. Casamirra, F. Castiglia, M. Giardina (2008), "Decay Heat Removal and Transient Analysis in Accidental Conditions in the EFIT Reactor", Science and Technology of Nuclear Installations, Volume 2008 (2008). Proceeding of International Conference New Energy for New Europe 2007, Portoroz, Slovenia, September 10-13, 2007. DOI:10.1155/2008/681847. ISSN: 1687-6083.
- [24] G. Bandini, P. Meloni, M. Polidori (2009), "Thermal-Hydraulics Analyses of ELSY Lead Fast Reactor with Open Square Core Option", Nuclear Engineering and Design, 241 (2011) 1165–1171. Proceedings of the International Conference New Energy for New Europe 2009, Bled, Slovenia, September 14-17, 2009. DOI:10.1016/j.nucengdes.2010.04.034. ISSN: 0029-5493.
- [25] G. Bandini, et al. (2013), "Safety Analysis Results of Representative DEC Accidental Transients for the ALFRED Reactor", Fast Reactors and Related Fuel Cycles: Safe Technologies and Sustainable Scenarios (FR13) p. CD Track 3 pages 170-179, ISBN: 978-92-0-104114-2.
- [26] I.E. Idelchik (2003), *Handbook of Hydraulic Resistance*, third Edition, Published by Jaico Publishing House.
- [27] K. Rehme (1973), "Pressure drop correlations for fuel elements spacers", *Nuclear Technology*, 43:17, 1973.
- [28] Korea Atomic Energy Research Institute (KAERI) (2006), *MARS Code Manual Volume I – Code Structure, System Models and Solution Methods*, Daejeon, Korea.
- [29] D. Balestri (2013), "Benchmarking Thermal-Hydraulic Analysis Code Relap5/Mod3.2.2 Beta For Lead-Bismuth Eutectic Alloy On Nacie Facility Tests Of Natural And Gas Enhanced Circulation", Master Thesis, Politecnico di Milano.
- [30] RELAP5/MOD3 CODE MANUAL, "RELAP5/MOD3 CODE MANUAL", SCIENTECH, Inc. Rockville, Maryland, Idaho Falls, Idaho.
- [31] I. E. Idelchik et al. (1987), "Handbook of Hydraulic resistance", Second edition, Erwin Fried, General Electric, Schenectady, New York.
- [32] R. Lobello, A. Alemberti, "Technical report – RELAP5 Code Modifications for ADS Demonstration Facility Simulation", Ansaldo Nucleare, Doc. ADS 1 TRIX 0243.

- [33] A. Mangialardo, "Design and CFD analysis of a lead jet pump for a GEN IV LFR Nuclear Power Plant", Università di Genova, Chapter 6.

4. Experiments and results

4.1 HELIOS

4.1.1 Setup and test procedure

The HELIOS facility has a lead-bismuth eutectic (LBE) storage tank where the LBE can be drained from the main loop when it is not in operation. Before the filling of the loop with LBE, the outer surface of the loop piping was heated to about 200°C, which is higher than the melting point of LBE (125°C) with adequate margin. When pre-heating is completed, the loop is filled with LBE by pressure; argon or 4% hydrogen with argon balance gas is injected in the storage tank and the gas pushes up LBE into the main loop.

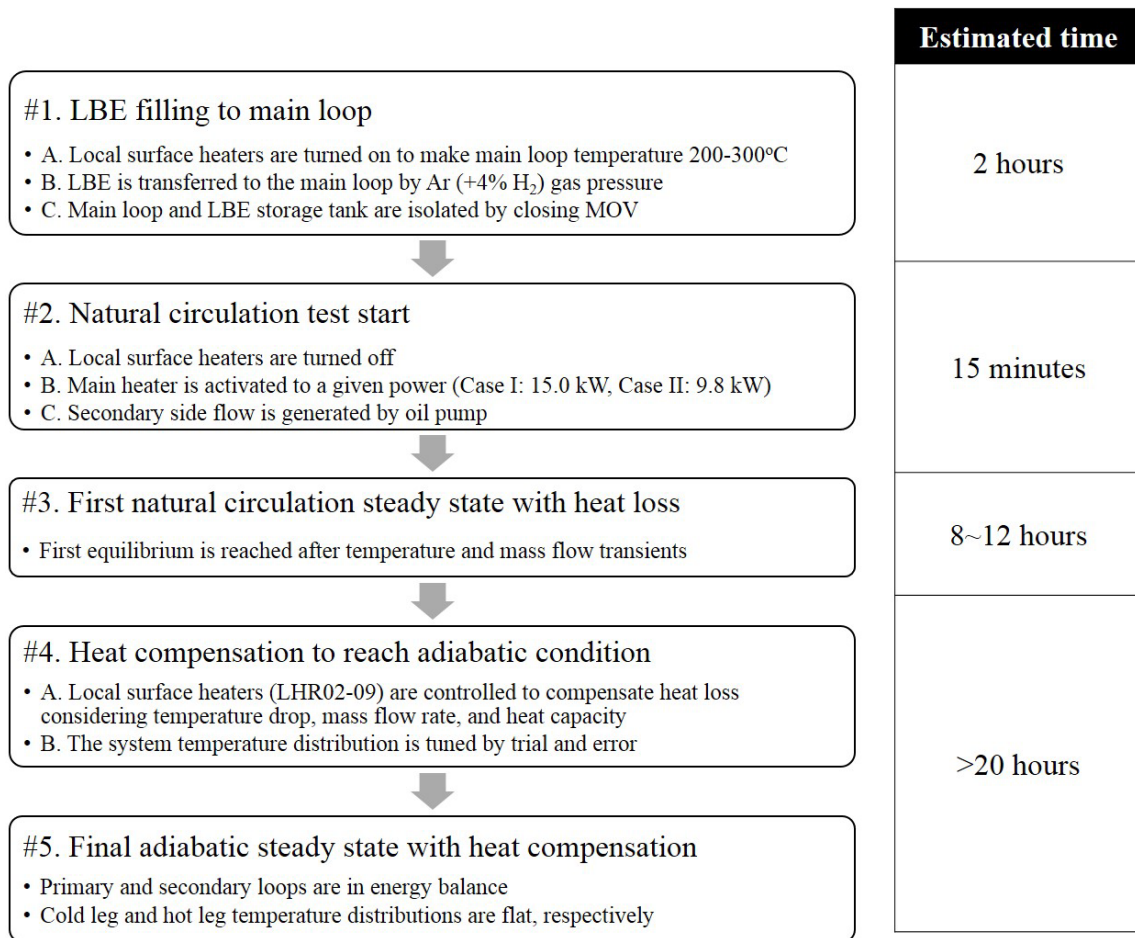
After LBE filling, the storage tank and main loop are isolated by closing the motor-operated valve in the connecting pipe. The gate valve, positioned at the inlet branch of the mechanical pump, is closed and the pump bypass valve is opened in order to make the natural circulation flow path.

All local surface heaters are turned off, besides, the main heater is activated to a given core power correspondent to the benchmark specification. In the meantime, the secondary side flow pump begins to circulate the diathermic oil. The energy produced in the core (heat source) is now removed in the heat exchanger (heat sink), starting the natural circulation flow. A temperature transient lasts until the system reaches the new equilibrium state.

Following the transient, reached without turning on the local surface heaters, the first steady state is obtained. In this condition, the thermocouples along the loop show some temperature drops due to heat loss through the outer surface of pipes and vessels. The local surface heaters are activated one by one after rough estimation of heat loss using a measured LBE flow rate, temperature drop and heat capacity to compensate heat loss section by section. Controlling the local surface heaters with a trial-and-error approach, the final steady state is reached when the primary loop and the secondary loop results in energy balance in terms of heat transfer, and when the temperature distributions in hot leg and cold leg are respectively in close ranges of few °C.

The experiment procedure for non-isothermal natural circulation tests is summarised in Figure 4.1.

Figure 4.1 – Test procedure for HELIOS non-isothermal natural circulation test campaigns



4.1.2 Instrumentation

There are three types of instrumentation systems in HELIOS: an orifice flow metre, the differential pressure transducers (Rosemount 3051 CD3A) and k-type thermocouples, as depicted in Figure 4.2. Differential pressure transducers are installed over three regions to measure pressure loss in each region: the inlet and outlet of mock-up core, the upstream and downstream regions of the orifice, and a combined region, which covers from the downstream of orifice to the mock-up core outlet. They show total measurement error as ±0.065% of 0.8 bar. These regions are expected to have large pressure losses compared to other parts. The mock-up core has the largest pressure loss due to three spacers holding heater rods rigidly. Detailed design of the spacer can be seen in the Phase I report [1]. The orifice also gives comparatively large pressure losses associated with sudden area change so that mass flow rate of LBE can be obtained even in low flow rate conditions exerted by natural circulation.

Thermocouples are installed along the loop through the piping to measure fluid temperature distribution and their error is about ±1.0 K. In Table 4.1, thermocouple locations are described with accumulated length, which is defined by the distance from the mock-up core inlet to a certain point along the LBE flow path.

Figure 4.2 – Position of orifice flow metre and thermocouples in HELIOS

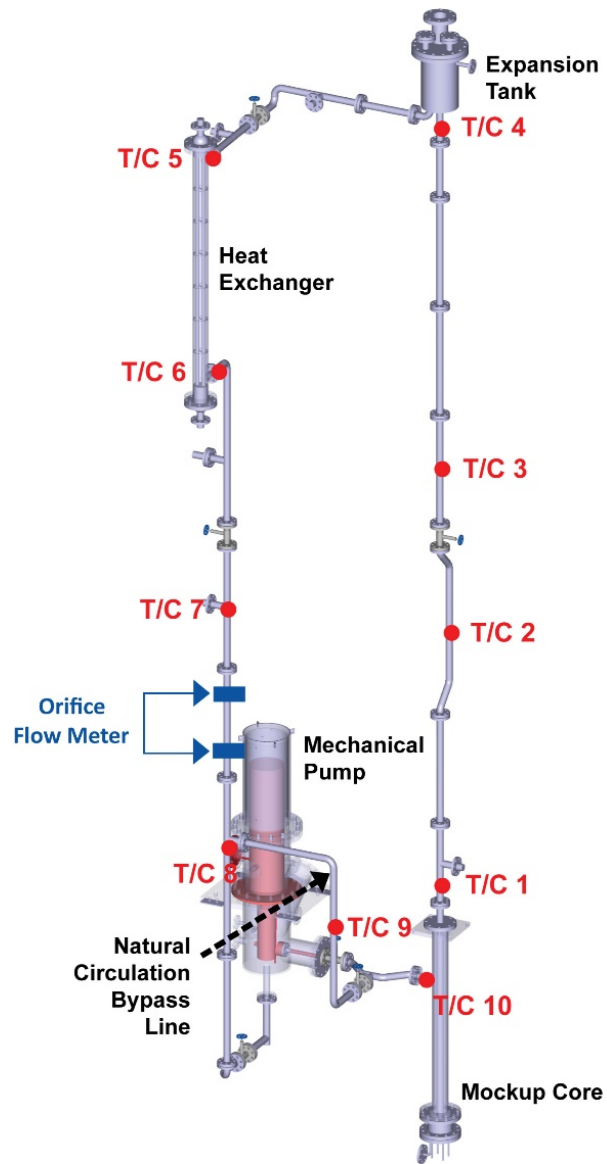


Table 4.1 – Thermocouple locations in HELIOS in terms of accumulated length

No.	Description/position	Accumulated Length (m)
T/C 1	Mock-up core inlet	0.00
T/C 2	Mock-up core outlet	3.72
T/C 3	Along hot leg (1)	6.54
T/C 4	Along hot leg (2)	9.47
T/C 5	Expansion tank inlet	10.88
T/C 6	Heat exchanger inlet	14.32
T/C 7	Heat exchanger outlet	16.52
T/C 8	Along cold leg (1)	19.23
T/C 9	Along cold leg (2)	21.42
T/C 10	Along cold leg (3); in natural circulation bypass	22.65

4.1.3 Benchmark approach

In order to evaluate and predict natural circulation phenomena of a hydraulic system, information on heat source, heat sink and component geometries, other system descriptions and the hydraulic resistance are necessary. Fixed parameters such as mock-up core power, secondary loop conditions and the geometries of the loop are provided to the Working Group participants. For the pressure drop prediction in each section, it is recommended to follow the best practice guideline given in the first phase, isothermal forced convection benchmark [1].

For the benchmark activities, each participant receives benchmark specifications for two different natural circulation cases. Three conditions are given explicitly: mock-up core power rating, secondary loop oil inlet temperature and secondary side oil mass flow rate. From these conditions, other parameters such as temperature distribution along the primary loop, mass flow rate of LBE, oil side outlet temperature and so on, can be calculated using own (or commercialised) system codes.

After completing the calculation from the participants, a table is filled out with hydraulic loss coefficients and pressure drop values in each section and temperature distributions and mass flow rates as well. These tables are for a thorough investigation and comparison between participants' calculation to minimise any unpredictable errors expected to be given in input preparation. Pressure loss comparison table for the HELIOS natural circulation cases are provided in Appendix 2.

4.1.4 Benchmark specifications and test results

Table 4.2 provides two natural circulation test conditions on the non-isothermal natural circulation test with the HELIOS facility. Two specific core power ratings are selected.

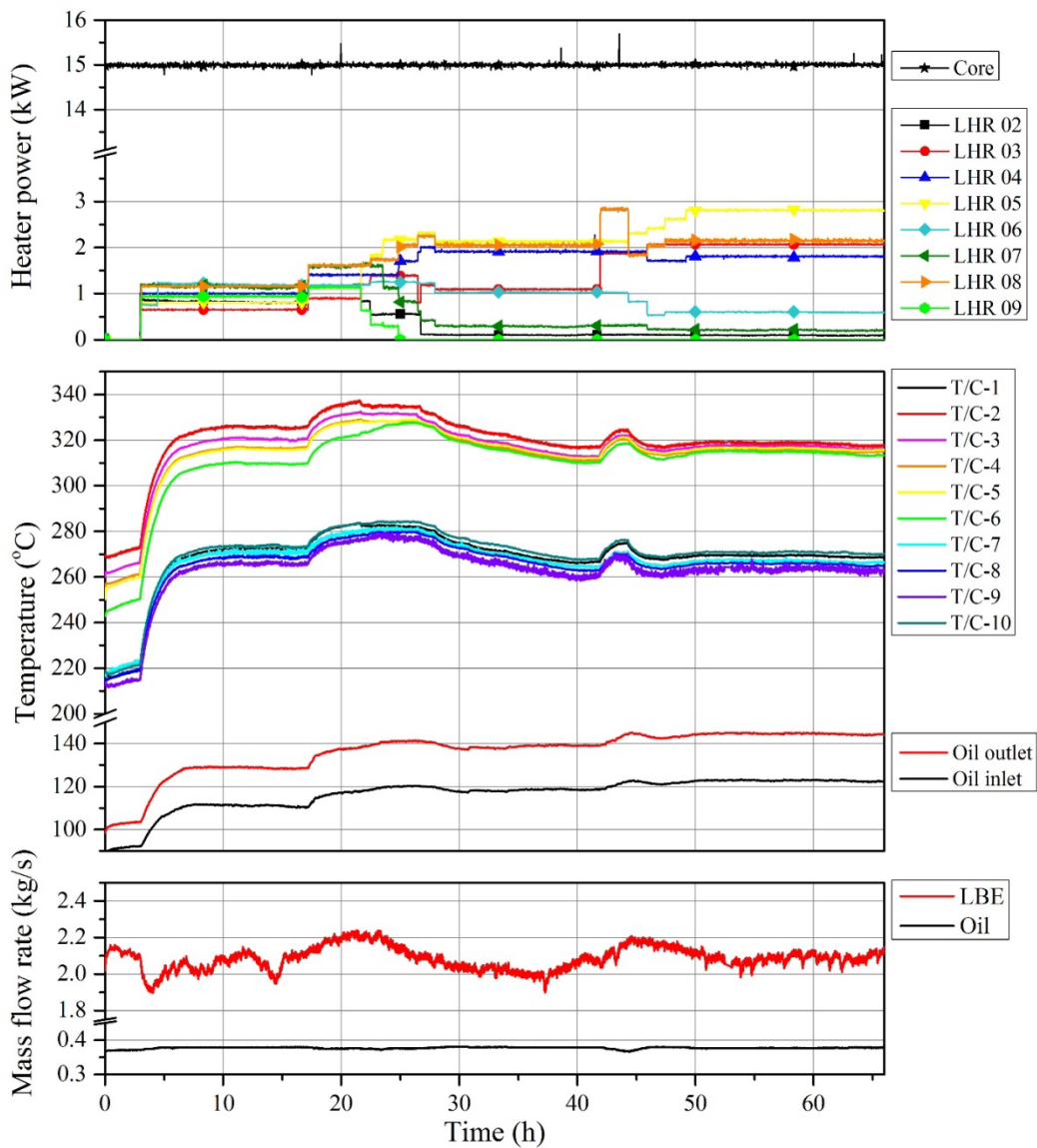
Table 4.2 – Case definition for HELIOS natural circulation tests

Case no.	Core power (kW)
Case I	15.0
Case II	9.8

- Case I: 15.0 kW core power

The first case of the HELIOS natural circulation tests was performed for about 70 hours. At first, no heat compensation was performed to the loop and by trial-and-error approach, electric power given to local surface heaters was changed to meet the balance of energy transferred to mock-up core and energy removed from the secondary loop. Temperature distributions along hot leg and cold leg were also of interest, so that they were flat in each leg. The system finally reached heat-compensated steady state after 50 hours, but still there was a temperature swing of the whole system expected to be given by ambient temperature change for a day. The full history of finding the adiabatic condition for Case I is depicted in Figure 4.3: electric power ratings given to the mock-up core and changes to local heaters, temperature variations, and mass flow rate changes, from top to bottom, respectively.

Figure 4.3 – Case I (15.0 kW) results: variation of power given to main loop, temperature distributions and mass flow rates of the HELIOS



Considering ambient temperature fluctuation in day and night, the actual steady state was designated as averaged data from 60 hours to 66 hours. In this regard, the steady-state temperature distributions for hot leg and cold leg lay in 5°C ranges, respectively. The data utilised for the steady-state natural circulation test results are given in Figure 4.4 and Figure 4.5: steady-state temperature distributions, and steady-state mass flow rates, respectively.

Figure 4.4 – Case I (15.0 kW) steady-state results: HELIOS temperature distributions

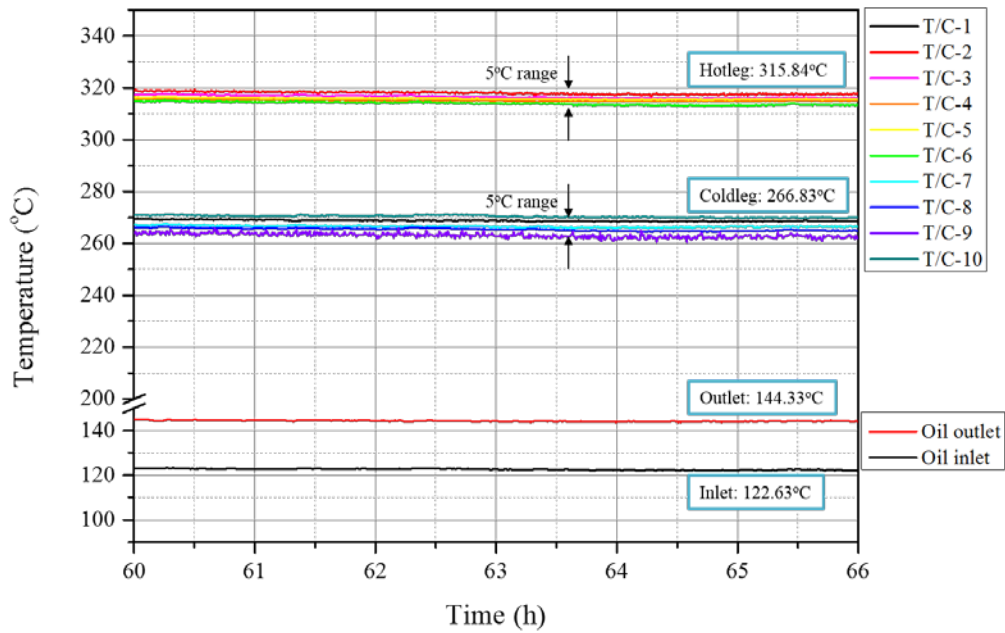
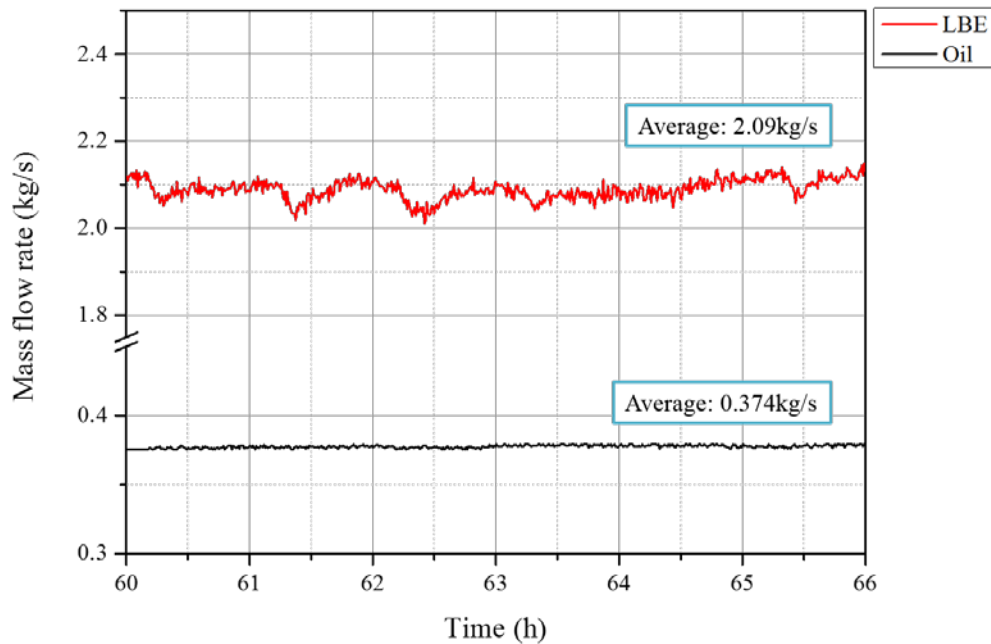


Figure 4.5 – Case I (15.0 kW) steady-state results: HELIOS mass flow rates



The primary loop temperature distribution, which is also a benchmark target, is depicted as Figure 4.6 with accumulated length, defined by the flow path length starting from the mock-up core inlet where thermocouple T/C-1 is located. The averaged, steady-state test results for Case I is summarised in Table 4.3. Hot leg average temperature is a mean value of temperatures measured by T/C-2 to T/C-6, and cold leg average temperature is averaged with T/C-7 to T/C-10 and T/C-1.

Figure 4.6 – Case I (15.0 kW) steady-state results: HELIOS primary loop temperature distribution

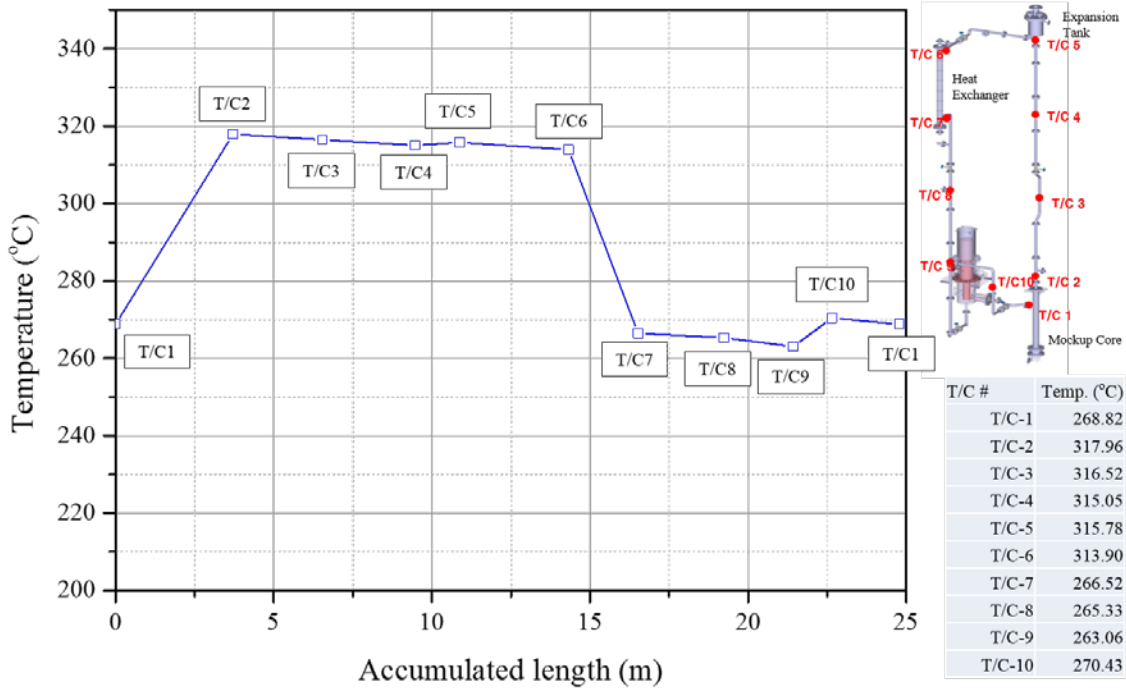


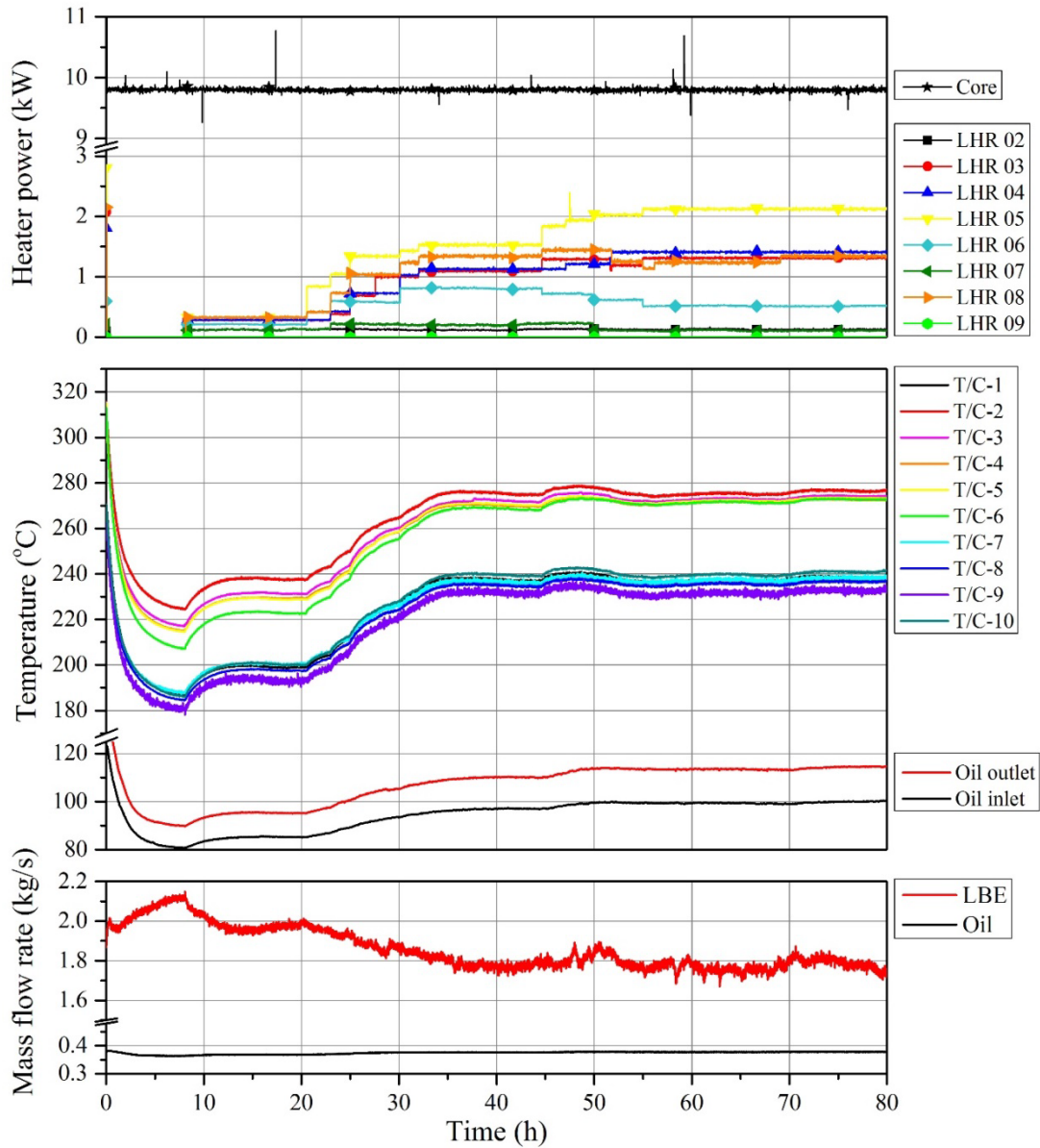
Table 4.3 –Averaged steady-state test results for Case I: 15.0 kW core power

Core power (kW)	15.0
Hot leg average temperature (°C)	315.84
Cold leg average temperature (°C)	266.83
LBE average mass flow rate (kg/s)	2.09
Oil side inlet average temperature (°C)	122.63
Oil side outlet average temperature (°C)	144.33
Oil average mass flow rate (kg/s)	0.374

- Case II: 9.8 kW core power

The second case of the HELIOS natural circulation tests was performed for about 80 hours, once the first case was terminated. As found in the first case, no heat compensation was made from the beginning and the system finally reached its adiabatic, steady state through the same trial-and-error approach. Results of Case II are described in Figure 4.7: power given to the mock-up core and local surface heaters, temperature variations and mass flow rate changes, from top to bottom, respectively. Note that temperatures and mass flow rates are decreased at the beginning because the test was continued from the previous condition, as described in Case I.

Figure 4.7 – Case II (9.8 kW) results: variation of power given to main loop, temperature distributions and mass flow rates of the HELIOS



Due to ambient temperature change, for the same reason of Case I, the actual steady state was designated as averaged data from 70 hours to 76 hours. In this regard, the steady-state temperature distributions for hot leg and cold leg ranged in 5°C and 7°C, respectively, because cold leg temperature flattening was more difficult in this case due to local surface heater arrangements and their power ratings. The steady-state test results are shown in Figure 4.8 and Figure 4.9: steady-state temperature distributions, and steady-state mass flow rates, respectively.

Figure 4.8 – Case II (9.8 kW) steady-state results: HELIOS temperature distributions

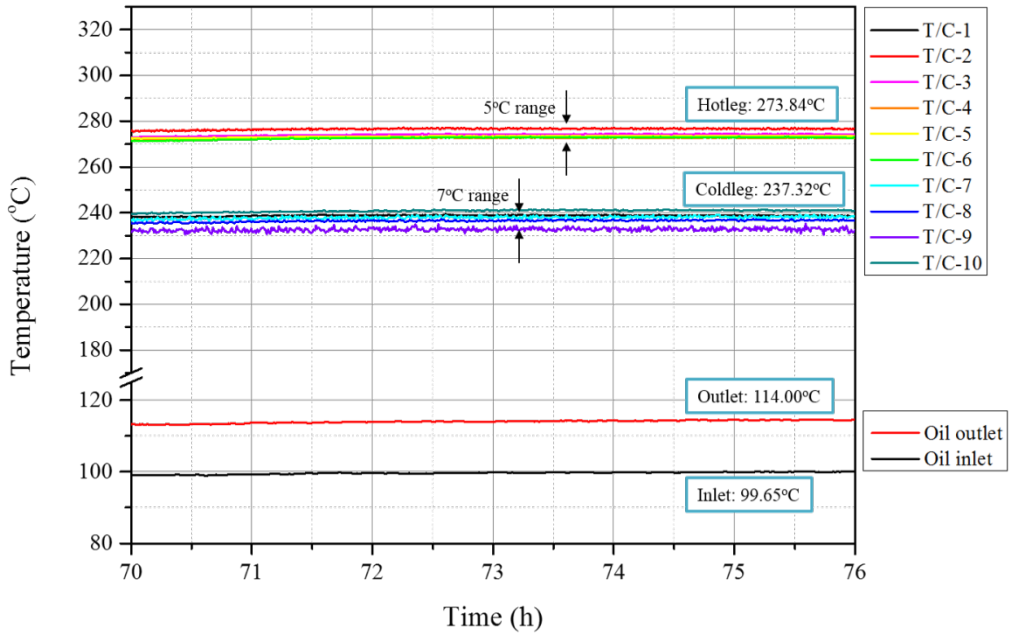
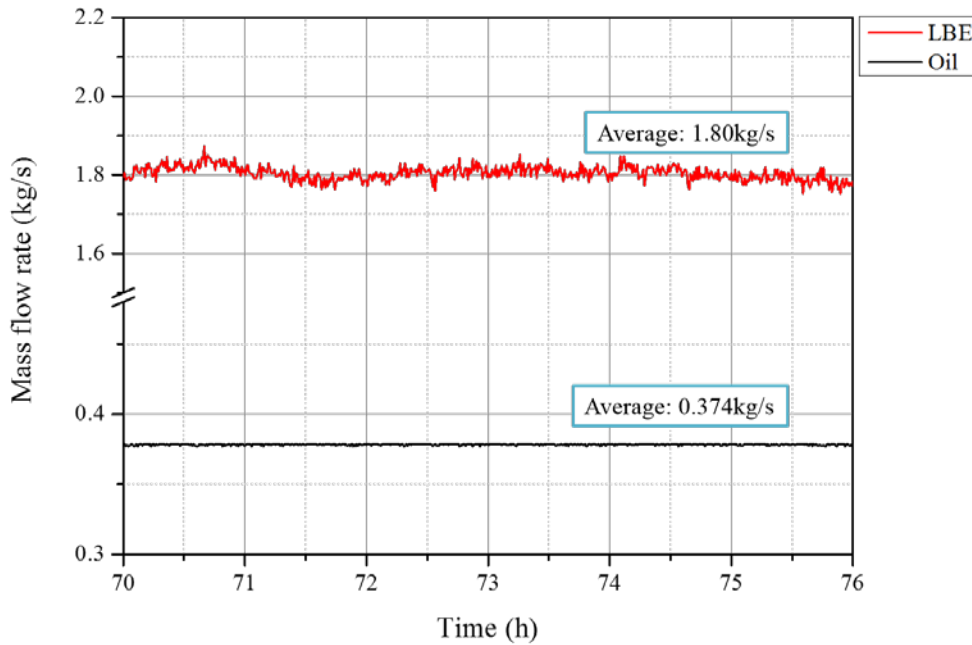


Figure 4.9 – Case II (9.8 kW) steady-state results: HELIOS mass flow rates



In Figure 4.10, the primary loop temperature distribution is given in terms of the accumulated length, and subsequently in Table 4.4, the averaged, steady-state test results for Case I is summarised.

Figure 4.10 – Case II (9.8 kW) steady-state results: HELIOS primary loop temperature distribution

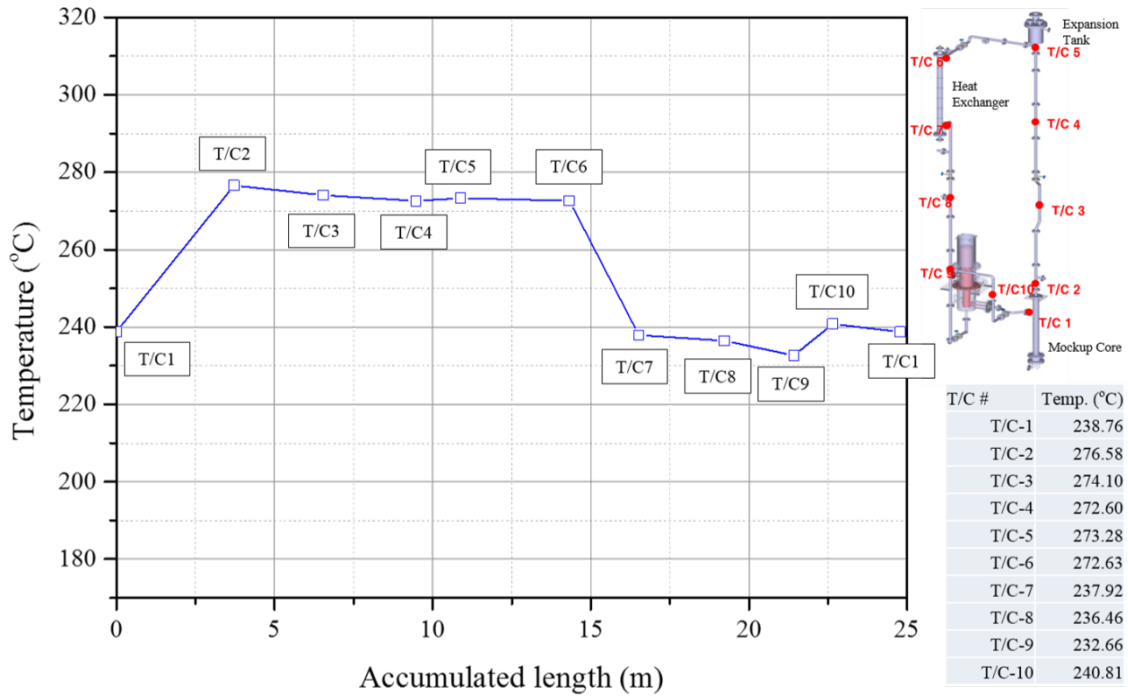


Table 4.4 –Averaged steady-state test results for Case II: 9.8 kW core power

Core power (kW)	9.8
Hot leg average temperature (°C)	273.84
Cold leg average temperature (°C)	237.32
LBE average mass flow rate (kg/s)	1.80
Oil side inlet average temperature (°C)	99.65
Oil side outlet average temperature (°C)	114.00
Oil average mass flow rate (kg/s)	0.374

- Benchmark specifications

Following the benchmark approach, only the values for mock-up core power rating, secondary side oil inlet temperature and oil mass flow rate are given to the participants, for both Case I and Case II. The benchmark specification are summarised in Table 4.3 and Table 4.4. In addition the MARS-LBE calculations performed before the benchmark specification were distributed and showed that the temperature distribution of the primary loop was underestimated by about 25°C in Case II. Consequently, three potential causes were considered in order to understand the causes of this discrepancy:

1. MARS-LBE calculation: a code-to-code comparison between the participants’ results was carried out for both cases. Good agreement but there was found among predictions given by the participants and it was concluded that the temperature discrepancy was not due to modelling.

2. Convective heat transfer coefficient of oil side: possibility possible explanation could be that oil flow condition was out of range in using the Sieder-Tate's correlation. In Case II, the secondary oil was under low turbulent regime ($Re \sim 6\ 000$), whereas it is recommended to use at least $Re > 10\ 000$ for high turbulent flow regime. However, the disagreement in the Case II was simply too large to be caused by the moderate Reynolds number deviation from the limit. So the Working Group did not accept this cause.
3. Flowmeter calibration: the secondary loop flow measurement, a turbine flowmeter has been used. It is known that a turbine flowmeter can give incorrect results when flow rate is low; this error misleads to an error in the calculation of the power removed by the secondary side. To make sure that the flowmeter caused incorrect measurement, the HELIOS operators tried to reproduce the calibration curve under varying flow rates, but unfortunately, flow rate cannot be measured by the flowmeter due to its failure. The Working Group concluded that the conditions given in Table 4.4 for the Case II could not be reproduced, even though the flowmeter was repaired.

i Consequently, the benchmark specifications were modified for Case II by changing the oil mass flow rate so that only the primary loop temperature distribution and LBE mass flow rate are asked to be benchmarked. On the other hand, the focus of the present work remains the simulation of the LBE under natural circulation condition; therefore, as long as the correct power removal is ensured, the benchmark results will be considered consistent. Through an energy balance in the heat exchanger (HX) secondary side, the oil mass flow rate of Case II is modified to 0.27 kg/s from 0.374 kg/s. The finalised benchmark specifications are shown in Table 4.5. Note that the other conditions are not amended for both cases.

Table 4.5 – Modified benchmark specifications for HELIOS natural circulation tests

Case no.	Core power (kW)	Oil inlet temperature (°C)	Oil mass flow rate (kg/s)
Case I	15.0	122.63	0.374
Case II	9.8	99.65	0.27*

* Oil mass flow rate of Case II is modified from the experimental results to benchmark LBE side properly.

4.2 NACIE

4.2.1 Experimental campaign

The experimental activity performed on the NACIE facility includes several tests concerning natural circulation (NC) and gas enhanced circulation (GEC). Each test has been performed with only one pin activated inside the test section, with a nominal power of 22.5 kW.

In the following Table 4.6, the test matrix is reported highlighting the flow regime investigated, the gas injection flow rate in the case of gas enhanced circulation test (G_{lift}), the total power supplied to the system through the heating section as well as the ramp time imposed at the power supply system to get the chosen values. Finally, the LBE average temperature in the loop has been indicated (T_{av}). Different T_{av} are obtained imposing different boundary conditions on the secondary side of the HX, in terms of water flow rate as well as water inlet temperature. The range of LBE average temperature considered in the experimental campaign is 200-360°C. The typical time-scale for a single test is a few hours.

Table 4.6 – Test matrix of the experimental campaign in the NACIE loop

ID	T_{av} [°C]	Power %	Power [kW]	Ramp t [min]	Heat Sink	Glift [NI/min]	Transition NC to GLC	Transition GLC to NC
201	200-250	50	9.5	5	YES	0	NO	NO
203	200-250	50	9.5	5	YES	5	NO	YES
204	200-250	50	9.5	5	YES	2,4,5,6,8, 10,6,5,4,2	YES	NO
206	200-250	0	0	-	NO	2,4,5,6,8, 10,6,5,4,3	NO	NO
301	300-350	100	21.5	5	YES	0	NO	NO
303	300-350	100	21.5	5	YES	5	NO	YES
304	300-350	100	21.5	5	YES	2,4,5,6,8, 10,6,5,4,2	YES	NO
305	300-350	50	9.5	5	YES	0	NO	NO
306	300-350	0	0	-	NO	2,4,5,6,8, 10,6,5,4,2	NO	NO
406	350-360	25	3.5	5	NO	2,4,5,6,8, 10,6,5,4,2	NO	NO

Keeping in mind that the flow rate measured by new inductive flowmeter MP101 can be compared with the thermal balance through the test section only when the thermo-fluid-dynamic equilibrium is reached, the main achievements obtained with the experimental campaign are as follows:

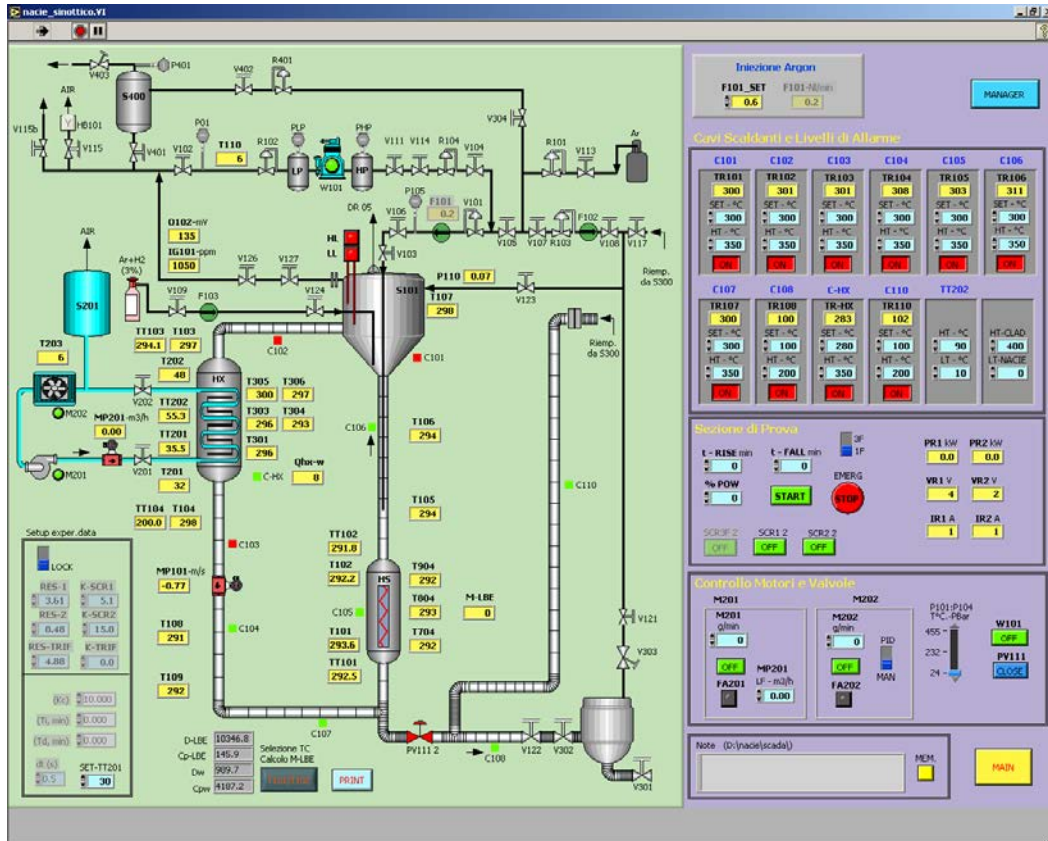
- The results confirm that the induction flow meter technique is valid and accurate for high mass flow rate, in the range 5-20 kg/s.
- The uncertainty of the measurement is of the order of ~1 kg/s, and thus it can be relevant at the low mass flow rates, but it is satisfactory in the high mass flow rate range 5-20 kg/s.
- The reasons of such an uncertainty are clear and are tied to the diameter of the pipe in which the induction effect is measured, i.e. 2.5" diameter pipe.
- Starting from this experience, a new induction flow meter mounted on a smaller tube (20 mm diameter pipe) is going to be manufactured to be accurate in the range 0-5 kg/s and it will be mounted in the upgrade of the facility NACIE, called NACIE-UP.

- Another weak point is the calibration procedure, and this point will be addressed by installing ball valves in the facility upgrade NACIE-UP in order to set the zero point more accurately.

4.2.2 Instrumentation

In the following Figure 4.11, a view of the NACIE facility synoptic is reported. Here can be appreciated the entire NACIE layout and the position of the instrumentation. A more detailed piping and instrumentation (P&I) scheme is attached in Appendix A.

Figure 4.11 – Synoptic view of NACIE facility

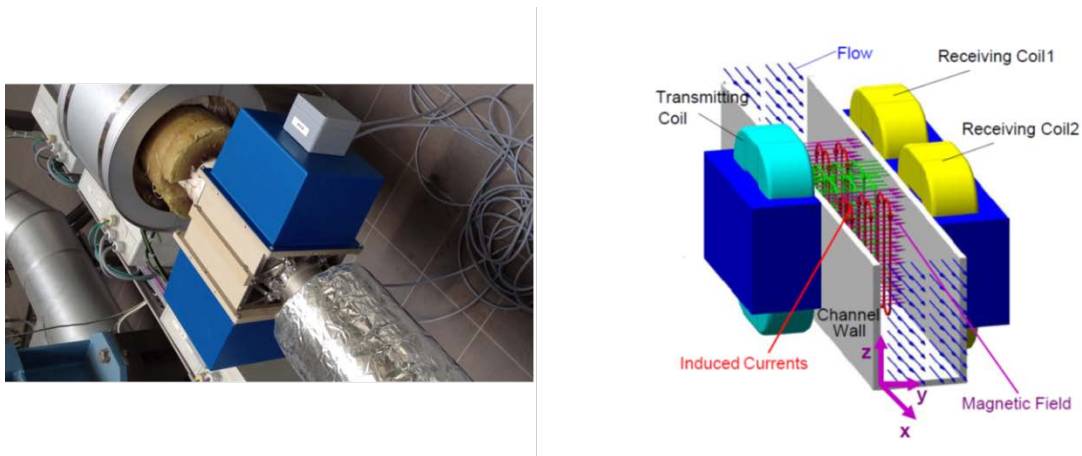


- T201 HX water inlet temperature
- T202 HX water outlet temperature
- VR2 rod bundle tension [V]

4.2.3 The induction flowmeter MP101

A non-intrusive induction flow meter has been developed through a collaboration with the Helmholtz-Zentrum Dresden-Rossendorf (HZDR; Dresden, Germany), and it was designed and realised by Systemanalyse & Automatisierungsservice GmbH (SAAS GmbH; Bannewitz, Allemagne). The induction flow meter was installed in the NACIE facility in July 2012 and was calibrated later on. A sketch of the induction flow meter is reported in Figure 4.12. The flow meter is mounted directly on the 2.5” primary pipe.

Figure 4.12 – Sketch of the Induction flow meter MP101 installed in the NACIE primary loop



Due to the absence of a valve in the NACIE loop, the calibration procedure was repeated several times to determine the zero point correctly. For the calibration, a thermal balance mass flow rate (TBMFR) across the bundle was used as reference:

$$\dot{m} = \frac{Q}{c_p \Delta T} \tag{1}$$

where ΔT is the temperature drop across the bundle, Q is the bundle power and c_p is the LBE specific heat. The calculated quantity computed according to Eq. (1) is a correct evaluation of the mass flow rate when the system has reached the stationary condition. During the thermal transient, a large imbalance can occur and the reference value expressed by Eq. (1) must not be considered correct. Without a valve, it was found that the best way to carry out a two-point calibration is the following:

1. The loop is filled with LBE and kept at constant temperature, i.e. 300°C.
2. The heating cables are switched off.
3. The bundle is started up with a ramp of 5 minutes at full power (20 kW).
4. The secondary side is filled with water and the secondary pump and air-cooler are switched on.
5. A transient starts, after a few hours the system reaches the thermo-fluid dynamic equilibrium state, characterised by quantities not varying with time.
6. In this NC condition, an equilibrium mass flow rate can be evaluated according to Eq. (1), this mass flow rate is of the order of ~5 kg/s: the first calibration point is fixed in instrument.

7. The gas lift is switched on at the maximum flow rate (20 NI/min) and the equilibrium steady state is reached in a few hours.
8. In this enhanced circulation condition, an equilibrium mass flow rate can be evaluated according to Eq. (1), this mass flow rate is of the order of 18 kg/s: the second calibration point is fixed in instrument.

4.2.4 Benchmark approach

The Working Group agreed to use recent experimental tests carried out on LBE-cooled NACIE facility to continue the investigation on heavy liquid metal (HLM) NC conditions. Using NACIE experimental data, allows greater confidence based on:

- the simplicity of the loop (straight tubes without valves, no mechanical pump, water on the secondary side, etc.);
- better insulation to represent adiabatic conditions;
- higher consistency between the forced circulation and the NC due to an unchanged loop configuration (there is no pump bypass line).

Nonetheless, awaiting the upgrade planned for the loop (NACIE-UP), the NACIE experimental campaign considered for the present activity has some deficiencies:

- no measurements of pressure drops are available;
- little-known thermal properties of the steel powder set in the HX between the primary and secondary side;
- high uncertainty on the mass flow rate measurement shown by the induction flowmeter, especially at mass flow rates consistent with the NC operating condition.

The previous activities conducted within LACANES gave the opportunity to assess the approach on the pressure losses calculation against experimental data conducted in isothermal forced convection. On the other side, they show a high level of uncertainties on heat losses and also on the pressure loss along the pump bypass line in NC tests.

With the experimental data coming from NACIE, a complementary study will be attempted. The measures of pressure losses not being available, but the heat losses values being reasonably accurate, the following steps will be pursued:

- due to the high level of uncertainties of the experimental mass flow rate, characterisation of the pressure losses of the loop with the “best practice” gained in Phase I of the benchmark and the help of correlation in literature;
- the simulation of a selected NC test (low mass flow rate) mainly with a code-to-code approach and secondly with a code-to-experiment comparison, in particular regarding the mass flow rate

If many of the codes involved in the benchmark are not able to manage the gas injection for the gas lifting enhanced circulation, only the NC tests are taken into account.

4.2.5 Test specification

Suggestions for the preparation of the code models:

- limit the description of the secondary side to the explicit nodalisation of heat exchanger plus boundary conditions at inlet and outlet;
- the conductivity of the steel powder in the HX is about a tenth (1/10) of the steel, but the value should be tuned to agree with the experimental data;

- pay attention on the evaluation of the k-factors of the heating section spacer grids shown in Figure 2.5 positioned around the middle and exit part of the rod bundle, and in general, the pressure drop coefficient evaluation should take advantage of the best practices gained during Phase I;
- the LBE thermodynamic properties evaluation should be based on the NEA handbook [2].

The Test 301 in NC is considered for the benchmark. The power supplied through the heating section is 21.8 kW. The participants should simulate the steady-state condition. In Figure 4.13 and Figure 4.14, the experimental data collected are plotted:

Figure 4.13 – Test 301: LBE mass flow rate measured (MP101) and estimated with thermal balance

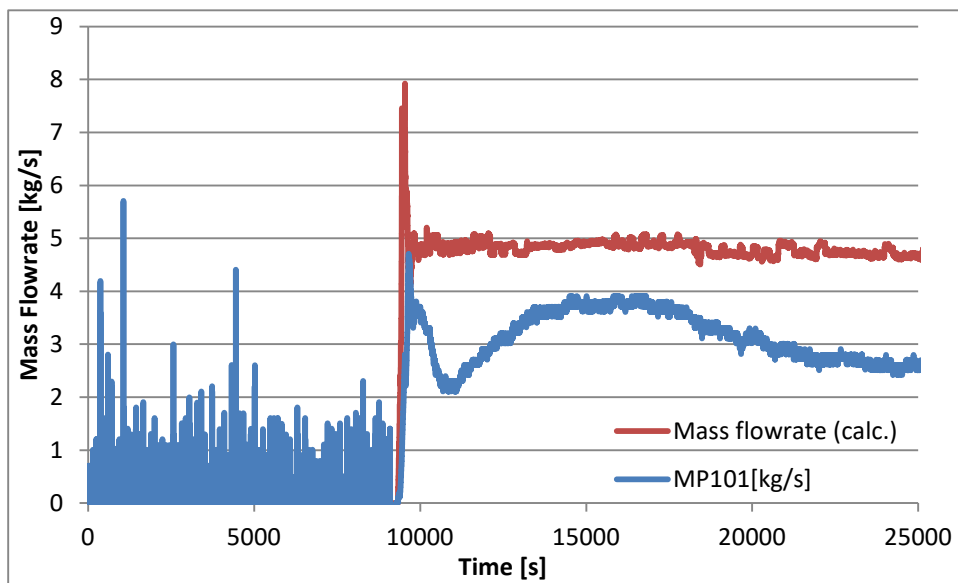


Figure 4.14 – Test 301: LBE and water temperatures.

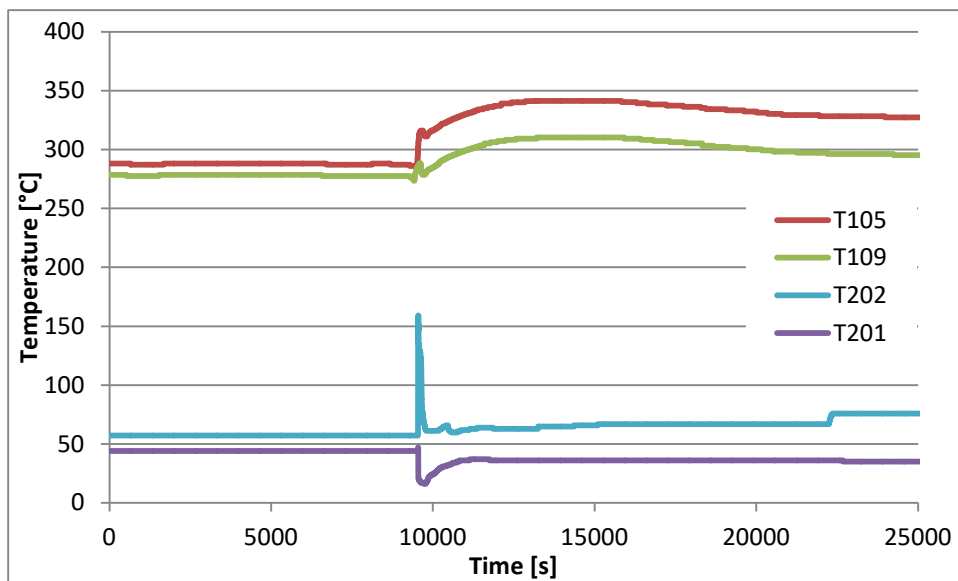


Table 4.7 collects the main NACIE loop steady-state experimental data in NC Test 301. The data have been averaged along a time interval of one hour of steady state.

Table 4.7 – Test 301 main averaged experimental data (1 h)

Parameter (TEST 301)	Unit	Value	Instrument	Note
Time interval (1h)	s	23400-27000		
Argon injection flow rate	NI/min	0.0	F101	
LBE flow rate	kg/s	4.712		Calculated
Water flow rate	m ³ /h	0.47	MP201	
Rod power	kW	21.798	PR2	
Temperature T102	°C	327.7	T102	
Temperature T103	°C	324.3	T103	HX inlet
Temperature T104	°C	297.1	T104	HX outlet
Temperature T105	°C	326.9	T105	Core outlet
Temperature T106	°C	326.4	T106	
Temperature T107	°C	326.6	T107	Expansion vessel
Temperature T109	°C	295.1	T109	Core inlet
Secondary inlet temperature	°C	35.1	T201	
Secondary outlet temperature	°C	75.8	T202	

References

- [1] NEA (2012), *Benchmarking of thermal-hydraulic loop models for lead-alloy-cooled advanced nuclear energy systems – Phase I: Isothermal forced convection case*, OECD, Paris.
- [2] NEA (2007), *Handbook on Lead-bismuth Eutectic Alloy and Lead Properties, Materials Compatibility, thermal-hydraulics and Technologies*, OECD, Paris.

5. Comparison and discussion

5.1 HELIOS

, Four out of five taskforce members have participated to the benchmark on HELIOS natural circulation experiments: the Italian National Agency for New Technologies, Energy and Sustainable Economic Development (ENEA), Ricerca sul Sistema Energetico (RSE, Italy), Seoul National University (SNU), and the Institute of Nuclear Energy Safety Technology (INEST). The participants established their own calculation models and boundary conditions complying with the given benchmark approach and specifications as described in sections 4.1.3 and 4.1.4 Each calculation model has been illustrated throughout Chapter 3. In this activity, several parameters of interest have been defined: temperature distribution along the main loop, secondary side oil outlet temperature, mass flow rate of lead-bismuth eutectic (LBE), and pressure drop over each main component. The participants submitted their benchmarking results including these parameters of interest. In addition, pressure loss coefficient including both friction factors and form loss coefficients in both cases are contained in Appendix B in detail.

5.1.1 Calculation results on loop temperature distribution and mass flow rate

In both experiment and simulation, temperature in several specific points and total mass flow rate in a system can be obtained at first hand. In this regard, calculated temperature distributions and mass flow rates for the Case I at 15.0 kW and the Case II at 9.8 kW are summarised in Table 5.1 and Table 5.2. Regarding the temperature distributions, the hot leg and cold leg average temperatures and oil outlet temperatures are compared. Since the enthalpy change over heat source and heat sink can be described with the temperature change, the temperature differences between hot leg and cold leg average temperatures (ΔT) are also included. Any deviations and/or discrepancies are defined by difference between calculation results and measurements.

As shown in Table 5.1 and Table 5.2, all of the parameters of interest in natural circulation (NC) conditions show good agreement between experiments and code benchmark results, which is no larger than 10% deviations, in both cases. The LBE temperature distributions along the primary loop for two benchmark cases are plotted in Figure 5.1 and Figure 5.2 in detail. All of the calculation results on temperature distributions are in good agreement with the experimental data in less than 7 °C deviation. There are several potential causes for this deviation resulted in the absolute temperatures because the primary loop temperatures are determined by temperature profile over heat exchanger, which can be affected by three parameters: primary side (LBE) convective heat transfer coefficient, thermal conductivity of the wall that constitutes the interface between the primary and secondary loops where conductive heat transfer occurs, and secondary side (oil) heat transfer coefficient.

Table 5.1 – Summary of benchmark results from participants: Case I (15.0 kW)

	Experiment	ENEA (RELAP5)	RSE (LegoPST)	SNU (MARS-LBE)	INEST (RELAP5)
Hot leg average temperature (°C) [deviation from measurement (°C)]	315.84	312.37 [-3.47]	311.83 [-4.01]	313.87 [-1.97]	317.91 [2.07]
Cold leg average temperature (°C) [deviation from measurement (°C)]	266.83	265.48 [-1.35]	267.12 [0.29]	269.02 [2.19]	268.89 [2.06]
Average temperature difference (°C) [discrepancy with experiment (%)]	49.01	46.89 [-4.3%]	44.71 [-8.8%]	44.85 [-8.5%]	49.02 [0.0%]
Oil outlet temperature (°C) [deviation from measurement (°C)]	144.33	143.48 [-0.85]	143.17 [-1.16]	144.33 [0.00]	143.07 [-1.26]
LBE mass flow rate (kg/s) [discrepancy with experiment (%)]	2.09	2.19 [4.8%]	2.23 [6.7%]	2.27 [8.8%]	2.10 [0.5%]

Table 5.2 – Summary of benchmark results from participants: Case II (9.8 kW)

	Experiment	ENEA (RELAP5)	RSE (LegoPST)	SNU (MARS-LBE)	INEST (RELAP5)
Hot leg average temperature (°C) [deviation from measurement (°C)]	273.84	277.51 [3.67]	268.16 [-5.68]	274.36 [0.53]	274.99 [1.15]
Cold leg average temperature (°C) [deviation from measurement (°C)]	237.32	242.12 [4.80]	234.99 [-2.33]	240.36 [3.04]	238.13 [0.81]
Average temperature difference (°C) [discrepancy with experiment (%)]	36.52	35.39 [-3.1%]	33.16 [-9.2%]	34.00 [-6.9%]	36.86 [0.9%]
Oil outlet temperature (°C) [deviation from measurement (°C)]	118.86	119.34 [0.48]	118.87 [0.01]	118.86 [0.00]	118.86 [0.00]
LBE mass flow rate (kg/s) [discrepancy with experiment (%)]	1.80	1.89 [4.9%]	1.94 [7.8%]	1.94 [7.9%]	1.81 [0.6%]

As summarised in Table 5.1 and Table 5.2, calculated oil outlet temperatures are in less than 1.5 °C deviations. It means that heat balance between two systems, primary and secondary sides, is properly simulated and the secondary side thermal-hydraulic conditions such as temperature and flow velocity are almost the same among calculations. As described through Chapter 3, all participants used the same convective heat transfer correlations for both LBE (Seban-Shimazaki correlation) and secondary side oil (modified Sieder-Tate correlation). In addition, calculation schemes on conductive and/or convective heat transfer used in each code would not be the cause of the discrepancy because the codes have similar structure, in other words, most of participants used RELAP and its variant except RSE that used LegoPST. Therefore, the deviations in the absolute temperature distributions along the primary loop may be resulted from the thermal conductivity values of the stainless steel in the heat exchanger used by each participant in both cases.

Figure 5.1 – Calculated LBE temperature distributions along main loop: Case I (15.0 kW)

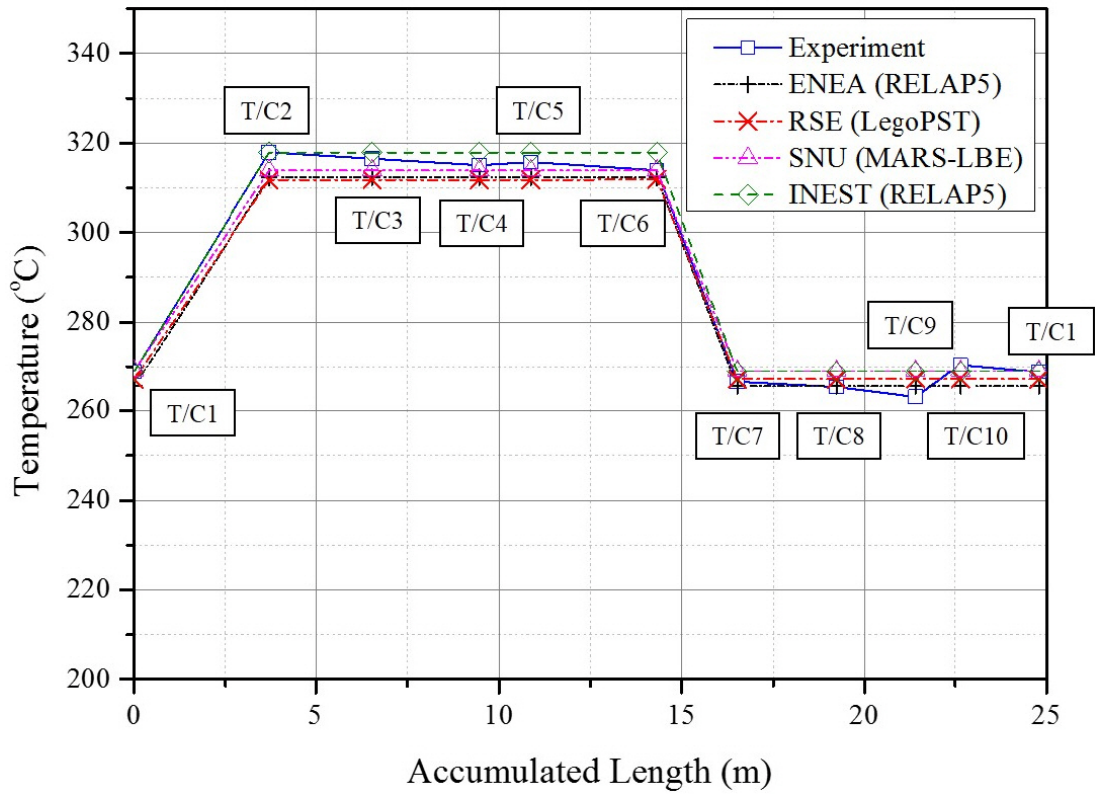
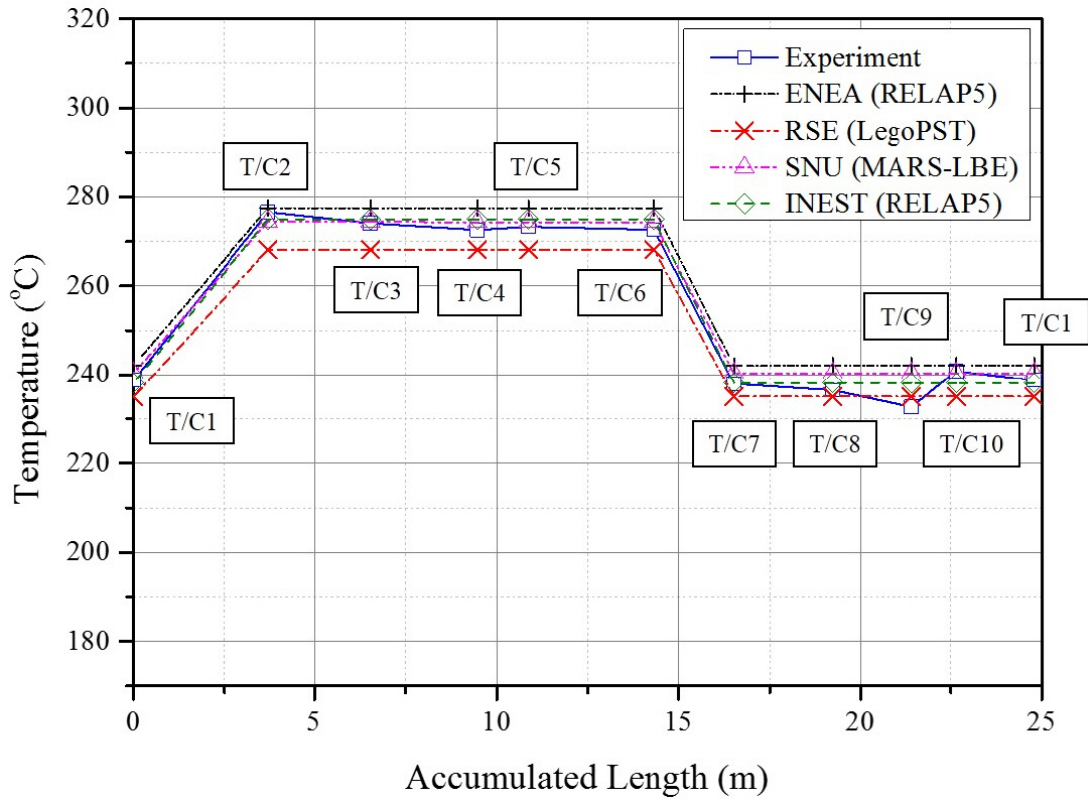


Figure 5.2 – Calculated LBE temperature distributions along main loop: Case II (9.8 kW)



The LBE mass flow rates calculated by the system codes and the average temperature difference between hot leg and cold leg for both Case I and Case II are summarised in Figure 5.3 and Figure 5.4, respectively. Benchmark results show good agreement with measurement data within maximum 9% discrepancies, both in mass flow rate and average temperature difference. The absolute magnitudes of discrepancies in average temperature difference and LBE mass flow rate are similar and the signs are opposite for each participant's result, as power given to a system can be expressed with the thermal balance, product of mass flow rate and temperature difference (also with heat capacity, i.e. $Q = \dot{m}C_p\Delta T$). For example, ENEA's computational code estimated that LBE mass flow rate was larger than the measurement while temperature difference was smaller.

Figure 5.3 – LBE mass flow rate comparisons on Case I (15.0 kW) and Case II (9.8 kW)

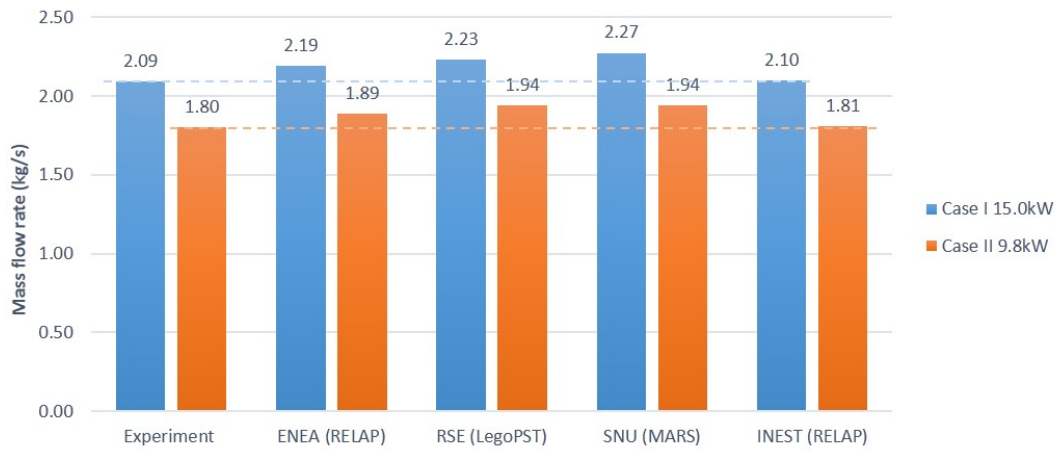
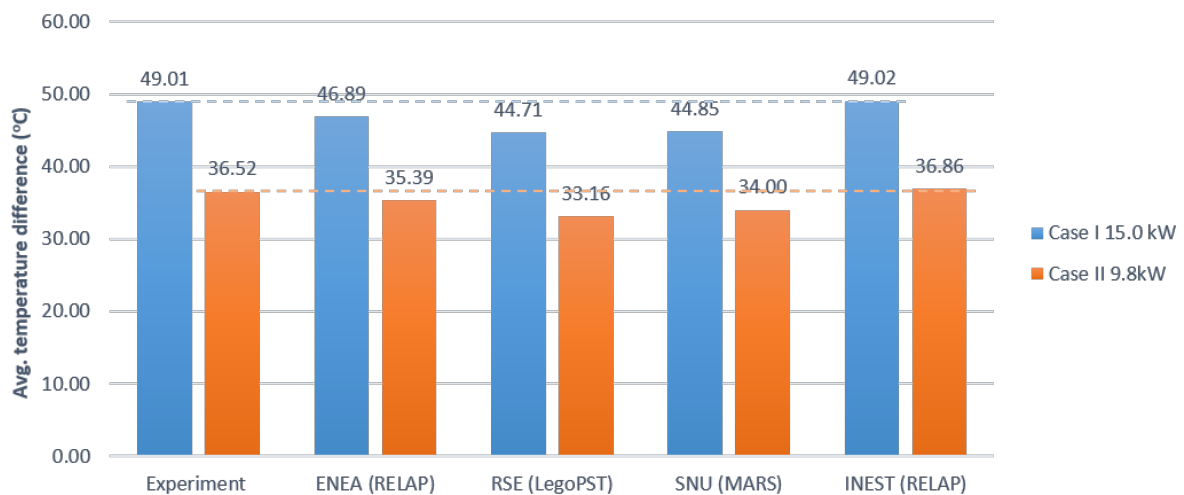


Figure 5.4 – Comparisons on average temperature differences between hot leg and cold leg in Case I (15.0 kW) and Case II (9.8 kW)



In addition to the discrepancies, it is notable that all the calculation results showed overestimation compared to the measurement. Viewing from a different point of view, this overestimation would not be the ‘overestimation’ that originally resulted from flow decrease made out of some flow condition changes. In this context, the long-term chemical condition change in LBE could affect the surface friction that finally led to decreased flow rate. At this moment, this cannot be found nor concluded but can be a future research subject.

5.1.2 Pressure drop estimation

As hydraulic loss configuration has not been a main target for the benchmark activity, pressure loss measurements were not made for the HELIOS. However, total pressure loss over a system is an important parameter in NC because mass flow rate is highly dependent on it. In this regard, the hydraulic loss calculation results from all participants in terms of hydraulic loss coefficients with reference velocity of each component were collected. The detailed comparison between the results are summarised in Appendix B. In this section, total and local pressure loss estimations will be mainly discussed.

As the HELIOS main loop has many components as listed in Table 2.2, it is not practical to compare each component side by side. In this regard, several sub-parts are grouped together for a better resolution. Table 5.3 defines eight component groups by means of LBE flow path and contribution to the total pressure loss of the main loop. Especially, core and heat exchanger (HX) are treated into two parts, the total form loss given by grid spacers and the others. The orifice also grouped itself due to its high contribution to total hydraulic loss. Figure 5.5 illustrates these groups graphically.

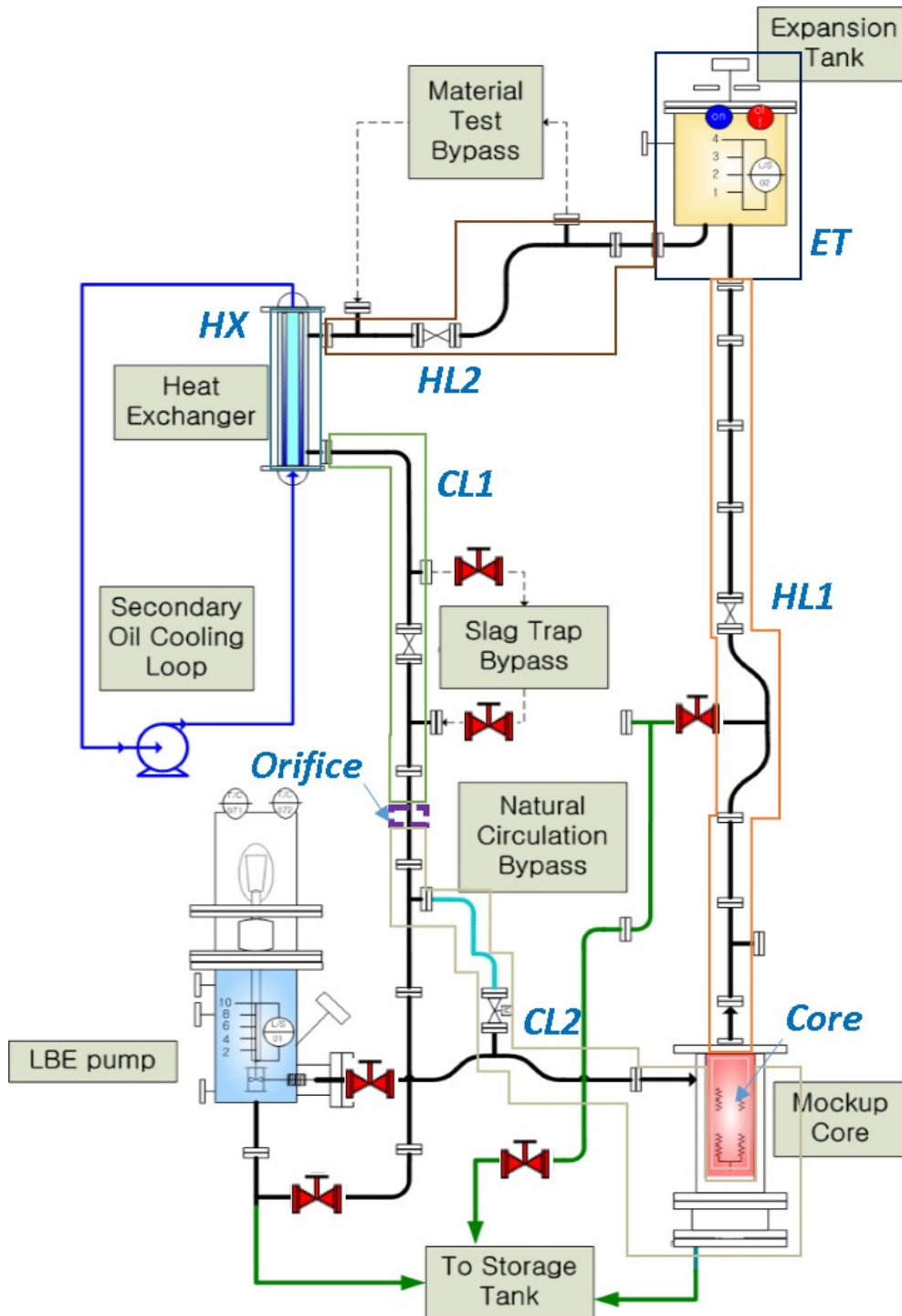
Table 5.3 – Grouping of HELIOS sub-parts for pressure loss comparison

Grouped part	Sub-part no.*
Core**	1-4
HL1	1-5, 1-6, 2-1, 2-2, 2-3, 2-4, 3-1, 3-2, 4-1, 4-2, 4-3, 4-4, 4-5, 4-6, 4-7, 4-8, 4-9, 4-10, 5-1, 5-2, 6-1, 6-2, 7-1, 7-2, 19-1, 8-4, 9-1, 9-2
ET	10-1, 10-2
HL2	11-1, 11-2, 12-1, 12-2, 12-3, 12-4, 12-5, 12-6, 12-7, 13-1, 13-2, 14-1, 14-2, 14-3, 14-4
HX**	15-1, 15-2, 15-3, 15-4
CL1	16-1, 16-2, 16-3, 16-4, 16-5, 16-6, 17-1, 17-2, 18-1, 18-2, 18-3, 18-4, 8-1
Orifice	8-2
CL2	8-3, 19-2, 20-1, 20-2, 20-3, 20-4, 21-1, 21-2, 21-3, 21-4, 21-5, 21-6, 22-1, 22-2, 23-1, 23-2, 23-3, 23-4, 23-5, 23-6, 1-1, 1-2, 1-3

* Each of sub-part numbers are the same with the sub-part numbers as defined in Appendix B.

** Components with grid spacers.

Figure 5.5 – Graphical illustration of pressure loss comparison groups for HELIOS loop



The total and local pressure loss evaluated by each participant for both Cases I and II are summarised in Table 5.4, while the results are visualised in Figure 5.6. In addition, accumulated pressure losses for both cases are illustrated in Figure 5.7 in terms of accumulated length in flow path.

Table 5.4 – Comparison of total and local pressure loss of HELIOS for (a) Case I (15.0 kW) and (b) Case II (9.8 kW)

Group		Pressure loss (Pa)							
		(a) Case I (15.0 kW)				(b) Case II (9.8 kW)			
		ENEA	RSE	SNU	INEST	ENEA	RSE	SNU	INEST
Core	Other than grids	222.8	757.5	259.7	262.4	174.4	575.5	200.4	277.5
	Form loss by grids	1209.1	1423.2	1682.0	2416.5	895.5	1118.5	1280.4	1783.8
HL1		550.2	558.6	506.1	200.7	416.6	423.5	383.2	205.3
ET		154.0	86.2	71.6	86.7	114.7	65.6	53.7	65.8
HL2		264.9	200.1	265.8	117.2	199.2	152.7	199.4	148.0
HX	Other than grids	90.9	118.1	88.8	90.0	67.6	15.7	65.8	70.6
	Form loss by grids	18.0	25.4	77.4	449.8	13.4	19.7	10.2	348.8
CL1		324.7	234.1	279.5	109.8	245.0	179.8	210.7	102.9
Orifice		637.0	516.3	591.3	25.5	472.1	392.5	437.0	19.0
CL2		597.6	574.9	635.9	543.4	444.1	439.7	474.8	431.4
Total pressure loss (Pa)		4069.2	4494.3	4458.1	4301.9	3042.4	3383.3	3315.7	3453.0

Figure 5.6 – Comparison of total and local pressure loss of HELIOS for (a) Case I (15.0 kW) and (b) Case II (9.8 kW)

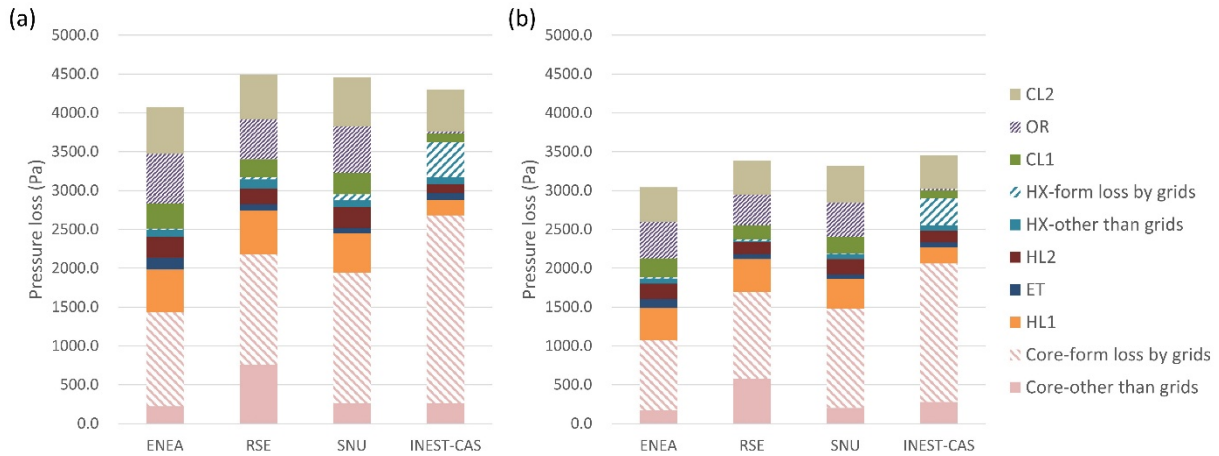
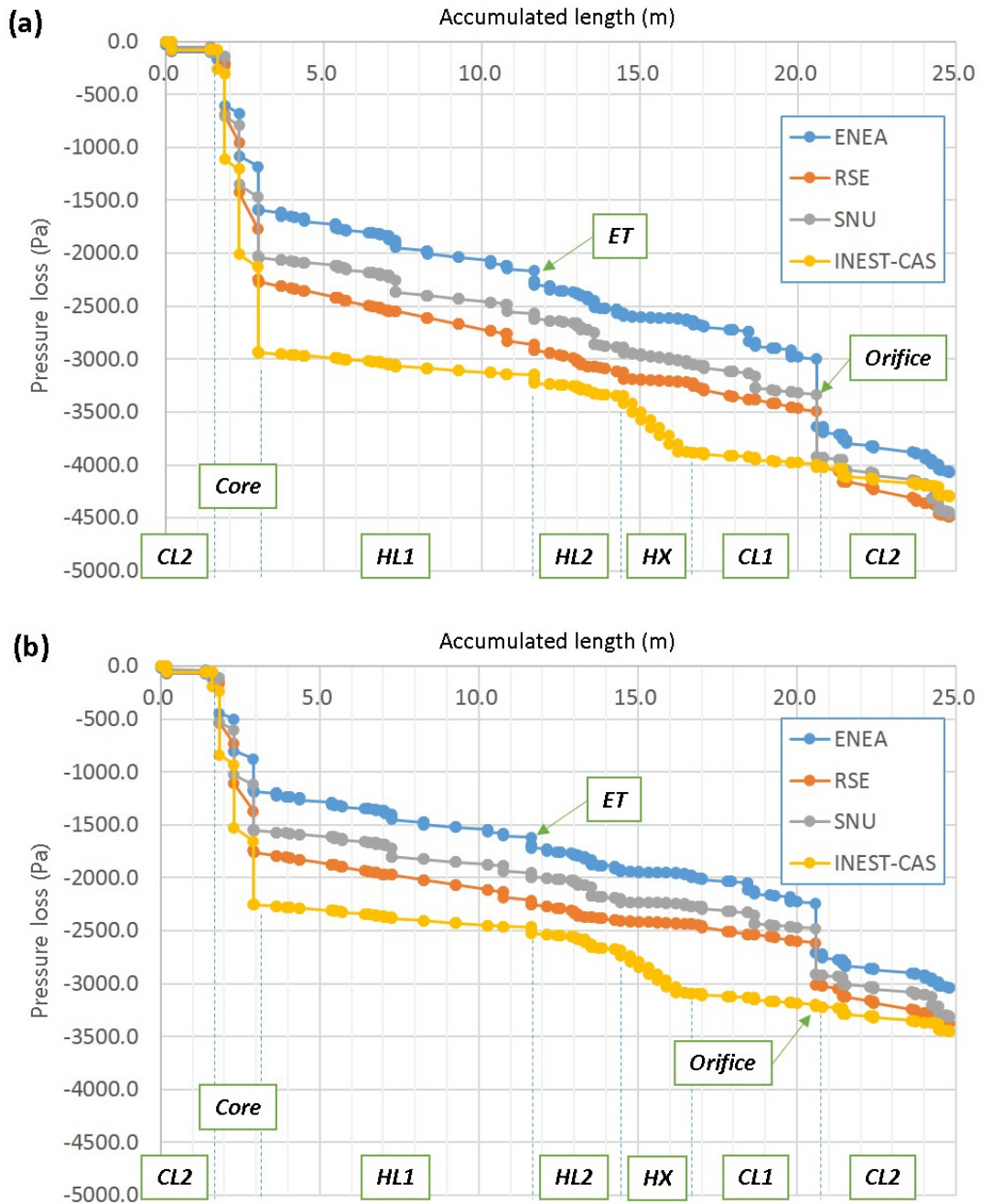


Figure 5.7 – Comparison of accumulated pressure loss of HELIOS for (a) Case I (15.0 kW) and (b) Case II (9.8 kW)



As shown in Table 5.4 and Figure 5.6, all participants estimated total pressure loss for the Case I as about 4000-4500 Pa, and that for the Case II as about 3000-3500 Pa. The mock-up core is the region where most of pressure drop takes place because all participants calculated as much as 35-66% and 26-51% of total pressure loss occurs in that region for the Case I and Case II, respectively. However, the heat exchanger, which has six grid spacers, shows rather small amount of local pressure loss compared to the mock-up core; about 3-13% of total pressure loss in Case I and 2-10% of that in Case II, respectively. This difference can be made from the

ratio between flow area (undisturbed area) and grid spacer projected area, because the same correlation (Rehme) was applied to both components.

Other than two components, local pressure loss in orifice is shown to be large with respect to other pressure loss comparison groups, except from the results INEST submitted. Their results show negligible pressure loss while others presents 13-16% and 10-12% of total pressure loss for the Case I and the Case II, respectively. This can be resulted from the calculation of pressure loss coefficient as shown in section 3.6.2 where INEST described their calculation models.

In Figure 5.7, pressure loss over a component can be seen with the gradient change of a curve, which means higher pressure loss with a drastic change. Pressure drops given by three grid spacers in the mock-up core can also be identified with three steep changes in that region. It is noted that the gradients over comparison groups except for core, heat exchanger, and orifice are almost similar, in other words, estimated pressure drops are almost in good agreement.

5.2 NACIE

In the present section have been collected and benchmarked the results obtained with the models and codes presented in Chapter 3 for the NACIE NC Test 301 described in section 4.2.5.

5.2.1 Result of system code simulation

In the following tables are shown the pressure loss results obtained by each participant as were submitted. Each table provides, the main geometrical quantities of the model, the mass flow rate obtained in NC, the equivalent coefficients of distributed pressure loss (f^*L/D), the form loss coefficients (K), the reference velocities in each section and the relative pressure loss calculated in each sections and flow accidents. The template covers the entire flow path of NACIE facility gathering all the information both for distributed and concentrated pressure loss. Some differences in the geometry of the models may be due to different assumptions and nodalisation choices that can be analysed in detail in Chapter 3.

Table 5.5 reports the ENEA results obtained with RELAP5 mod3.3, Table 5.6 reports the RSE results obtained with LegOPST, Table 5.7 reports the SNU results obtained with MARS-LBE,

Component	flow area (m ²)	hyd. dia. (m)	length (m)	roughness (mm)	mass flow rate (kg/s)	$f^*(L/D)$	K	Ref. velocity (m/s)	press. loss (Pa)
Heating section	2.88E-03	3.84E-02	0.85	32	5.31	0.51572		0.179	453
Grid spacer	2.68E-03						0.0681	0.192	14
Upper grid	1.69E-03						0.697	0.305	345
Riser w/o Ar inj. Line	3.09E-03	6.27E-02	1.500	32		0.53306		0.167	76
Area change due to the gas injection line	2.31E-04						0.0759	0.181	13
Riser with Ar inj. Line	2.86E-03	5.27E-02	5.326	32		2.28253		0.181	377
Riser to E/V	2.86E-03	5.27E-02		32			0.8266	0.181	147
E/V to upper horizontal pipe							0.5000	0.167	76
Upper Horizontal pipe	3.09E-03	6.27E-02	0.923	32		0.32791		0.167	43
90 deg elbow	3.09E-03	6.27E-02		32			0.3177	0.167	48
Down c	3.09	6.27	7	32		2.66532		0.167	377

o m e r	E - 0 3	E - 0 2	5					
90 deg elbow	3.09E-03	6.27E-02		32		0.3177	0.167	48
Lower h o r i z o n t a l p i p e	3.0 9 E - 0 3	6.2 7 E - 0 2	1 . 0 0 0	3 2	0.3 5 5 3 8		0 . 1 6 7	4 8
Tee	3.0 9 E - 0 3	6.2 7 E - 0 2		3 2		1. 2 9 0 0	0 . 1 6 7	1 9 6

Table 5.8 reports the Ansaldo results obtained with RELAP5 mod3.2.2beta and Table 5.9 reports the INEST results obtained with RELAP5 mod4.0.

Table 5.5 – ENEA pressure loss results of NACIE Test 301 (RELAP5 mod3.3)

Component	flow area (m ²)	hyd. dia. (m)	length (m)	roughness (µm)	mass flow rate (kg/s)	f*(L/D)	K	Ref. velocity (m/s)	press. loss (Pa)
Heating section	2.86E-03	3.83E-02	0.854	32	5.28	0.6184		0.178	427
Grid spacer	2.87E-03	3.67E-02					0.06887	0.193	13
Upper grid	1.74E-03	1.18E-02					0.697	0.295	313
Riser w/o Ar inj. Line	3.09E-03	6.27E-02	1.500	32			0.52178	0.166	74
Area change due to the gas injection line	2.94E-03	4.55E-02						0.0374	6
Riser with Ar inj. Line	2.85E-03	4.55E-02	5.326	32			2.52449	0.179	419
Riser to E/V	2.85E-03	4.55E-02						0.89062	148
E/V to upper horizontal pipe	3.09E-03	1.82E-01						0.6200	88
Upper Horizontal pipe	3.09E-03	6.27E-02	0.923	32			0.33161	0.166	47
90 deg elbow	3.09E-03	6.27E-02						0.3134	44
Downcomer	3.09E-03	6.27E-02	7.5	32			2.64206	0.165	375
90 deg elbow	3.09E-03	6.27E-02						0.3134	44
Lower horizontal pipe	3.09E-03	6.27E-02	1.000	32			0.3847	0.165	54
Tee	3.09E-03	6.27E-02						2.0200	311

Table 5.6 – RSE pressure loss results of NACIE Test 301 (LegoPST)

Component	flow area (m ²)	hyd. dia. (m)	length (m)	roughness (mm)	mass flow rate (kg/s)	f*(L/D)	K	Ref. velocity (m/s)	press. loss (Pa)
Heating section	2.88E-03	3.84E-02	0.85	32	5.66	0.67987		0.190	270
Grid spacer	2.68E-03						0.0653	0.190	12
Upper grid	1.89E-03						0.697	0.190	131
Riser w/o Ar inj. Line	3.09E-03	6.27E-02	1.500	32		0.51756		0.178	84
Area change due to the gas injection line	2.31E-04						0.07193	0.178	12
Riser with Ar inj. Line	2.86E-03	4.56E-02	5.029	32		2.65676		0.192	505
Riser to E/V	2.86E-03	4.56E-02	0.121	32		0.06392	0.89039	0.192	181
E/V to upper horizontal pipe							0.5000	0.178	81
Upper Horizontal pipe	3.09E-03	6.27E-02	0.828	32		0.28578		0.178	47
90 deg elbow	3.09E-03	6.27E-02	0.14954	32		0.05192	0.24351	0.178	48
Downcomer	3.09E-03	6.27E-02	7.53292	32		2.54116		0.178	412
90 deg elbow	3.09E-03	6.27E-02	0.14954	32		0.05206	0.24598	0.178	48
Lower horizontal pipe	3.09E-03	6.27E-02	0.829	32		0.28861		0.178	47
Tee	3.09E-03	6.27E-02	0.152	32		0.05292	1.2900	0.178	218

Table 5.7 – SNU pressure loss results of NACIE Test 301 (MARS)

Component	flow area (m ²)	hyd. dia. (m)	length (m)	roughness (mm)	mass flow rate (kg/s)	f*(L/D)	K	Ref. velocity (m/s)	press. loss (Pa)
Heating section	2.88E-03	3.84E-02	0.85	32	5.31	0.51572		0.179	453
Grid spacer	2.68E-03						0.0681	0.192	14
Upper grid	1.69E-03						0.697	0.305	345
Riser w/o Ar inj. Line	3.09E-03	6.27E-02	1.500	32		0.53306		0.167	76
Area change due to the gas injection line	2.31E-04						0.0759	0.181	13
Riser with Ar inj. Line	2.86E-03	5.27E-02	5.326	32		2.28253		0.181	377
Riser to E/V	2.86E-03	5.27E-02		32			0.8266	0.181	147
E/V to upper horizontal pipe							0.5000	0.167	76
Upper Horizontal pipe	3.09E-03	6.27E-02	0.923	32		0.32791		0.167	43
90 deg elbow	3.09E-03	6.27E-02		32			0.3177	0.167	48
Downcomer	3.09E-03	6.27E-02	7.5	32		2.66532		0.167	377

90 deg elbow	3.09E-03	6.27E-02		32		0.3177	0.167	48
Lower horizontal pipe	3.09E-03	6.27E-02	1.000	32	0.35538		0.167	48
Tee	3.09E-03	6.27E-02		32		1.2900	0.167	196

Table 5.8 – Ansaldo pressure loss results of NACIE Test 301 (RELAP5 mod3.3.2b)

Component	flow area (m ²)	hyd. dia. (m)	length (m)	roughness (mm)	mass flow rate (kg/s)	f*(L/D)	K	Ref. velocity (m/s)	press. loss (Pa)
Heating section	2.90E-03	3.83E-02	0.85	32	5.19	0.53931	-	0.175	397
Grid spacer	2.60E-03	-	-	32		-	0.05	0.190	9
Upper grid	1.70E-03	-	-	32		-	0.6965	0.291	302
Riser w/o Ar inj. Line	3.10E-03	6.27E-02	1.500	32		0.53222	-	0.164	73
Area change due to the gas injection line	2.90E-03	4.55E-02	-	32		-	0.0719	0.177	12
Riser with Ar inj. Line	2.90E-03	4.55E-02	5.355	32		2.76474	-	0.177	444
Riser to E/V	2.90E-03	4.55E-02	-	32		-	0.889	0.177	143
E/V to upper horizontal pipe	3.10E-03	6.27E-02	-	32		-	0.8540	0.164	117
Upper Horizontal pipe	3.10E-03	6.27E-02	0.873	32		0.30643	-	0.164	42
90 deg elbow	3.10E-03	6.27E-02	-	32		-	0.3192	0.164	45
Downcomer	3.10E-03	6.27E-02	7.5	32		2.68136	-	0.164	368
90 deg elbow	3.10E-03	6.27E-02	-	32		-	0.3192	0.163	44
Lower horizontal pipe	3.10E-03	6.27E-02	1.000	32		0.35155	-	0.163	48
Tee	3.10E-03	6.27E-02	-	32		-	1.4880	0.163	204

Table 5.9 – INEST pressure loss results of NACIE Test 301 (RELAP5 mod4.0)

Component	flow area (m ²)	hyd. dia. (m)	length (m)	roughness (mm)	mass flow rate (kg/s)	f*(L/D)	K	Ref. velocity (m/s)	press. loss (Pa)
Heating section	2.88E-03	3.83E-02	0.85	32	5.49	0.54395		0.184	462
Grid spacer	2.67E-03						0.0681	0.199	14
Upper grid	1.70E-03						0.697	0.313	352
Riser w/o Ar inj. Line	3.09E-03	6.27E-02	1.500	32		0.52527		0.172	80
Area change due to the gas injection line	2.30E-04						0.0719	0.186	13
Riser with Ar inj. Line	2.86E-03	5.27E-02	5.335	32		2.28515		0.186	408
Riser to E/V	2.97E-03						0.8865	0.186	158
E/V to upper horizontal pipe	3.09E-03						0.5000	0.172	77

Upper Horizontal pipe	3.09E-03	6.27E-02	1.000	32		0.3497		0.172	54
90 deg elbow	3.09E-03	6.27E-02		32			0.3125	0.172	48
Downcomer	3.09E-03	6.27E-02	7.5	32		2.64656		0.172	404
90 deg elbow	3.09E-03	6.27E-02		32			0.3125	0.172	48
Lower horizontal pipe	3.09E-03	6.27E-02	1.000	32		0.35287		0.172	54
Tee	3.09E-03	6.27E-02		32			1.2900	0.172	197

The total and partial pressure loss evaluated by each model are collected in the following Table 5.10 for a direct comparison. Since the reconstruction of the pressure field along the loop cannot be evaluated due to the lack of any pressure or differential pressure measurement, the simulation results can only be compared one against the other.

As can be seen, the distributed pressure loss are slightly prevailing the concentrated ones for the whole set of models, ranging from 52 to 62% of the total pressure loss. The most relevant concentrated pressure loss are those relative to the upper grid spacer, the riser to expansion volume and then to the upper horizontal pipe, where the LBE flow enters and exits from the expansion tank, and the tee at the inlet of the heating section.

Table 5.10 – Comparison of the partial and total pressure loss of NACIE Test 301

	Pressure loss (Pa)				
	ENEA	RSE	SNU	Ansaldo	INEST
Heating Section lower half	50.7	63.6	47.1	42.6	47.8
Lower grid spacer	13.2	12.2	13.7	9.3	13.9
Heating Section upper half	50.7	63.6	47.1	42.6	47.8
Upper grid spacer	312.6	130.7	344.8	302.3	352.3
Riser w/o Ar inj. line	74.0	84.2	76.3	73.1	80.5
Area change due to the gas injection line	6.2	11.7	12.8	11.5	12.8
Riser with Ar inj. Line	418.6	505.1	377.1	444.1	408.0
Riser to E/V	147.7	181.4	146.6	142.8	158.3
E/V to upper horizontal pipe	88.0	81.4	76.3	117.3	76.6
Upper Horizontal pipe	47.1	46.5	43.4	42.1	53.6
90 deg elbow	44.5	48.0	48.5	45.4	47.9
Downcomer	375.0	412.4	376.6	368.3	404.1
90 deg elbow	44.3	48.3	48.3	43.7	47.7
Lower horizontal pipe	54.4	46.8	47.9	48.1	53.9
Tee	310.6	217.8	196.1	203.8	197.0
TOTAL DP	2037.4	1954.1	1902.3	1937.0	2002.1
Total distributed DP	1070.5	1222.4	1015.4	1060.9	1095.6
Total concentrated DP	967.0	731.7	886.9	876.1	906.5

Figure 5.8 shows the comparison of the total and partial loss of the NACIE Test 301 carried out in NC, and Figure 5.9 shows the comparison of the accumulated pressure loss against the length of NACIE primary loop.

The methodologies to evaluate the form loss coefficients have been widely discussed during the benchmark activities in order to find some guidelines for better use the correlations in literature. In those cases where the accident is hardly traceable to a form present in literature (e.g. prototypical spacer grid), the use of CFD codes may be helpful to improve the system code models. The result of this work is a quite good agreement among the simulations where, apart from small deviations, the worth of each pressure loss is coherent among the simulations.

Figure 5.8 – Comparison of total and partial pressure loss of NACIE Test 301

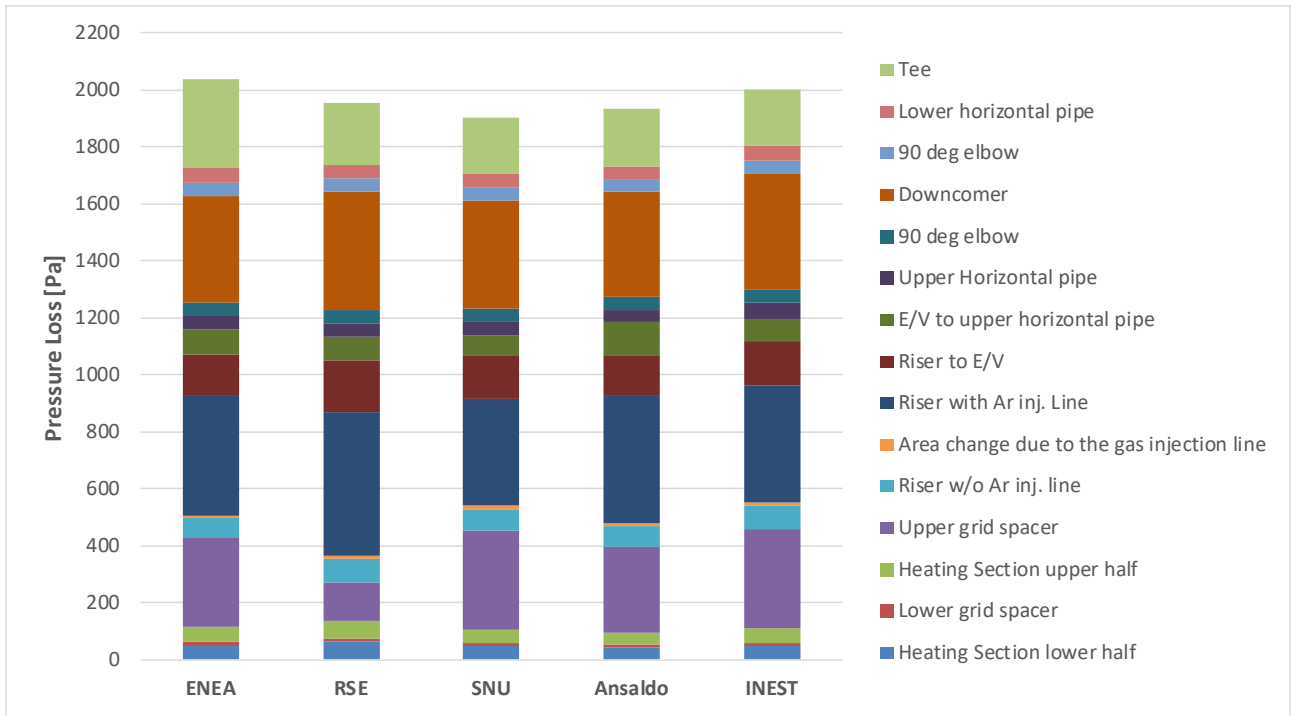


Figure 5.9 – Comparison of the accumulated pressure loss of NACIE Test 301

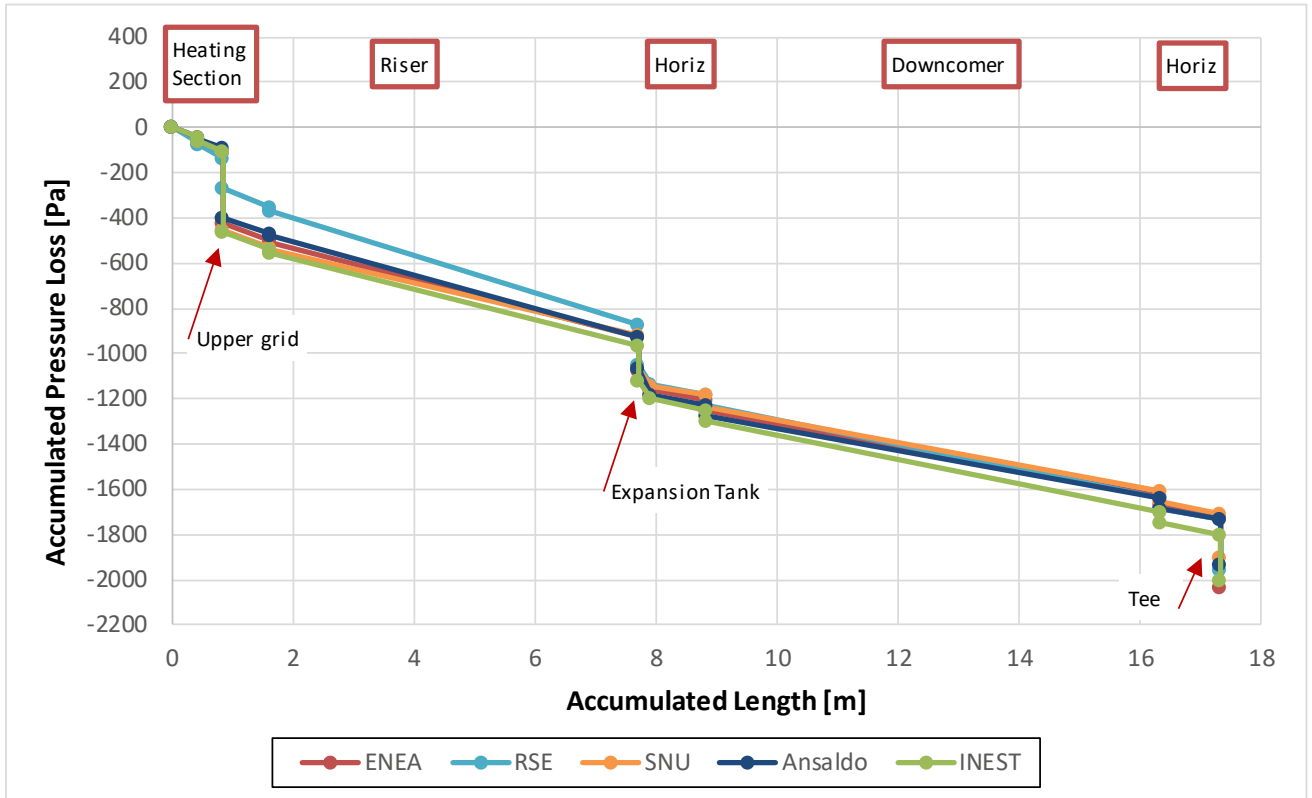


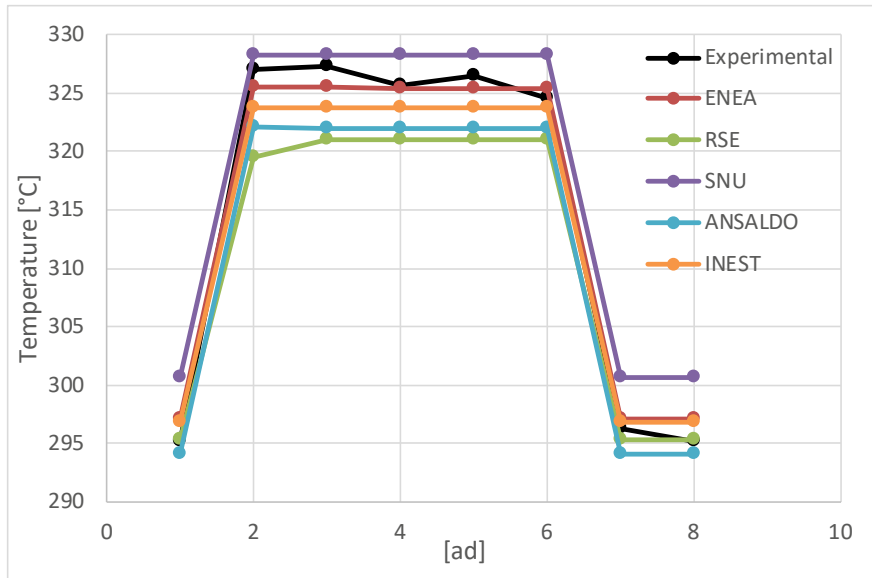
Table 5.11 shows the comparison of the experimental data against the simulations of all the participants. The place of the measurements can be found in the piping and instrumentation (P&I) in Appendix A.

Table 5.11 – Comparison of the experimental data against simulations of NACIE Test 301

		Experiments	ENEA	RSE	SNU	Ansaldo	INEST	Note
Variable	Unit		<i>RELAP5 Mod 3.3</i>	<i>Lego PST</i>	<i>MARS-LBE</i>	<i>RELAP5 mod3.2.2b</i>	<i>RELAP5 mod4.0</i>	
T109	°C	295.2	297.1	295.4	300.6	294.1	296.8	Lower part of downcomer
T102	°C	327.0	325.5	319.5	328.3	322.1	323.7	Heating section outlet
T105	°C	327.3	325.5	321.1	328.3	322.0	323.7	Riser
T106	°C	325.7	325.5	321.1	328.2	322.0	323.7	Tank inlet
T107	°C	326.4	325.5	321.1	328.2	322.0	323.7	Tank
T103	°C	324.6	325.5	321.1	328.2	322.0	323.7	HX inlet
T104	°C	296.2	297.1	295.4	300.6	294.0	296.8	HX outlet
LBE Mass Flow rate	kg/s	4.71	5.28	5.66	5.32	5.19	5.49	
T H ₂ O inlet	°C	35.1	35.1	35.0	35.1	35.1	35.1	
T H ₂ O outlet	°C	75.9	76.0	75.1	75.2	75.9	75.2	
H ₂ O Mass Flow rate	kg/s	0.128	0.128	0.130	0.128	0.129	0.128	
Tank Pressure	bar	-	1.013	1.500	1.000	1.000	1	abs pressure in tank
Tank Level	m	-	0.038	0.520	0.285	0.249	0.193	above the riser outlet

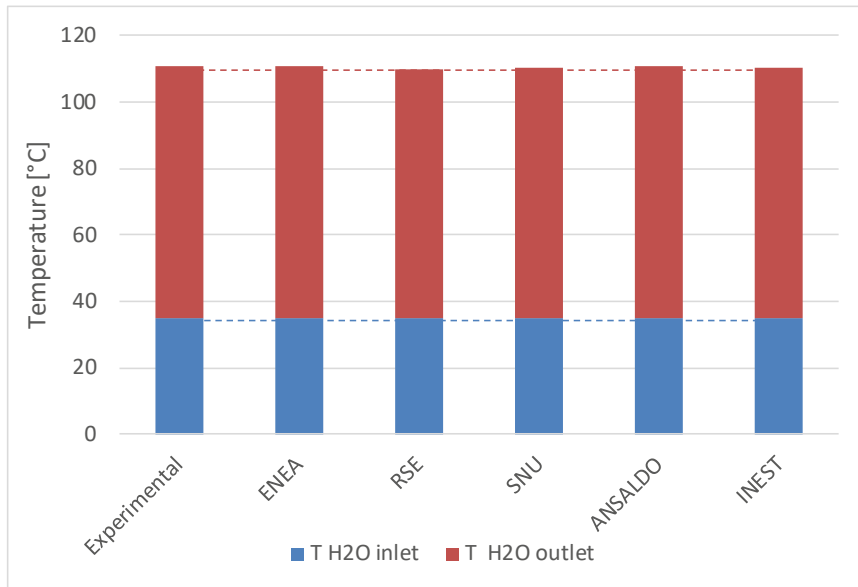
Figure 5.10 plots the LBE temperature distributions along the primary loop from a qualitative point of view. The profiles are in good agreement against the experimental data both in terms of heat-up in the heating section as well as in terms of cooling in the heat exchanger. The highest discrepancy is around 5 °C, meaning a maximum deviation of about 1.5%.

Figure 5.10 – Qualitative comparison of the temperature distributions of NACIE Test 301



In order to understand the slight differences between the experimental data and the simulations, in Figure 5.11 is reported the inlet and outlet temperature comparison of the water in the secondary side, simulated by all the participant as the secondary side of the heat exchanger driven by boundary conditions. While the water mass flow rate and inlet temperature are imposed through the boundary conditions, the outlet temperature results from the simulations. The enthalpy jump in the secondary side is very well reproduced by the participants.

Figure 5.11 – Comparison of the inlet/outlet water temperatures of NACIE Test 301

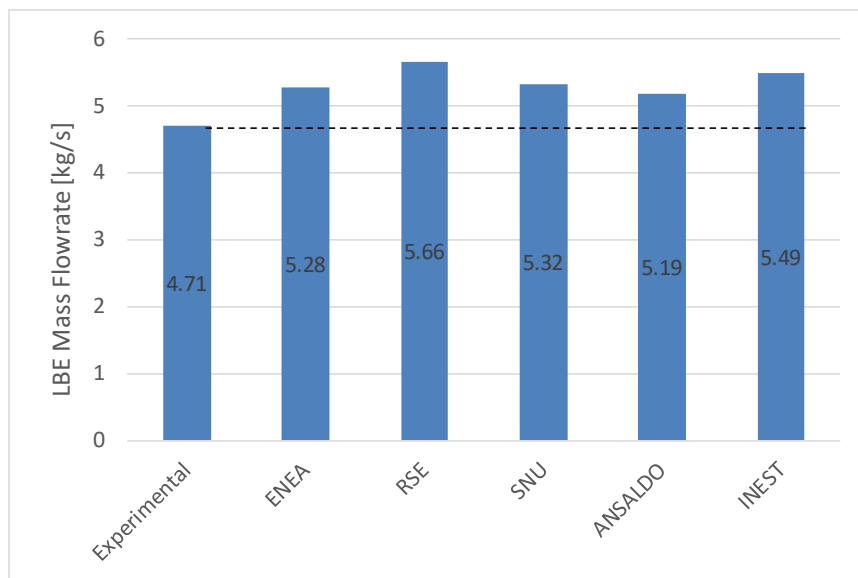


All the simulations are carried out with the same heat transfer correlations for water side, Dittus-Boelter, and LBE side, Seban-Shimazaki. For this reason, the slight differences in the temperature values may be due

also to the slight difference on the thermal conductivity of the steel powder layer in the heat exchanger considered by each participant, that impact heat transfer resistance between the primary and secondary side, besides the differences in flow resistance (at least among the participants).

In Figure 5.12 is reported a graph with the comparison of the LBE mass flow rate in NC calculated by the participants, in which the overestimation of the experimental mass flow rate is evident for all the models with a discrepancy that ranges from 10 to 20%. Since NACIE in this configuration did not implement a mass flowmeter device, the experimental value has been derived through a thermal balance between the inlet and outlet section of the heating region. The thermocouple detections considered are those relative to T109 (inlet) and T102 (outlet) that, as can be seen from the P&I in Appendix A, are positioned quite far from the active heating region. This means that the calculation of the experimental mass flow rate may be affected by large uncertainty due to possible heat losses in the loop section. In other words, the comparison shown in Figure 5.12 is more interesting looking at the comparison among the codes in which the mass flow rate difference is within an acceptable range of 10%.

Figure 5.12 – Comparison of mass flow rates in natural circulation of NACIE Test 301



The benchmark exercise conducted with experimental data of NACIE facility, together with HELIOS, have allowed to test and benchmark different codes and users in the simulations of system cooled by LBE and operating in NC. This is one of the R&D main topic for future nuclear power systems that rely on passive safety feature.

6. Summary and conclusion

6.1 Summary

The LACANES (Lead-Alloy-Cooled Advanced Nuclear Energy Systems) benchmark exercise began in 2007 under the auspices of the Nuclear Energy Agency Nuclear Science Committee with the purpose of carrying out a thermal-hydraulic benchmarking for system analysis computer codes by using experimental data on isothermal forced convection and non-isothermal natural circulation, both obtained from lead-bismuth eutectic (LBE) coolant test loops. The task has been divided in two phases: forced convection (Phase I) and natural circulation (NC; Phase II).

Phase I was completed in 2012 with the publication of the NEA Report on the best practice guidelines for pressure loss coefficient estimation for isothermal forced circulation conditions, based on experimental data obtained from the heavy eutectic liquid metal loop for integral test of operability and safety (HELIOS) test loop located at Seoul National University (SNU). Phase II has been motivated by growing interests in NC capability of lead and lead-alloy systems using the characteristics of the primary cooling mechanism either for pumpless LFR designs and/or for passive cooling under the loss of flow accidents in all LACANES designs.

During Phase II, thermal-hydraulic benchmark studies have been carried out using system codes against a set of natural circulation experiments that were conducted with the HELIOS test loop of SNU, Korea and the NATural Circulation Experiment (NACIE) test loop of the National Agency for New Technologies, Energy and Sustainable Economic Development (ENEA), Italy. Participants in the second phase included the representatives of China, Italy and Korea. This report summarised the objective, rationale, procedures and results of Phase II benchmarks.

As a part of Phase II, a set of three experimental data sets obtained from two test loops including HELIOS of SNU and NACIE of ENEA based on natural circulation (NC) of lead-bismuth eutectic (LBE) have been utilised. Two test data sets with the HELIOS loops and one with the NACIE loop were employed as well-characterised test results for code benchmark activities. Participants of the Phase II were requested to employ the best practice guidelines for pressure loss coefficient estimation given in the Phase I report, to perform modelling for NC. Temperature distributions along the loops, mass flow rates and pressure loss predictions were taken as principal results for comparison with experimental data.

1. Two sets of natural circulation experiments with HELIOS including different mock-up core power ratings of 15.0 kW and 9.8 kW, respectively, provided data sets that can be accepted for Phase II benchmarking. The single NC test set was obtained with NACIE at a heater power rating of 22 kW (referred to as Test #301).
2. Participants established their own benchmark models by closely following the benchmark specifications on the set of three experiments. To ensure a consistent basis on which results can be compared among participants, correlations on wall heat transfer coefficient with LBE and with Dowtherm® cooling oil as well as with ultimate cooling water, respectively, were prescribed by the benchmark controller, SNU.
3. For the experiment at 15.0 kW of heater power with HELIOS (Case I), all four participants predicted temperature, pressure and LBE flow rates that are in agreement with experimental data within about 9% for flow rate and 9% for average temperature difference. All predictions on flow rate were greater than the measurement.

4. For the 9.8 kW of heater power case (Case II) of NACIE with HELIOS, however, a systematic underestimation of LBE temperature distributions was consistently observed by all participants. It was found that the Case II experiment had a low oil flow rate that may have caused flow rate measurement error. Unfortunately, the actual error cannot be estimated due to flowmeter irregularities at low flow rates. The LBE temperature underestimation was corrected by reducing the oil flow rate by 30%. The predicted mass flow rates of LBE were in agreement with experimental data within 10% for all four participants. Total pressure drop under NC is also in good agreement between participants once the temperature distribution was matched.
5. For the estimation of pressure loss coefficients in the case of NACIE, however, no closed-form correlation in the best practice guidelines could properly characterise heater spacer configurations. Therefore, computational fluid dynamics (CFD) calculation was conducted by Ansaldo Nucleare on the form loss coefficient for upper grid in the heating section. When complete, NACIE benchmark results also showed good agreement with experimental data on LBE temperature distributions even though there was uncertainty in the thermophysical properties of metal powder introduced at the gap of the double-wall heat exchanger tube.
6. Mass flow rates predicted by participants are about 10% greater than NACIE measurements. This may be a result of the uncertainty in mass flow rate data that was obtained by indirect measurement through thermal balance between the inlet and outlet sections of the heater region.
7. The overestimation of mass flow rates for both HELIOS and NACIE cases by most models may have been caused by certain inherent characteristics that have not been identified in this work. Future studies on this issue are recommended.

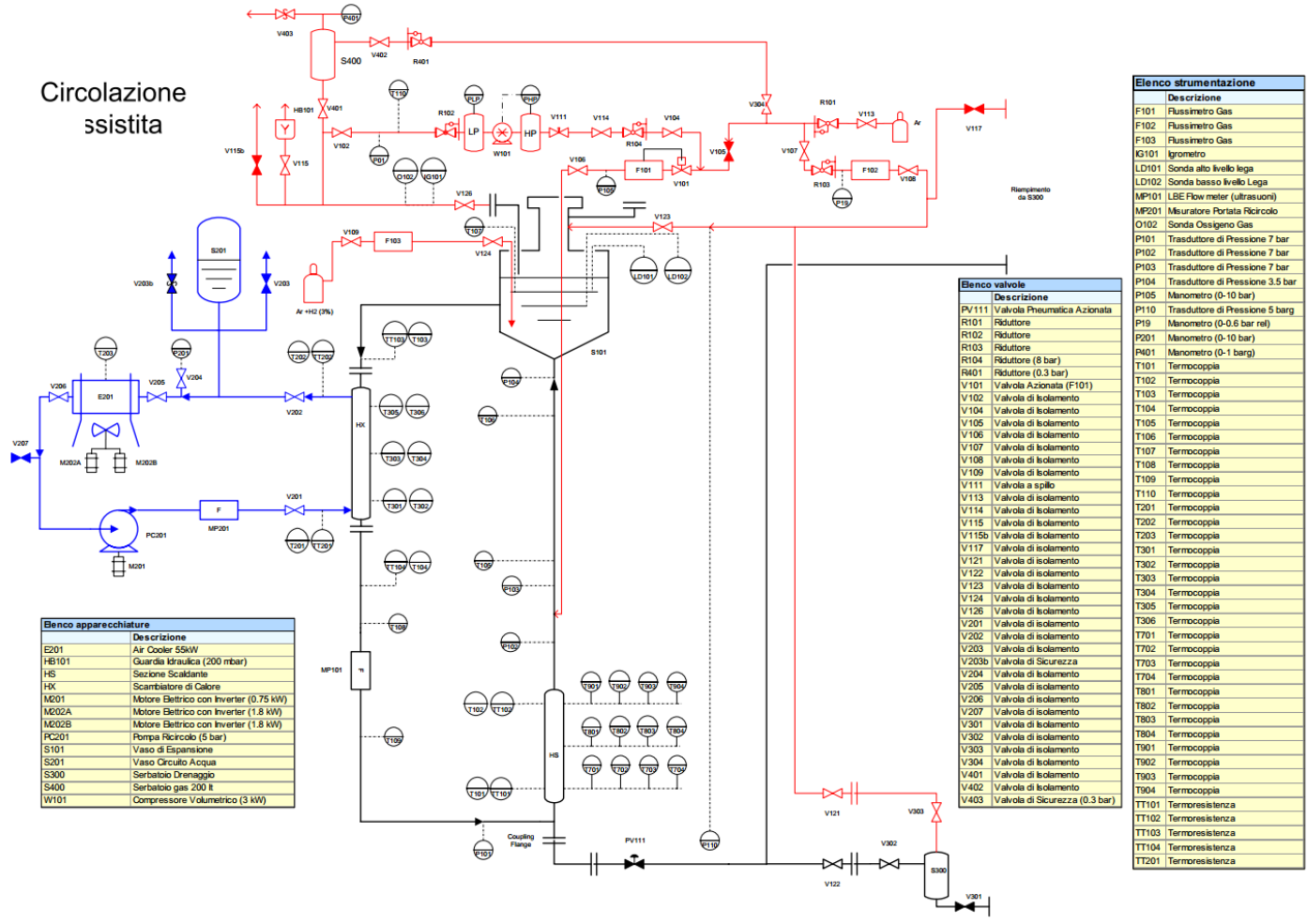
6.2 Conclusion

Lead and lead-bismuth eutectic (LBE) have been widely investigated for the development of Generation IV nuclear reactor coolant owing to their outstanding characteristics: high thermal conductivity, relatively low melting temperature and high boiling temperature, chemical stability with oxidants and good neutron transparency. The engineering designs on lead and lead-alloy-cooled fast reactors (LFR) and accelerator-driven systems (ADS) have been developed as small modular reactors or large-scale nuclear waste transmutation systems. The NEA Task Force on Benchmarking Thermal-Hydraulic Loop Models for Lead-Alloy-Cooled Advanced Nuclear Energy Systems (LACANES) has conducted a thermal-hydraulic benchmark programme launched in 2007 in support of Generation-IV lead fast reactor (LFR) development.

In this LACANES Phase II report, the natural circulation has been studied by a task force consisting of five participants.

Good agreement was found between predicted and measured LBE natural circulation (NC) flow rates for three sets of data produced by the heavy eutectic liquid metal loop for integral test of operability and safety (HELIOS) at Seoul National University (SNU) and the NATural Circulation Experiment (NACIE) at the National Agency for New Technologies, Energy and Sustainable Economic Development (ENEA). However, discrepancies up to 10%, observed in the benchmark, could not be explained and will therefore necessitate further investigations. Advances in modelling of NC through LACANES Phase II have provided a valuable foundation for the development of innovative designs and safety analysis of lead and lead-alloy-cooled advanced nuclear energy systems.

Appendix A: NACIE drawings

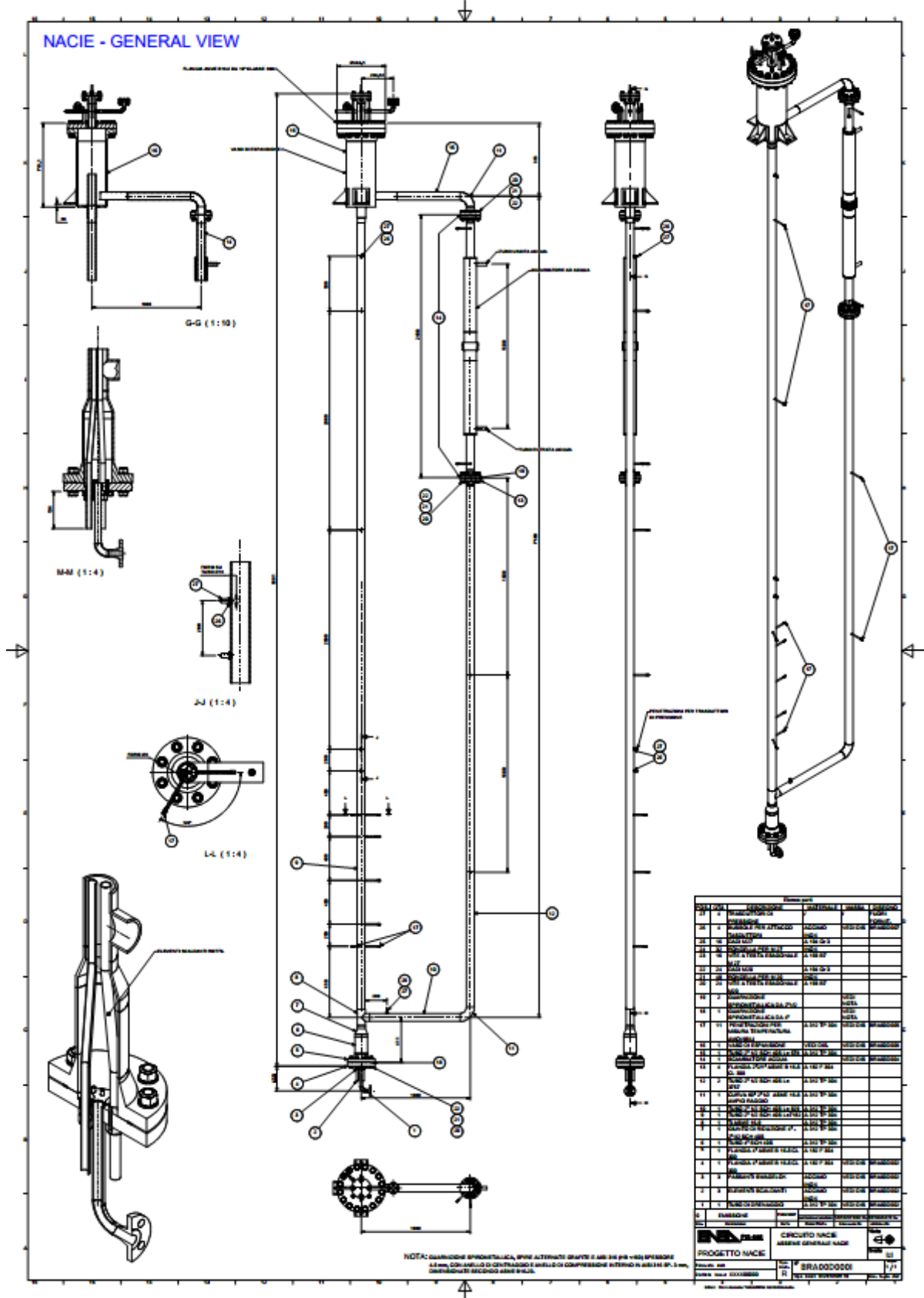


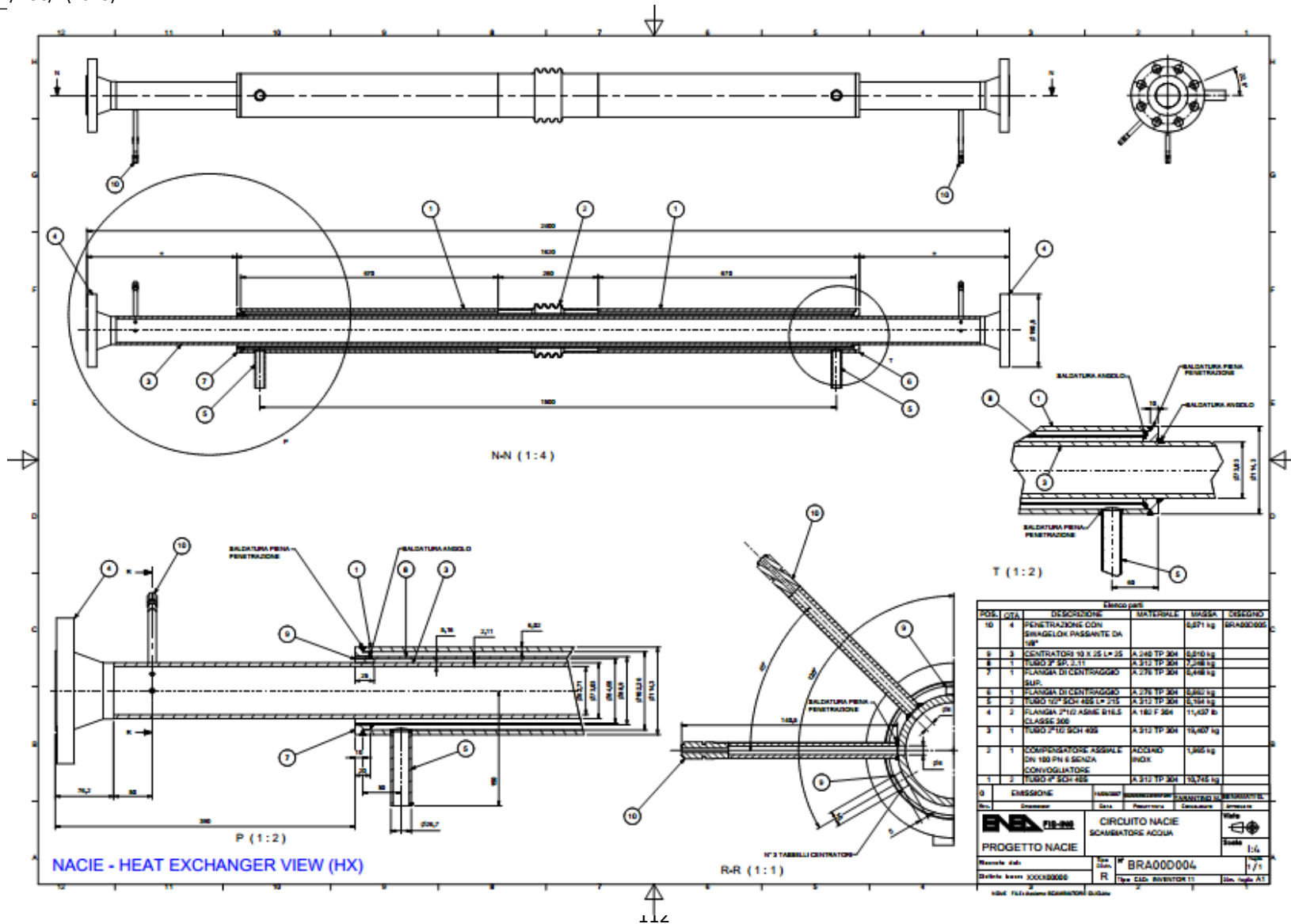
Circolazione assistita

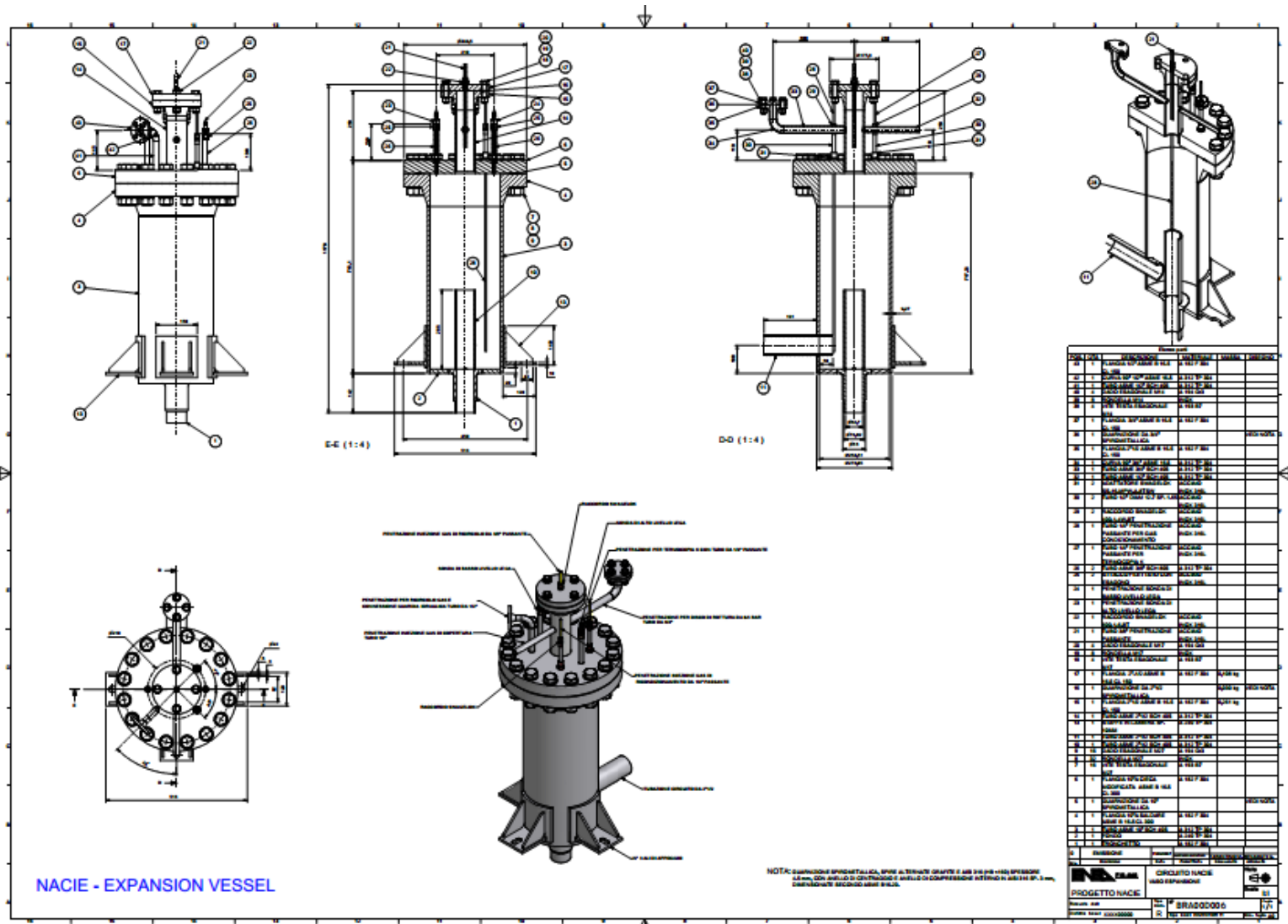
Elenco apparecchiature	
Descrizione	
E201	Air Cooler 55kW
HB101	Guardia Idraulica (200 mbar)
HS	Sezione Scaldante
HX	Scambiatore di Calore
M201	Motore Elettrico con Inverter (0.75 kW)
M202A	Motore Elettrico con Inverter (1.8 kW)
M202B	Motore Elettrico con Inverter (1.8 kW)
PC301	Pompa Ricircolo (5 bar)
S101	Vaso di Espansione
S201	Vaso Circolo Acqua
S300	Serbatoio Drenaggio
S400	Serbatoio gas 200 l
W101	Compressore Volumetrico (3 kW)

Elenco valvole	
Descrizione	
PV111	Valvola Pneumatica Azionata
R101	Riduttore
R102	Riduttore
R103	Riduttore
R104	Riduttore (8 bar)
RA01	Riduttore (0.3 bar)
V101	Valvola Azionata (F101)
V102	Valvola di isolamento
V104	Valvola di isolamento
V105	Valvola di isolamento
V106	Valvola di isolamento
V107	Valvola di isolamento
V108	Valvola di isolamento
V109	Valvola di isolamento
V111	Valvola a spillo
V113	Valvola di isolamento
V114	Valvola di isolamento
V115	Valvola di isolamento
V115b	Valvola di isolamento
V117	Valvola di isolamento
V121	Valvola di isolamento
V122	Valvola di isolamento
V123	Valvola di isolamento
V124	Valvola di isolamento
V126	Valvola di isolamento
V201	Valvola di isolamento
V202	Valvola di isolamento
V203	Valvola di isolamento
V203b	Valvola di Sicurezza
V204	Valvola di isolamento
V205	Valvola di isolamento
V206	Valvola di isolamento
V207	Valvola di isolamento
V301	Valvola di isolamento
V302	Valvola di isolamento
V303	Valvola di isolamento
V304	Valvola di isolamento
V401	Valvola di isolamento
V402	Valvola di isolamento
V403	Valvola di Sicurezza (0.3 bar)

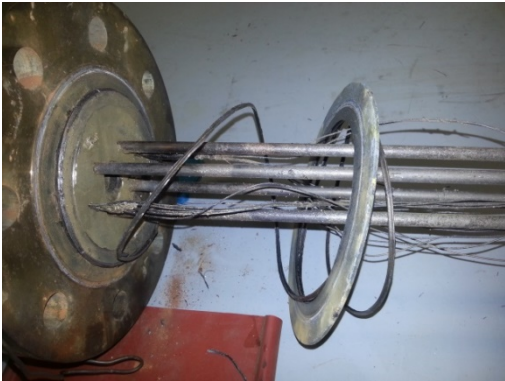
Elenco strumentazione	
Descrizione	
F101	Flussimetro Gas
F102	Flussimetro Gas
F103	Flussimetro Gas
IG101	Igrometro
LD101	Sonda alto livello lega
LD102	Sonda basso livello Lega
MP101	LBE Flow meter (ultrasuoni)
MP201	Msuratore Portata Ricircolo
O102	Sonda Ossigeno Gas
P101	Trasduttore di Pressione 7 bar
P102	Trasduttore di Pressione 7 bar
P103	Trasduttore di Pressione 7 bar
P104	Trasduttore di Pressione 3.5 bar
P105	Manometro (0-10 bar)
P110	Trasduttore di Pressione 5 bar
P19	Manometro (0-0.6 bar rel)
P201	Manometro (0-10 bar)
RA01	Manometro (0-1 bar)
T101	Termocoppia
T102	Termocoppia
T103	Termocoppia
T104	Termocoppia
T105	Termocoppia
T106	Termocoppia
T107	Termocoppia
T108	Termocoppia
T109	Termocoppia
T110	Termocoppia
T201	Termocoppia
T202	Termocoppia
T203	Termocoppia
T301	Termocoppia
T302	Termocoppia
T303	Termocoppia
T304	Termocoppia
T305	Termocoppia
T306	Termocoppia
T701	Termocoppia
T702	Termocoppia
T703	Termocoppia
T704	Termocoppia
T801	Termocoppia
T802	Termocoppia
T803	Termocoppia
T804	Termocoppia
T901	Termocoppia
T902	Termocoppia
T903	Termocoppia
T904	Termocoppia
TT101	Termoresistenza
TT102	Termoresistenza
TT103	Termoresistenza
TT104	Termoresistenza
TT201	Termoresistenza







NACIE rod bundle pictures



Appendix B: HELIOS pressure loss result comparison tables

Table B.1 – Friction loss coefficient (f/l/d) at Case I: 15.0 kW

Sub-part No.	Sub-part name	Part length (mm)	Accumulated length (mm)	Accumulated elevation (mm)	ENE A			RSE			SNU			IN EST		
					f(l/d)	Ref.	Ref. Velocity (m/s)	f(l/d)	Ref.	Ref. Velocity (m/s)	f(l/d)	Ref.	Ref. Velocity (m/s)	f(l/d)	Ref.	Ref. Velocity (m/s)
1-1	Core Inlet	180.7	180.7	0.0	0.0241	*	0.1097	0.1719	**	0.1116	0.0448	***	0.1139	0.0894	****	0.0905
1-2	Downcomer	1222.6	1403.3	-1222.6	0.5920	"	0.0217	1.0499	"	0.0221	0.6005	"	0.0226	0.1974	"	0.0045
1-3	Lower Plenum	212.8	1616.1	-1299.5	0.1254	"	0.1489	0.0649	"	0.0073	0.1160	"	0.0226	0.0133	"	0.0054
1-4	Core	1330.9	2946.9	31.3	1.8740	"	0.1488	6.2454	"	0.1522	2.0234	"	0.1547	0.9376	"	0.2326
1-5	Upper Plenum	681.6	3628.6	713.0	0.3196	"	0.1103	0.6463	"	0.1122	0.3372	"	0.1145	0.3288	"	0.0909
1-6	Gasket [Between Flanges]	4.5	3633.1	717.5	0.0000	"	0.0000							0.0022	"	0.0909
2-1	Pipe [One Side Flange]	300.0	3933.1	1017.5	0.7873	"	0.1103	0.2844	"	0.1122	0.1010	"	0.1145	0.1447	"	0.0909
2-2	Tee	127.0	4060.1	1144.5	0.7873	"	0.1103	0.1204	"	0.1122	0.1010	"	0.1145	0.0613	"	0.0909
2-3	Pipe [One Side Flange]	300.0	4360.1	1444.5	0.7873	"	0.1103	0.2844	"	0.1122	0.1181	"	0.1145	0.1447	"	0.0909
2-4	Gasket [Between Flanges]	4.5	4364.6	1449.0	0.7873	"	0.1103							0.0022	"	0.0909
3-1	Pipe [Both Side Flange]	1000.0	5364.6	2449.0	0.7873	"	0.1103	0.9482	"	0.1122	0.4417	"	0.1145	0.4824	"	0.0909
3-2	Gasket [Between Flanges]	4.5	5369.1	2453.5	0.0000	"	0.0000							0.0022	"	0.0909
4-1	45 Degree Elbow [One Side Flange]	82.5	5451.6	2529.9	0.7818	"	0.1103	0.0000	"	0.0000	0.0627	"	0.1145	0.0368	"	0.0909

4-2	Pipe	180.7	5632.3	2657.6	0.7818	"	0.1103	0.3276	"	0.1122	0.0563	"	0.1145	0.0616	"	0.0909
4-3	45 Degree Elbow	60.0	5692.3	2711.5	0.7818	"	0.1103	0.0000	"	0.0000	0.0701	"	0.1145	0.0260	"	0.0909
4-4	Pipe	718.9	6411.1	3430.4	0.7818	"	0.1103	0.6816	"	0.1122	0.3102	"	0.1145	0.3468	"	0.0909
4-5	Tee	127.0	6538.1	3557.4	0.7818	"	0.1103	0.1204	"	0.1122	0.0698	"	0.1145	0.0613	"	0.0909
4-6	Pipe	171.1	6709.2	3728.5	0.7818	"	0.1103	0.1622	"	0.1122	0.0541	"	0.1145	0.0825	"	0.0909
4-7	45 Degree Elbow	60.0	6769.2	3782.4	0.7818	"	0.1103	0.0000	"	0.0000	0.0563	"	0.1145	0.0260	"	0.0909
4-8	Pipe	180.7	6949.9	3910.1	0.7818	"	0.1103	0.3063	"	0.1122	0.0616	"	0.1145	0.0616	"	0.0909
4-9	45 Degree Elbow [One Side Flange]	82.5	7032.4	3986.5	0.7818	"	0.1103	0.0000	"	0.0000	0.0286	"	0.1145	0.0368	"	0.0909
4-10	Gasket [Between Flanges]	4.5	7036.9	3991.0	0.7818	"	0.1103							0.0022	"	0.0909
5-1	Gate Valve	216.0	7252.9	4207.0	1.7911	"	0.1103	0.0000	"	0.0000	0.1345	"	0.2050	0.1042	"	0.0909
5-2	Gasket [Between Flanges]	4.5	7257.4	4211.5	1.7911	"	0.1103							0.0022	"	0.0909
6-1	Pipe [Both Side Flange]	1000.0	8257.4	5211.5	1.7911	"	0.1103	0.9482	"	0.1122	0.4703	"	0.1145	0.4824	"	0.0909
6-2	Gasket [Between Flanges]	4.5	8261.9	5216.0	1.7911	"	0.1103							0.0022	"	0.0909
7-1	Pipe [Both Side Flange]	1000.0	9261.9	6216.0	1.7911	"	0.1103	0.9482	"	0.1122	0.4703	"	0.1145	0.4824	"	0.0909
7-2	Gasket [Between Flanges]	4.5	9266.4	6220.5	1.7911	"	0.1103							0.0022	"	0.0909
19-1	Pipe [Both Side Flange]	1000.0	10266.4	7220.5	1.7911	"	0.1103	0.9482	"	0.1122	0.4823	"	0.1145	0.4824	"	0.0909

8-4	Gasket [Between Flanges]	4.5	10270.9	7225.0	1.7911	"	0.1103							0.0022	"	0.0909
9-1	Pipe [Both Side Flange]	500.0	10770.9	7725.0	1.7911	"	0.1103	0.4741	"	0.1122	0.2556	"	0.1145	0.2412	"	0.0909
9-2	Gasket [Between Flanges]	4.5	10775.4	7729.5	1.7911	"	0.1103							0.0022	"	0.0909
10-1	Expansion Tank	868.2	11643.6	7933.8	0.2954	"	0.1103	0.5526	"	0.1122	0.2700	"	0.1145	0.0986	"	0.0909
10-2	Gasket [Between Flanges]	4.5	11648.1	7933.8	0.0000	"	0.0000							0.0022	"	0.0909
11-1	Pipe [Both Side Flange]	500.0	12148.1	7933.8	0.2383	"	0.1103	0.4741	"	0.1122	0.2469	"	0.1145	0.2412	"	0.0909
11-2	Gasket [Between Flanges]	4.5	12152.6	7933.8	0.0000	"	0.0000							0.0022	"	0.0909
12-1	Pipe [One Side Flange]	300.0	12452.6	7933.8	0.9902	"	0.1103	0.2844	"	0.1122	0.1010	"	0.1145	0.1447	"	0.0909
12-2	Tee	127.0	12579.6	7933.8	0.9902	"	0.1103	0.1204	"	0.1122	0.1012	"	0.1145	0.0613	"	0.0909
12-3	Pipe	305.4	12885.0	7933.8	0.9902	"	0.1103	0.2896	"	0.1122	0.0996	"	0.1145	0.1473	"	0.0909
12-4	90 Degree Elbow	120.0	13005.0	7857.6	0.9902	"	0.1103	0.2270	"	0.1122	0.0562	"	0.1145	0.0368	"	0.0909
12-5	90 Degree Elbow	120.0	13125.0	7781.4	0.9902	"	0.1103	0.2270	"	0.1122	0.0760	"	0.1145	0.0368	"	0.0909
12-6	Pipe [One Side Flange]	200.0	13325.0	7781.4	0.9902	"	0.1103	0.1896	"	0.1122	0.0563	"	0.1145	0.0965	"	0.0909
12-7	Gasket [Between Flanges]	4.5	13329.5	7781.4	0.9902	"	0.1103							0.0022	"	0.0909
13-1	Gate Valve	216.0	13545.5	7781.4	0.9902	"	0.1103	0.0000	"	0.0000	0.1351	"	0.2050	0.0915	"	0.1627

13-2	Gasket [Between Flanges]	4.5	13550.0	7781.4	0.9902	"	0.1103							0.0019	"	0.1627
14-1	Pipe [One Side Flange]	200.0	13750.0	7781.4	0.9902	"	0.1103	0.2370	"	0.1122	0.0776	"	0.1145	0.0965	"	0.0909
14-2	Tee	127.0	13877.0	7781.4	0.9902	"	0.1103	0.1204	"	0.1122	0.0745	"	0.1145	0.0613	"	0.0909
14-3	Pipe [One Side Flange]	382.3	14259.3	7781.4	0.9902	"	0.1103	0.3625	"	0.1122	0.1827	"	0.1145	0.1844	"	0.0909
14-4	Gasket [Between Flanges]	4.5	14263.8	7781.4	0.9902	"	0.1103							0.0022	"	0.0909
15-1	Heat Exchanger Vessel Inlet	202.5	14466.3	7781.4	0.0345	"	0.1103	0.1320	"	0.1122	0.0506	"	0.1145	0.0977	"	0.0909
15-2	Heat Exchanger Internal	2010.5	16476.8	5770.9	0.9494	"	0.0197	1.6192	"	0.0199	0.8591	"	0.0204	1.2341	"	0.0213
15-3	Heat Exchanger Outlet	202.5	16679.3	5770.9	0.0390	"	0.1103	0.1324	"	0.1116	0.1024	"	0.1139	0.1002	"	0.0905
15-4	Gasket [Between Flanges]	4.5	16683.8	5770.9	0.0000	"	0.0000							0.0011	"	0.0905
16-1	Pipe [One Side Flange]	219.8	16903.6	5770.9	1.9558	"	0.1097	0.2090	"	0.1116	0.0815	"	0.1139	0.0708	"	0.0905
16-2	90 Degree Elbow	120.0	17023.6	5694.7	1.9558	"	0.1097	0.1138	"	0.1116	0.0759	"	0.1139	0.0245	"	0.0905
16-3	Pipe	785.5	17809.1	4909.2	1.9558	"	0.1097	0.7471	"	0.1116	0.3603	"	0.1139	0.2529	"	0.0905
16-4	Tee	127.0	17936.1	4782.2	1.9558	"	0.1097	0.1208	"	0.1116	0.0910	"	0.1139	0.0409	"	0.0905
16-5	Pipe [One Side Flange]	500.0	18436.1	4282.2	1.9558	"	0.1097	0.4755	"	0.1116	0.1902	"	0.1139	0.1610	"	0.0905
16-6	Gasket [Between Flanges]	4.5	18440.6	4277.7	1.9558	"	0.1097							0.0014	"	0.0905

17-1	Gate Valve	216.0	18656.6	4061.7	1.9558	"	0.1097	0.0000	"	0.0000	0.1498	"	0.2038	0.1068	"	0.0905
17-2	Gasket [Between Flanges]	4.5	18661.1	4057.2	1.9558	"	0.1097							0.0022	"	0.0905
18-1	Pipe[One Side Flange]	500.0	19161.1	3557.2	1.9558	"	0.1097	0.4755	"	0.1116	0.2120	"	0.1139	0.2473	"	0.0905
18-2	Tee	127.0	19288.1	3430.2	1.9558	"	0.1097	0.1208	"	0.1116	0.0904	"	0.1139	0.0628	"	0.0905
18-3	Pipe [One Side Flange]	500.0	19788.1	2930.2	1.9558	"	0.1097	0.4755	"	0.1116	0.2290	"	0.1139	0.2473	"	0.0905
18-4	Gasket [Between Flanges]	4.5	19792.6	2925.7	1.9558	"	0.1097							0.0022	"	0.0905
8-1	Pipe [One Side Flange]	200.0	19992.6	2725.7	1.9558	"	0.1097	0.1902	"	0.1116	0.1014	"	0.1139	0.0989	"	0.0905
8-2	Orifice	600.0	20592.6	2125.7	1.9558	"	0.1097	0.5232	"	0.0977	0.2382	"	0.0997	0.2968	"	0.0905
8-3	Pipe [One Side Flange]	200.0	20792.6	1925.7	1.9558	"	0.1097	0.1902	"	0.1116	0.1090	"	0.1139	0.0989	"	0.0905
19-2	Gasket [Between Flanges]	4.5	20797.1	1921.2	1.9558	"	0.1097							0.0022	"	0.0905
20-1	Pipe[One Side Flange]	500.0	21297.1	1421.2	0.2858	"	0.1097	0.4755	"	0.1116	0.2104	"	0.1139	0.2473	"	0.0905
20-2	Tee	127.0	21424.1	1357.0	1.7422	"	0.1097	0.2740	"	0.1116	0.0555	"	0.1139	0.0317	"	0.0905
20-3	Pipe [One Side Flange]	100.0	21524.1	1357.0	1.7422	"	0.1097	0.0000	"	0.0000	0.0856	"	0.1139	0.0495	"	0.0905
20-4	Gasket [Between Flanges]	4.5	21528.6	1357.0	1.7422	"	0.1097							0.0022	"	0.0905

21-1	Pipe [One Side Flange]	757.1	22285.7	1357.0	1.7422	"	0.1097	0.7201	"	0.1116	0.3316	"	0.1139	0.3745	"	0.0905
21-2	90 Degree Elbow	120.0	22405.7	1280.8	1.7422	"	0.1097	0.2277	"	0.1116	0.0770	"	0.1139	0.0377	"	0.0905
21-3	Pipe	1204.6	23610.3	76.2	1.7422	"	0.1097	1.1457	"	0.1116	0.5587	"	0.1139	0.5959	"	0.0905
21-4	90 Degree Elbow	120.0	23730.3	0.0	1.7422	"	0.1097	0.2277	"	0.1116	0.0961	"	0.1139	0.0377	"	0.0905
21-5	Pipe [One Side Flange]	276.3	24006.6	0.0	1.7422	"	0.1097	0.2627	"	0.1116	0.0760	"	0.1139	0.1367	"	0.0905
21-6	Gasket [Between Flanges]	4.5	24011.1	0.0	1.7422	"	0.1097							0.0022	"	0.0905
22-1	Gate Valve	216.0	24227.1	0.0	1.7422	"	0.1097	0.0000	"	0.0000	0.1144	"	0.2038	0.1068	"	0.0905
22-2	Gasket [Between Flanges]	4.5	24231.6	0.0	1.7422	"	0.1097							0.0022	"	0.0905
23-1	Pipe [One Side Flange]	100.0	24331.6	0.0	1.7422	"	0.1097	0.2737	"	0.1116	0.0555	"	0.1139	0.0495	"	0.0905
23-2	Tee	127.0	24458.6	0.0	1.7422	"	0.1097	0.0000	"	0.0000	0.0449	"	0.1139	0.0628	"	0.0905
23-3	45 Degree Elbow	60.0	24518.6	0.0	0.2382	"	0.1097	0.0768	"	0.1116	0.0577	"	0.1139	0.0297	"	0.0905
23-4	Pipe	180.7	24699.2	0.0	0.2382	"	0.1097	0.1536	"	0.1116	0.0642	"	0.1139	0.0894	"	0.0905
23-5	45 Degree Elbow [One Side Flange]	82.5	24781.7	0.0	0.2382	"	0.1097	0.0768	"	0.1116	0.0642	"	0.1139	0.0408	"	0.0905
23-6	Gasket [Between Flanges]	4.5	24786.2	0.0	0.0000	"	0.0000	0.0000	"	0.0000	0.0000	"	0.0000	0.0022	"	0.0905

- * Zigrang-Sylvester approximation of Colebrook-White correlation, calculated by RELAP5 mod3.3
- ** Colebrook-White correlation, calculated by LegoPST
- *** Colebrook-White correlation, calculated by MARS-LBE 3.11
- **** Zigrang-Sylvester correlation, calculated by RELAP5 MOD 4.0

Table B.2 – Form loss coefficient (K) at Case I: 15.0 kW

Connection/ point	ENEA			RSE			SNU			INEST		
	K	Ref.	Ref. Velocity (m/s)	K	Ref.	Ref. Velocity (m/s)	K	Ref.	Ref. Velocity (m/s)	K	Ref.	Ref. Velocity (m/s)
23-6 → 1-1	0.4978	Idelchik I.E, Handbook of Hydraulic Resistance, 3 rd edition, Jaico Publishing House, 2003	0.1097							0.0042	Trubenok, V.D.	0.1050
1-1 → 1-2	0.9942	Idelchik I.E, Handbook of Hydraulic Resistance, 3 rd edition, Jaico Publishing House, 2003	0.1097	1.1390	Idelchik I.E, Handbook of Hydraulic Resistance, 3 rd edition, CRC press, 1994, calculated by MARS-LBE 3.11	0.1116	0.6996	Idelchik I.E, Handbook of Hydraulic Resistance, 3 rd edition, CRC press, 1994, calculated by MARS-LBE 3.11	0.1139	1.2900	Verein Deutscher Ingenieure, VDI	0.1050
1-2 → 1-3	0.4064	Idelchik I.E, Handbook of Hydraulic Resistance, 3 rd edition, Jaico Publishing House, 2003	0.0217	0.4910	Idelchik I.E, Handbook of Hydraulic Resistance, 3 rd edition, CRC press, 1994, calculated by MARS-LBE 3.11	0.0221	0.3959	Idelchik I.E, Handbook of Hydraulic Resistance, 3 rd edition, CRC press, 1994, calculated by MARS-LBE 3.11	0.1546	0.0388	Idelchik I.E	0.0062
1-3 → 1-4	0.4557	Idelchik I.E, Handbook of Hydraulic Resistance, 3 rd edition, Jaico Publishing House, 2003	0.1488	0.6260	Idelchik I.E, Handbook of Hydraulic Resistance, 3 rd edition, CRC press, 1994, calculated by MARS-LBE 3.12	0.0073				0.4839	Idelchik I.E	0.2694
in 1-4	10.4929	Rehme, K., Pressure Drop Correlations for Fuel Element Spacers, Nuclear Technology, Vol.17, pp.15-23, 1973	0.1492	11.8698	Rehme, K., Pressure Drop Correlations for Fuel Element Spacers, Nuclear Technology, Vol.17, pp.15-23, 1973 – Drag coefficient modified according to phase I	0.1522	4.5243	Rehme, K., Pressure Drop Correlations for Fuel Element Spacers, Nuclear Technology, Vol.17, pp.15-23, 1973	0.1548	2.1324*3	Idelchik I.E	0.2703
1-4 → 1-5	0.0692	Idelchik I.E, Handbook of Hydraulic Resistance, 3 rd edition, Jaico Publishing House, 2003	0.1497	0.0690	Idelchik I.E, Handbook of Hydraulic Resistance, 3 rd edition, CRC press, 1994, calculated by MARS-LBE 3.11	0.1523	0.0736	Idelchik I.E, Handbook of Hydraulic Resistance, 3 rd edition, CRC press, 1994, calculated by MARS-LBE 3.11	0.1554			

1-5 → 1-6										0.0042	Trubenok, V.D.	0.1057
1-6 → 2.1	0.4978	Idelchik I.E., Handbook of Hydraulic Resistance, 3 rd edition, Jaico Publishing House, 2003	0.1103									
in 2-2												
2-3 → 2-4										0.0042	Trubenok, V.D.	0.1057
2-4 → 3-1	0.4978	Idelchik I.E., Handbook of Hydraulic Resistance, 3 rd edition, Jaico Publishing House, 2003	0.1103									
3-1 → 3-2										0.0042	Trubenok, V.D.	0.1057
3-2 → 4-1	0.4978	Idelchik I.E., Handbook of Hydraulic Resistance, 3 rd edition, Jaico Publishing House, 2003	0.1103									
in 4-1	0.1359	Idelchik I.E., Handbook of Hydraulic Resistance, 3 rd edition, Jaico Publishing House, 2003	0.1103	0.0993	Nippert, H., Über den Stromungsverlust in gekrümmten Kanälen, Forschungsarb. Geb. Ingenieurwes, no. 320, VDI, 1922, 85pp	0.1122	0.2161	Nippert, H., Über den Stromungsverlust in gekrümmten Kanälen, Forschungsarb. Geb. Ingenieurwes, no. 320, VDI, 1922, 85pp	0.1145	0.1678	Nippert H.	0.1057
in 4-3	0.1359	Idelchik I.E., Handbook of Hydraulic Resistance, 3 rd edition, Jaico Publishing House, 2003	0.1103	0.0993	Nippert, H., Über den Stromungsverlust in gekrümmten Kanälen, Forschungsarb. Geb. Ingenieurwes, no. 320, VDI, 1922, 85pp	0.1122	0.2161	Nippert, H., Über den Stromungsverlust in gekrümmten Kanälen, Forschungsarb. Geb. Ingenieurwes, no. 320, VDI, 1922, 85pp	0.1145			
in 4-5												
in 4-7	0.1359	Idelchik I.E., Handbook of Hydraulic Resistance, 3 rd edition, Jaico Publishing House, 2003	0.1103	0.0993	Nippert, H., Über den Stromungsverlust in gekrümmten Kanälen, Forschungsarb. Geb. Ingenieurwes, no. 320, VDI, 1922, 85pp	0.1122	0.2161	Nippert, H., Über den Stromungsverlust in gekrümmten Kanälen, Forschungsarb. Geb. Ingenieurwes, no. 320, VDI, 1922, 85pp	0.1145	0.1678	Nippert H.	0.1057

in 4-9	0.1359	Idelchik I.E, Handbook of Hydraulic Resistance, 3 rd edition, Jaico Publishing House, 2003	0.1103	0.0993	Nippert, H., Über den Stromungsverlust in gekrümmten Kanälen, Forschungsarb. Geb. Ingenieurwes, no. 320, VDI, 1922, 85pp	0.1122			0.1678	Nippert H.	0.1057	
4-9 → 4-10									0.0042	Trubenok, V.D.	0.1057	
4-10 → 5-1	0.4718	Idelchik I.E, Handbook of Hydraulic Resistance, 3 rd edition, Jaico Publishing House, 2003	0.1103			0.2257		Idelchik I.E, Handbook of Hydraulic Resistance, 3 rd edition, CRC press, 1994, calculated by MARS-LBE 3.11	0.1145			
in 5-1	0.1960	Idelchik I.E, Handbook of Hydraulic Resistance, 3 rd edition, Jaico Publishing House, 2003	0.1975	0.3900	Emerson – Fisher, Control valve handbook, 4 th edition / ISA 75.01.01 – 2007, Flow equation for sizing control valves (tuning according to phase I)	0.0000	0.5119	Idelchik I.E, Handbook of Hydraulic Resistance, 3 rd edition, CRC press, 1994, calculated by MARS-LBE 3.11	0.2050	0.1969	B.S.Massey	0.1057
5-1 → 5-2							0.0127	Idelchik I.E, Handbook of Hydraulic Resistance, 3 rd edition, CRC press, 1994, calculated by MARS-LBE 3.11	0.1145	0.0042	Trubenok, V.D.	0.1057
5-2 → 6-1	0.4487	Idelchik I.E, Handbook of Hydraulic Resistance, 3 rd edition, Jaico Publishing House, 2003	0.1103									
6-1 → 6-2									0.0042	Trubenok, V.D.	0.1057	
6-2 → 7-1	0.4978	Idelchik I.E, Handbook of Hydraulic Resistance, 3 rd edition, Jaico Publishing House, 2003	0.1103									
7-1 → 7-2									0.0042	Trubenok, V.D.	0.1057	
7-2 → 19-1												
19-1 → 8-4									0.0042	Trubenok, V.D.	0.1057	
8-4 → 9-1	0.4978	Idelchik I.E, Handbook of Hydraulic Resistance, 3 rd edition, Jaico Publishing House, 2003	0.1103									

9-1 → 9-2												
9-2 → 10-1	0.4978	Idelchik I.E, Handbook of Hydraulic Resistance, 3 rd edition, Jaico Publishing House, 2003	0.1103	1.0000	Idelchik I.E, Handbook of Hydraulic Resistance, 3 rd edition, CRC press, 1994, calculated by MARS-LBE 3.11	0.1122	0.9761	Idelchik I.E, Handbook of Hydraulic Resistance, 3 rd edition, CRC press, 1994, calculated by MARS-LBE 3.11	0.1145	0.0042	Trubenok, V.D.	0.1057
in 10-1	1.6572	Idelchik I.E, Handbook of Hydraulic Resistance, 3 rd edition, Jaico Publishing House, 2003	0.1103	0.7735	Idelchik I.E, Handbook of Hydraulic Resistance, 3 rd edition, CRC press, 1994, calculated by MARS-LBE 3.11	0.1122	0.3808	Idelchik I.E, Handbook of Hydraulic Resistance, 3 rd edition, CRC press, 1994, calculated by MARS-LBE 3.11	0.1145			
10-1 → 10-2							0.4083	Idelchik I.E, Handbook of Hydraulic Resistance, 3 rd edition, CRC press, 1994, calculated by MARS-LBE 3.11	0.1145	0.9482	Idelchik I.E	0.1057
10-2 → 11-1	0.4978	Idelchik I.E, Handbook of Hydraulic Resistance, 3 rd edition, Jaico Publishing House, 2003	0.1103							0.4818	B.S.Massey	0.1057
11-1 → 11-2										0.0042	Trubenok, V.D.	0.1057
11-2 → 12-1	0.4978	Idelchik I.E, Handbook of Hydraulic Resistance, 3 rd edition, Jaico Publishing House, 2003	0.1103									
in 12-2												
in 12-4	0.2222	Idelchik I.E, Handbook of Hydraulic Resistance, 3 rd edition, Jaico Publishing House, 2003	0.1103	0.2735	Nippert, H., Über den Stromungsverlust in gekrümmten Kanälen, Forschungsarb. Geb. Ingenieurwes, no. 320, VDI, 1922, 85pp	0.1122	0.3808	Nippert, H., Über den Stromungsverlust in gekrümmten Kanälen, Forschungsarb. Geb. Ingenieurwes, no. 320, VDI, 1922, 85pp	0.1145	0.2661	Nippert H.	0.1057
in 12-5	0.2222	Idelchik I.E, Handbook of Hydraulic Resistance, 3 rd edition, Jaico Publishing House, 2003	0.1103	0.2735	Nippert, H., Über den Stromungsverlust in gekrümmten Kanälen, Forschungsarb. Geb. Ingenieurwes, no. 320, VDI, 1922, 85pp	0.1122	0.3808	Nippert, H., Über den Stromungsverlust in gekrümmten Kanälen, Forschungsarb. Geb. Ingenieurwes, no. 320, VDI, 1922, 85pp	0.1145	0.2661	Nippert H.	0.1057
12-6 → 12-7										0.0042	Trubenok, V.D.	0.1057

12-7 → 13-1	0.4718	Idelchik I.E, Handbook of Hydraulic Resistance, 3 rd edition, Jaico Publishing House, 2003	0.1103				0.0096	Idelchik I.E, Handbook of Hydraulic Resistance, 3 rd edition, CRC press, 1994, calculated by MARS-LBE 3.11	0.1145	0.1969	B.S.Massey	0.1057
in 13-1	0.1960	Idelchik I.E, Handbook of Hydraulic Resistance, 3 rd edition, Jaico Publishing House, 2003	0.1975	0.3900	Emerson – Fisher, Control valve handbook, 4 th edition / ISA 75.01.01 – 2007, Flow equation for sizing control valves (tuning according to phase I)	0.0000	0.5119	Idelchik I.E, Handbook of Hydraulic Resistance, 3 rd edition, CRC press, 1994, calculated by MARS-LBE 3.11	0.2050	0.2438	Idelchik I.E	0.1057
13-1 → 13-2							0.0127	Idelchik I.E, Handbook of Hydraulic Resistance, 3 rd edition, CRC press, 1994, calculated by MARS-LBE 3.11	0.1145			
13-2 → 14-1	0.4487	Idelchik I.E, Handbook of Hydraulic Resistance, 3 rd edition, Jaico Publishing House, 2003	0.1103							0.0042	Trubenok, V.D.	0.1057
in 14-2												
14-3 → 14-4										0.0042	Trubenok, V.D.	0.1057
14-4 → 15-1	0.4978	Idelchik I.E, Handbook of Hydraulic Resistance, 3 rd edition, Jaico Publishing House, 2003	0.1103									
15-1 → 15-2	0.4972	Idelchik I.E, Handbook of Hydraulic Resistance, 3 rd edition, Jaico Publishing House, 2003	0.1103	1.0000	Idelchik I.E, Handbook of Hydraulic Resistance, 3 rd edition, CRC press, 1994, calculated by MARS-LBE 3.11	0.1122	0.7331	Idelchik I.E, Handbook of Hydraulic Resistance, 3 rd edition, CRC press, 1994, calculated by MARS-LBE 3.11	0.1145	1.2900	Verein Deutscher Ingenieure, VDI	0.1057
in 15-2	9.0360	Rehme, K., Pressure Drop Correlations for Fuel Element Spacers, Nuclear Technology, Vol.17, pp.15-23, 1973	0.0196	12.2990	Rehme, K., Pressure Drop Correlations for Fuel Element Spacers, Nuclear Technology, Vol.17, pp.15-23, 1973	0.0200	5.9738	Rehme, K., Pressure Drop Correlations for Fuel Element Spacers, Nuclear Technology, Vol.17, pp.15-23, 1973	0.0204	1.297445* 6	Idelchik I.E	0.1057

15-2 → 15-3	0.3526	Idelchik I.E, Handbook of Hydraulic Resistance, 3 rd edition, Jaico Publishing House, 2003	0.1097			0.4012	Idelchik I.E, Handbook of Hydraulic Resistance, 3 rd edition, CRC press, 1994, calculated by MARS-LBE 3.11	0.1139	1.2900	Verein Deutscher Ingenieure, VDI	0.0248	
15-3 → 15-4				0.5000	Idelchik I.E, Handbook of Hydraulic Resistance, 3 rd edition, CRC press, 1994, calculated by MARS-LBE 3.11	0.1122			0.0042	Trubenok, V.D.	0.1050	
15-4 → 16-1	0.4978	Idelchik I.E, Handbook of Hydraulic Resistance, 3 rd edition, Jaico Publishing House, 2003	0.1097									
in 16-2	0.2222	Idelchik I.E, Handbook of Hydraulic Resistance, 3 rd edition, Jaico Publishing House, 2003	0.1097	0.2789	Nippert, H., Über den Stromungsverlust in gekrümmten Kanälen, Forschungsarb. Geb. Ingenieurwes, no. 320, VDI, 1922, 85pp	0.1116	0.3810	Nippert, H., Über den Stromungsverlust in gekrümmten Kanälen, Forschungsarb. Geb. Ingenieurwes, no. 320, VDI, 1922, 85pp	0.1139	0.2661	Nippert H.	0.1050
in 16-4												
16-5 → 16-6									0.0042	Trubenok, V.D.	0.1050	
16-6 → 17-1	0.4718	Idelchik I.E, Handbook of Hydraulic Resistance, 3 rd edition, Jaico Publishing House, 2003	0.1963				0.0096	Idelchik I.E, Handbook of Hydraulic Resistance, 3 rd edition, CRC press, 1994, calculated by MARS-LBE 3.11	0.1139			
in 17-1	0.1960	Idelchik I.E, Handbook of Hydraulic Resistance, 3 rd edition, Jaico Publishing House, 2003	0.1097	0.3900	Emerson – Fisher, Control valve handbook, 4 th edition / ISA 75.01.01 – 2007, Flow equation for sizing control valves (tuning according to phase I)	0.0000	0.5121	Idelchik I.E, Handbook of Hydraulic Resistance, 3 rd edition, CRC press, 1994, calculated by MARS-LBE 3.11	0.2038	0.4406	B.S.Massey, Idelchik I.E	0.1050
17-1 → 17-2							0.0127	Idelchik I.E, Handbook of Hydraulic Resistance, 3 rd edition, CRC press, 1994, calculated by MARS-LBE 3.11	0.1139	0.0042	Trubenok, V.D.	0.1050

17-2 → 18-1	0.4487	Idelchik I.E, Handbook of Hydraulic Resistance, 3 rd edition, Jaico Publishing House, 2003	0.1097									
in 18-2												
18-3 → 18-4	0.4978	Idelchik I.E, Handbook of Hydraulic Resistance, 3 rd edition, Jaico Publishing House, 2003	0.1097							0.0042	Trubenok, V.D.	0.1050
18-4 → 8-1	0.4648	Idelchik I.E, Handbook of Hydraulic Resistance, 3 rd edition, Jaico Publishing House, 2003	0.1097	0.0155	Idelchik I.E, Handbook of Hydraulic Resistance, 3 rd edition, CRC press, 1994, calculated by MARS-LBE 3.11	0.1116	0.0169	Idelchik I.E, Handbook of Hydraulic Resistance, 3 rd edition, CRC press, 1994, calculated by MARS-LBE 3.11	0.1139			
in 8-2	10.2020	Idelchik, I.E., Determination of the resistance coefficients during discharge through orifices	0.0960	10.4250	Idelchik, I.E., Determination of the resistance coefficients during discharge through orifices, Gidrotekh. Stroit., no. 5, 31-36, 1953	0.2594	11.4725	Idelchik, I.E., Determination of the resistance coefficients during discharge through orifices, Gidrotekh. Stroit., no. 5, 31-36, 1953	0.0997	0.4460	Idelchik I.E	0.1050
8-3 → 19-2	0.4318	Idelchik I.E, Handbook of Hydraulic Resistance, 3 rd edition, Jaico Publishing House, 2003	0.0960	0.1047	Idelchik I.E, Handbook of Hydraulic Resistance, 3 rd edition, CRC press, 1994, calculated by MARS-LBE 3.11	0.0977	0.0223	Idelchik I.E, Handbook of Hydraulic Resistance, 3 rd edition, CRC press, 1994, calculated by MARS-LBE 3.11	0.1139	0.0042	Trubenok, V.D.	0.1050
19-2 → 20-1	0.4978	Idelchik I.E, Handbook of Hydraulic Resistance, 3 rd edition, Jaico Publishing House, 2003	0.1097									
in 20-2	0.7200	Idelchik I.E, Handbook of Hydraulic Resistance, 3 rd edition, Jaico Publishing House, 2003	0.1097	1.2900	Verein Deutscher Ingenieure, VDIWärmeatlas 3.0, Springer Verlag, Berlin Heidelberg, 2006	0.1116	1.4033	Verein Deutscher Ingenieure, VDIWärmeatlas 3.0, Springer Verlag, Berlin Heidelberg, 2006	0.1139	1.2900	Verein Deutscher Ingenieure, VDI	0.1050
20-3 → 20-4										0.0042	Trubenok, V.D.	0.1050
20-4 → 21-1	0.4978	Idelchik I.E, Handbook of Hydraulic Resistance, 3 rd edition, Jaico Publishing House, 2003	0.1097									

in 21-2	0.2222	Idelchik I.E, Handbook of Hydraulic Resistance, 3 rd edition, Jaico Publishing House, 2003	0.1097	0.2789	Nippert, H., Über den Stromungsverlust in gekrümmten Kanälen, Forschungsarb. Geb. Ingenieurwes, no. 320, VDI, 1922, 85pp	0.1116	0.3810	Nippert, H., Über den Stromungsverlust in gekrümmten Kanälen, Forschungsarb. Geb. Ingenieurwes, no. 320, VDI, 1922, 85pp	0.1139	0.2661	Nippert H.	0.1050
in 21-4	0.2222	Idelchik I.E, Handbook of Hydraulic Resistance, 3 rd edition, Jaico Publishing House, 2003	0.1097	0.2791	Nippert, H., Über den Stromungsverlust in gekrümmten Kanälen, Forschungsarb. Geb. Ingenieurwes, no. 320, VDI, 1922, 85pp	0.1116	0.3810	Nippert, H., Über den Stromungsverlust in gekrümmten Kanälen, Forschungsarb. Geb. Ingenieurwes, no. 320, VDI, 1922, 85pp	0.1139	0.2661	Nippert H.	0.1050
21-5 → 21-6										0.0042	Trubenok, V.D.	0.1050
21-6 → 22-1	0.4978	Idelchik I.E, Handbook of Hydraulic Resistance, 3 rd edition, Jaico Publishing House, 2003	0.1097				0.0096	Idelchik I.E, Handbook of Hydraulic Resistance, 3 rd edition, CRC press, 1994, calculated by MARS-LBE 3.11	0.1139			
in 22-1	0.1960	Idelchik I.E, Handbook of Hydraulic Resistance, 3 rd edition, Jaico Publishing House, 2003	0.1963	0.3900	Emerson – Fisher, Control valve handbook, 4 th edition / ISA 75.01.01 – 2007, Flow equation for sizing control valves (tuning according to phase I)	0.0000	0.5121	Idelchik I.E, Handbook of Hydraulic Resistance, 3 rd edition, CRC press, 1994, calculated by MARS-LBE 3.11	0.2038			
22-1 → 22-2							0.0127	Idelchik I.E, Handbook of Hydraulic Resistance, 3 rd edition, CRC press, 1994, calculated by MARS-LBE 3.11	0.1139			
22-2 → 23-1												
in 23-2	0.6940	Idelchik I.E, Handbook of Hydraulic Resistance, 3 rd edition, Jaico Publishing House, 2003	0.1097	1.2900	Verein Deutscher Ingenieure, VDIWärmeatlas 3.0, Springer Verlag, Berlin Heidelberg, 2006	0.1116	1.4033	Verein Deutscher Ingenieure, VDIWärmeatlas 3.0, Springer Verlag, Berlin Heidelberg, 2006	0.1139	1.2900	Verein Deutscher Ingenieure, VDI	0.1050

in 23-3	0.1359	Idelchik I.E, Handbook of Hydraulic Resistance, 3 rd edition, Jaico Publishing House, 2003	0.1097	0.1013	Nippert, H., Über den Stromungsverlust in gekrümmten Kanälen, Forschungsarb. Geb. Ingenieurwes, no. 320, VDI, 1922, 85pp	0.1116	0.2218	Nippert, H., Über den Stromungsverlust in gekrümmten Kanälen, Forschungsarb. Geb. Ingenieurwes, no. 320, VDI, 1922, 85pp	0.1139	0.1678	Nippert H.	0.1050
in 23-5	0.1359	Idelchik I.E, Handbook of Hydraulic Resistance, 3 rd edition, Jaico Publishing House, 2003	0.1097	0.1013	Nippert, H., Über den Stromungsverlust in gekrümmten Kanälen, Forschungsarb. Geb. Ingenieurwes, no. 320, VDI, 1922, 85pp	0.1116	0.2218	Nippert, H., Über den Stromungsverlust in gekrümmten Kanälen, Forschungsarb. Geb. Ingenieurwes, no. 320, VDI, 1922, 85pp	0.1139	0.1678	Nippert H.	0.1050
23-5 → 23-6										0.0042	Trubenok, V.D.	0.1050

Table B.3 – Friction loss coefficient (f/l/d) at Case II: 9.8 kW

Sub-part No.	Sub-part name	Part length (mm)	Accumulated length (mm)	Accumulated elevation (mm)	ENEA			RSE			SNU			INEST		
					f(l/d)	Ref.	Ref. Velocity (m/s)	f(l/d)	Ref.	Ref. Velocity (m/s)	f(l/d)	Ref.	Ref. Velocity (m/s)	f(l/d)	Ref.	Ref. Velocity (m/s)
1-1	Core Inlet	180.7	180.7	0.0	0.0253	*	0.0943	0.1730	**	0.0970	0.0474	***	0.0969	0.0943	****	0.0905
1-2	Downcomer	1222.6	1403.3	-1222.6	0.6274	"	0.0187	1.1580	"	0.0190	0.6406	"	0.0192	0.2103	"	0.0045
1-3	Lower Plenum	212.8	1616.1	-1299.5	0.1324	"	0.0947	0.0710	"	0.0060	0.1232	"	0.0192	0.0141	"	0.0054
1-4	Core	1330.9	2946.9	31.3	1.9810	"	0.1279	6.2820	"	0.1320	2.1500	"	0.1317	0.9869	"	0.2326
1-5	Upper Plenum	681.6	3628.6	713.0	0.3371	"	0.0947	0.6510	"	0.0970	0.3573	"	0.0974	0.3478	"	0.0909
1-6	Gasket [Between Flanges]	4.5	3633.1	717.5	0.0000	"	0.0000	0.0000		0.0000	0.0000		0.0000	0.0023	"	0.0909
2-1	Pipe [One Side Flange]	300.0	3933.1	1017.5	0.8304	"	0.0947	0.2870	"	0.0970	0.1070	"	0.0974	0.1531	"	0.0909
2-2	Tee	127.0	4060.1	1144.5	0.8304	"	0.0947	0.1210	"	0.0970	0.1070	"	0.0974	0.0648	"	0.0909
2-3	Pipe [One Side Flange]	300.0	4360.1	1444.5	0.8304	"	0.0947	0.2870	"	0.0970	0.1251	"	0.0974	0.1531	"	0.0909
2-4	Gasket [Between Flanges]	4.5	4364.6	1449.0	0.8304	"	0.0947	0.0000		0.0000	0.0000		0.0000	0.0023	"	0.0909
3-1	Pipe [Both Side Flange]	1000.0	5364.6	2449.0	0.8304	"	0.0947	0.9550	"	0.0970	0.4681	"	0.0974	0.5102	"	0.0909
3-2	Gasket [Between Flanges]	4.5	5369.1	2453.5	0.0000	"	0.0000	0.0000		0.0000	0.0000		0.0000	0.0023	"	0.0909
4-1	45 Degree Elbow [One Side Flange]	82.5	5451.6	2529.9	0.8246	"	0.0947	0.0000	"	0.0000	0.0664	"	0.0974	0.0390	"	0.0909
4-2	Pipe	180.7	5632.3	2657.6	0.8246	"	0.0947	0.3300	"	0.0970	0.0597	"	0.0974	0.0652	"	0.0909
4-3	45 Degree Elbow	60.0	5692.3	2711.5	0.8246	"	0.0947	0.0000	"	0.0000	0.0743	"	0.0974	0.0275	"	0.0909
4-4	Pipe	718.9	6411.1	3430.4	0.8246	"	0.0947	0.6870	"	0.0970	0.3287	"	0.0974	0.3668	"	0.0909
4-5	Tee	127.0	6538.1	3557.4	0.8246	"	0.0947	0.1210	"	0.0970	0.0740	"	0.0974	0.0648	"	0.0909

4-6	Pipe	171.1	6709.2	3728.5	0.8246	"	0.0947	0.1630	"	0.0970	0.0573	"	0.0974	0.0873	"	0.0909
4-7	45 Degree Elbow	60.0	6769.2	3782.4	0.8246	"	0.0947	0.0000	"	0.0000	0.0597	"	0.0974	0.0275	"	0.0909
4-8	Pipe	180.7	6949.9	3910.1	0.8246	"	0.0947	0.3090	"	0.0970	0.0653	"	0.0974	0.0652	"	0.0909
4-9	45 Degree Elbow [One Side Flange]	82.5	7032.4	3986.5	0.8246	"	0.0947	0.0000	"	0.0000	0.0303	"	0.0974	0.0390	"	0.0909
4-10	Gasket [Between Flanges]	4.5	7036.9	3991.0	0.8246	"	0.0947	0.0000		0.0000	0.0000		0.0000	0.0023	"	0.0909
5-1	Gate Valve	216.0	7252.9	4207.0	1.8890	"	0.0947	0.0000	"	0.0000	0.1423	"	0.1743	0.1102	"	0.0909
5-2	Gasket [Between Flanges]	4.5	7257.4	4211.5	1.8890	"	0.0947	0.0000		0.0000	0.0000		0.0000	0.0023	"	0.0909
6-1	Pipe [Both Side Flange]	1000.0	8257.4	5211.5	1.8890	"	0.0947	0.9550	"	0.0970	0.4984	"	0.0974	0.5102	"	0.0909
6-2	Gasket [Between Flanges]	4.5	8261.9	5216.0	1.8890	"	0.0947	0.0000		0.0000	0.0000		0.0000	0.0023	"	0.0909
7-1	Pipe [Both Side Flange]	1000.0	9261.9	6216.0	1.8890	"	0.0947	0.9550	"	0.0970	0.4984	"	0.0974	0.5102	"	0.0909
7-2	Gasket [Between Flanges]	4.5	9266.4	6220.5	1.8890	"	0.0947	0.0000		0.0000	0.0000		0.0000	0.0023	"	0.0909
19-1	Pipe [Both Side Flange]	1000.0	10266.4	7220.5	1.8890	"	0.0947	0.9550	"	0.0970	0.5111	"	0.0974	0.5102	"	0.0909
8-4	Gasket [Between Flanges]	4.5	10270.9	7225.0	1.8890	"	0.0947	0.0000		0.0000	0.0000		0.0000	0.0023	"	0.0909
9-1	Pipe [Both Side Flange]	500.0	10770.9	7725.0	1.8890	"	0.0947	0.4780	"	0.0970	0.2708	"	0.0974	0.2551	"	0.0909
9-2	Gasket [Between Flanges]	4.5	10775.4	7729.5	1.8890	"	0.0947	0.0000		0.0000	0.0000		0.0000	0.0023	"	0.0909
10-1	Expansion Tank	868.2	11643.6	7933.8	0.3122	"	0.0947	0.5570	"	0.0970	0.2861	"	0.0974	0.1042	"	0.0909
10-2	Gasket [Between]	4.5	11648.1	7933.8	0.0000	"	0.0000	0.0000		0.0000	0.0000		0.0000	0.0023	"	0.0909

	Flanges]															
11-1	Pipe [Both Side Flange]	500.0	12148.1	7933.8	0.2513	"	0.0947	0.4780	"	0.0970	0.2616	"	0.0974	0.2551	"	0.0909
11-2	Gasket [Between Flanges]	4.5	12152.6	7933.8	0.0000	"	0.0000	0.0000		0.0000	0.0000		0.0000	0.0023	"	0.0909
12-1	Pipe [One Side Flange]	300.0	12452.6	7933.8	1.0443	"	0.0947	0.2870	"	0.0970	0.1070	"	0.0974	0.1531	"	0.0909
12-2	Tee	127.0	12579.6	7933.8	1.0443	"	0.0947	0.1210	"	0.0970	0.1073	"	0.0974	0.0648	"	0.0909
12-3	Pipe	305.4	12885.0	7933.8	1.0443	"	0.0947	0.2920	"	0.0970	0.1055	"	0.0974	0.1558	"	0.0909
12-4	90 Degree Elbow	120.0	13005.0	7857.6	1.0443	"	0.0947	0.2290	"	0.0970	0.0595	"	0.0974	0.0389	"	0.0909
12-5	90 Degree Elbow	120.0	13125.0	7781.4	1.0443	"	0.0947	0.2290	"	0.0970	0.0805	"	0.0974	0.0389	"	0.0909
12-6	Pipe[One Side Flange]	200.0	13325.0	7781.4	1.0443	"	0.0947	0.1910	"	0.0970	0.0597	"	0.0974	0.1020	"	0.0909
12-7	Gasket [Between Flanges]	4.5	13329.5	7781.4	1.0443	"	0.0947	0.0000		0.0000	0.0000		0.0000	0.0023	"	0.0909
13-1	Gate Valve	216.0	13545.5	7781.4	1.0443	"	0.0947	0.0000	"	0.0000	0.1430	"	0.1743	0.0964	"	0.1627
13-2	Gasket [Between Flanges]	4.5	13550.0	7781.4	1.0443	"	0.0947	0.0000		0.0000	0.0000		0.0000	0.0020	"	0.1627
14-1	Pipe [One Side Flange]	200.0	13750.0	7781.4	1.0443	"	0.0947	0.2390	"	0.0970	0.0822	"	0.0974	0.1020	"	0.0909
14-2	Tee	127.0	13877.0	7781.4	1.0443	"	0.0947	0.1210	"	0.0970	0.0789	"	0.0974	0.0648	"	0.0909
14-3	Pipe [One Side Flange]	382.3	14259.3	7781.4	1.0443	"	0.0947	0.3650	"	0.0970	0.1936	"	0.0974	0.1951	"	0.0909
14-4	Gasket [Between Flanges]	4.5	14263.8	7781.4	1.0443	"	0.0947	0.0000		0.0000	0.0000		0.0000	0.0023	"	0.0909
15-1	Heat Exchanger Vessel Inlet	202.5	14466.3	7781.4	0.0364	"	0.0947	0.1330	"	0.0970	0.0536	"	0.0974	0.1033	"	0.0909

15-2	Heat Exchanger Internal	2010.5	16476.8	5770.9	1.0083	"	0.0169	1.7890	"	0.0170	0.9170	"	0.0174	1.3113	"	0.0213
15-3	Heat Exchanger Outlet	202.5	16679.3	5770.9	0.0410	"	0.0947	0.1330	"	0.0970	0.1082	"	0.0969	0.1056	"	0.0905
15-4	Gasket [Between Flanges]	4.5	16683.8	5770.9	0.0000	"	0.0000	0.0000		0.0000	0.0000		0.0000	0.0011	"	0.0905
16-1	Pipe [One Side Flange]	219.8	16903.6	5770.9	2.0554	"	0.0943	0.2110	"	0.0970	0.0861	"	0.0969	0.0736	"	0.0905
16-2	90 Degree Elbow	120.0	17023.6	5694.7	2.0554	"	0.0943	0.1150	"	0.0970	0.0802	"	0.0969	0.0255	"	0.0905
16-3	Pipe	785.5	17809.1	4909.2	2.0554	"	0.0943	0.7530	"	0.0970	0.3807	"	0.0969	0.2632	"	0.0905
16-4	Tee	127.0	17936.1	4782.2	2.0554	"	0.0943	0.1220	"	0.0970	0.0961	"	0.0969	0.0426	"	0.0905
16-5	Pipe [One Side Flange]	500.0	18436.1	4282.2	2.0554	"	0.0943	0.4790	"	0.0970	0.2010	"	0.0969	0.1676	"	0.0905
16-6	Gasket [Between Flanges]	4.5	18440.6	4277.7	2.0554	"	0.0943	0.0000		0.0000	0.0000		0.0000	0.0015	"	0.0905
17-1	Gate Valve	216.0	18656.6	4061.7	2.0554	"	0.0943	0.0000	"	0.0000	0.1581	"	0.1735	0.1127	"	0.0905
17-2	Gasket [Between Flanges]	4.5	18661.1	4057.2	2.0554	"	0.0943	0.0000		0.0000	0.0000		0.0000	0.0023	"	0.0905
18-1	Pipe [One Side Flange]	500.0	19161.1	3557.2	2.0554	"	0.0943	0.4790	"	0.0970	0.2241	"	0.0969	0.2608	"	0.0905
18-2	Tee	127.0	19288.1	3430.2	2.0554	"	0.0943	0.1220	"	0.0970	0.0956	"	0.0969	0.0662	"	0.0905
18-3	Pipe [One Side Flange]	500.0	19788.1	2930.2	2.0554	"	0.0943	0.4790	"	0.0970	0.2420	"	0.0969	0.2608	"	0.0905
18-4	Gasket [Between Flanges]	4.5	19792.6	2925.7	2.0554	"	0.0943	0.0000		0.0000	0.0000		0.0000	0.0023	"	0.0905
8-1	Pipe [One Side Flange]	200.0	19992.6	2725.7	2.0554	"	0.0943	0.1920	"	0.0970	0.1072	"	0.0969	0.1043	"	0.0905
8-2	Orifice	600.0	20592.6	2125.7	2.0554	"	0.0943	0.5280	"	0.0850	0.2518	"	0.0849	0.3129	"	0.0905
8-3	Pipe [One Side Flange]	200.0	20792.6	1925.7	2.0554	"	0.0943	0.1920	"	0.0970	0.1152	"	0.0969	0.1043	"	0.0905

19-2	Gasket [Between Flanges]	4.5	20797.1	1921.2	2.0554	"	0.0943	0.0000		0.0000	0.0000		0.0000	0.0023	"	0.0905
20-1	Pipe [One Side Flange]	500.0	21297.1	1421.2	0.3005	"	0.0943	0.4790	"	0.0970	0.2223	"	0.0969	0.2608	"	0.0905
20-2	Tee	127.0	21424.1	1357.0	1.8307	"	0.0943	0.2740	"	0.0970	0.0587	"	0.0969	0.0335	"	0.0905
20-3	Pipe [One Side Flange]	100.0	21524.1	1357.0	1.8307	"	0.0943	0.0000	"	0.0970	0.0905	"	0.0969	0.0522	"	0.0905
20-4	Gasket [Between Flanges]	4.5	21528.6	1357.0	1.8307	"	0.0943	0.0000		0.0000	0.0000		0.0000	0.0023	"	0.0905
21-1	Pipe [One Side Flange]	757.1	22285.7	1357.0	1.8307	"	0.0943	0.7260	"	0.0970	0.3503	"	0.0969	0.3949	"	0.0905
21-2	90 Degree Elbow	120.0	22405.7	1280.8	1.8307	"	0.0943	0.2290	"	0.0970	0.0813	"	0.0969	0.0397	"	0.0905
21-3	Pipe	1204.6	23610.3	76.2	1.8307	"	0.0943	1.1550	"	0.0970	0.5903	"	0.0969	0.6283	"	0.0905
21-4	90 Degree Elbow	120.0	23730.3	0.0	1.8307	"	0.0943	0.2290	"	0.0970	0.1016	"	0.0969	0.0397	"	0.0905
21-5	Pipe [One Side Flange]	276.3	24006.6	0.0	1.8307	"	0.0943	0.2650	"	0.0970	0.0803	"	0.0969	0.1441	"	0.0905
21-6	Gasket [Between Flanges]	4.5	24011.1	0.0	1.8307	"	0.0943	0.0000		0.0000	0.0000		0.0000	0.0023	"	0.0905
22-1	Gate Valve	216.0	24227.1	0.0	1.8307	"	0.0943	0.0000	"	0.0000	0.1207	"	0.1735	0.1127	"	0.0905
22-2	Gasket [Between Flanges]	4.5	24231.6	0.0	1.8307	"	0.0943	0.0000		0.0000	0.0000		0.0000	0.0023	"	0.0905
23-1	Pipe [One Side Flange]	100.0	24331.6	0.0	1.8307	"	0.0943	0.2737	"	0.0970	0.0587	"	0.0969	0.0522	"	0.0905
23-2	Tee	127.0	24458.6	0.0	1.8307	"	0.0943	0.0000	"	0.0000	0.0474	"	0.0969	0.0662	"	0.0905
23-3	45 Degree Elbow	60.0	24518.6	0.0	0.2504	"	0.0943	0.0770	"	0.0970	0.0610	"	0.0969	0.0313	"	0.0905
23-4	Pipe	180.7	24699.2	0.0	0.2504	"	0.0943	0.1550	"	0.0970	0.0679	"	0.0969	0.0942	"	0.0905
23-5	45 Degree Elbow [One Side Flange]	82.5	24781.7	0.0	0.2504	"	0.0943	0.0770	"	0.0970	0.0679	"	0.0969	0.0430	"	0.0905

23-6	Gasket [Between Flanges]	4.5	24786.2	0.0	0.0000		0.0000	0.0000		0.0000	0.0000		0.0000	0.0023	"	0.0905
------	--------------------------------	-----	---------	-----	--------	--	--------	--------	--	--------	--------	--	--------	--------	---	--------

* Zigrang-Sylvester approximation of Colebrook-White correlation, calculated by RELAP5 mod3.3

** Colebrook-White correlation, calculated by LegoPST

*** Colebrook-White correlation, calculated by MARS-LBE 3.11

**** Zigrang-Sylvester correlation, calculated by RELAP5 MOD 4.0

Table B.4 – Form loss coefficient (K) at Case II: 9.8 kW.

	ENEA			RSE			SNU			INEST		
	K	Ref.	Ref. Velocity (m/s)	K	Ref.	Ref. Velocity (m/s)	K	Ref.	Ref. Velocity (m/s)	K	Ref.	Ref. Velocity (m/s)
23-6 → 1-1	0.4978	Idelchik I.E., Handbook of Hydraulic Resistance, 3 rd edition, Jaico Publishing House, 2003	0.0943							0.0042	Trubenok, V.D.	0.0905
1-1 → 1-2	0.9942	Idelchik I.E., Handbook of Hydraulic Resistance, 3 rd edition, Jaico Publishing House, 2003	0.0943	1.1390	Idelchik I.E., Handbook of Hydraulic Resistance, 3 rd edition, CRC press, 1994	0.0970	0.7095	Idelchik I.E., Handbook of Hydraulic Resistance, 3 rd edition, CRC press, 1994, calculated by MARS-LBE 3.11	0.0969	1.2900	Verein Deutscher Ingenieure, VDI	0.0905
1-2 → 1-3	0.4064	Idelchik I.E., Handbook of Hydraulic Resistance, 3 rd edition, Jaico Publishing House, 2003	0.0187	0.4910	Idelchik I.E., Handbook of Hydraulic Resistance, 3 rd edition, CRC press, 1994	0.0190	0.4002	Idelchik I.E., Handbook of Hydraulic Resistance, 3 rd edition, CRC press, 1994, calculated by MARS-LBE 3.11	0.1316	0.0388	Idelchik I.E.	0.0054
1-3 → 1-4	0.4557	Idelchik I.E., Handbook of Hydraulic Resistance, 3 rd edition, Jaico Publishing House, 2003	0.1279	0.6260	Idelchik I.E., Handbook of Hydraulic Resistance, 3 rd edition, CRC press, 1994	0.0060				0.4839	Idelchik I.E.	0.2321
in 1-4	10.4929	Rehme, K., Pressure Drop Correlations for Fuel Element Spacers, Nuclear Technology, Vol.17, pp.15-23, 1973	0.1282	12.430 0	Rehme, K., Pressure Drop Correlations for Fuel Element Spacers, Nuclear Technology, Vol.17, pp.15-23, 1973 – Drag coefficient modified according to phase I	0.1316	4.7339	Rehme, K., Pressure Drop Correlations for Fuel Element Spacers, Nuclear Technology, Vol.17, pp.15-23, 1973	0.1317	2.11528*3	Idelchik I.E.	0.2326
1-4 → 1-5	0.0692	Idelchik I.E., Handbook of Hydraulic Resistance, 3 rd edition, Jaico Publishing House, 2003	0.1285	0.0690	Idelchik I.E., Handbook of Hydraulic Resistance, 3 rd edition, CRC press, 1994	0.1321	0.0744	Idelchik I.E., Handbook of Hydraulic Resistance, 3 rd edition, CRC press, 1994, calculated by MARS-LBE 3.11	0.1321			
1-5 → 1-6										0.0042	Trubenok, V.D.	0.0909
1-6 → 2.1	0.4978	Idelchik I.E., Handbook of Hydraulic Resistance, 3 rd edition, Jaico Publishing House, 2003	0.0947									

in 2-2												
2-3 → 2-4									0.0042	Trubenok, V.D.		0.0909
2-4 → 3-1	0.4978	Idelchik I.E, Handbook of Hydraulic Resistance, 3 rd edition, Jaico Publishing House, 2003	0.0947									
3-1 → 3-2									0.0042	Trubenok, V.D.		0.0909
3-2 → 4-1	0.4978	Idelchik I.E, Handbook of Hydraulic Resistance, 3 rd edition, Jaico Publishing House, 2003	0.0947									
in 4-1	0.1359	Idelchik I.E, Handbook of Hydraulic Resistance, 3 rd edition, Jaico Publishing House, 2003	0.0947	0.1040	Nippert, H., Über den Stromungsverlust in gekrümmten Kanälen, Forschungsarb. Geb. Ingenieurwes, no. 320, VDI, 1922, 85pp	0.0970	0.2287	Nippert, H., Über den Stromungsverlust in gekrümmten Kanälen, Forschungsarb. Geb. Ingenieurwes, no. 320, VDI, 1922, 85pp	0.0974	0.1579	Nippert H.	0.0909
in 4-3	0.1359	Idelchik I.E, Handbook of Hydraulic Resistance, 3 rd edition, Jaico Publishing House, 2003	0.0947	0.1040	Nippert, H., Über den Stromungsverlust in gekrümmten Kanälen, Forschungsarb. Geb. Ingenieurwes, no. 320, VDI, 1922, 85pp	0.0970	0.2287	Nippert, H., Über den Stromungsverlust in gekrümmten Kanälen, Forschungsarb. Geb. Ingenieurwes, no. 320, VDI, 1922, 85pp	0.0974	0.1579	Nippert H.	0.0909
in 4-5												
in 4-7	0.1359	Idelchik I.E, Handbook of Hydraulic Resistance, 3 rd edition, Jaico Publishing House, 2003	0.0947	0.1040	Nippert, H., Über den Stromungsverlust in gekrümmten Kanälen, Forschungsarb. Geb. Ingenieurwes, no. 320, VDI, 1922, 85pp	0.0970	0.2287	Nippert, H., Über den Stromungsverlust in gekrümmten Kanälen, Forschungsarb. Geb. Ingenieurwes, no. 320, VDI, 1922, 85pp	0.0974	0.1579	Nippert H.	0.0909
in 4-9	0.1359	Idelchik I.E, Handbook of Hydraulic Resistance, 3 rd edition, Jaico Publishing House, 2003	0.0947	0.1040	Nippert, H., Über den Stromungsverlust in gekrümmten Kanälen, Forschungsarb. Geb. Ingenieurwes, no. 320, VDI, 1922, 85pp	0.0970				0.1579	Nippert H.	0.0909
4-9 → 4-10									0.0042	Trubenok, V.D.		0.0909

4-10 → 5-1	0.4718	Idelchik I.E, Handbook of Hydraulic Resistance, 3 rd edition, Jaico Publishing House, 2003	0.0947			0.2385	Idelchik I.E, Handbook of Hydraulic Resistance, 3 rd edition, CRC press, 1994, calculated by MARS-LBE 3.11	0.0974				
in 5-1	0.1960	Idelchik I.E, Handbook of Hydraulic Resistance, 3 rd edition, Jaico Publishing House, 2003	0.1695	0.3900	Emerson – Fisher, Control valve handbook, 4 th edition / ISA 75.01.01 – 2007, Flow equation for sizing control valves (tuning according to phase I)	0.0000	0.5162	Idelchik I.E, Handbook of Hydraulic Resistance, 3 rd edition, CRC press, 1994, calculated by MARS-LBE 3.11	0.1743	0.1969	B.S.Massey	0.0909
5-1 → 5-2							0.0129	Idelchik I.E, Handbook of Hydraulic Resistance, 3 rd edition, CRC press, 1994, calculated by MARS-LBE 3.11	0.0974	0.0042	Trubenok, V.D.	0.0909
5-2 → 6-1	0.4487	Idelchik I.E, Handbook of Hydraulic Resistance, 3 rd edition, Jaico Publishing House, 2003	0.0947									
6-1 → 6-2										0.0042	Trubenok, V.D.	0.0909
6-2 → 7-1	0.4978	Idelchik I.E, Handbook of Hydraulic Resistance, 3 rd edition, Jaico Publishing House, 2003	0.0947									
7-1 → 7-2										0.0042	Trubenok, V.D.	0.0909
7-2 → 19-1												
19-1 → 8-4										0.0042	Trubenok, V.D.	0.0909
8-4 → 9-1	0.4978	Idelchik I.E, Handbook of Hydraulic Resistance, 3 rd edition, Jaico Publishing House, 2003	0.0947									
9-1 → 9-2												
9-2 → 10-1	0.4978	Idelchik I.E, Handbook of Hydraulic Resistance, 3 rd edition, Jaico Publishing House, 2003	0.0947	1.0000	Idelchik I.E, Handbook of Hydraulic Resistance, 3 rd edition, CRC press, 1994	0.0970	0.9900	Idelchik I.E, Handbook of Hydraulic Resistance, 3 rd edition, CRC press, 1994, calculated by MARS-LBE 3.11	0.0974	0.0042	Trubenok, V.D.	0.0909

in 10-1	1.6572	Idelchik I.E, Handbook of Hydraulic Resistance, 3 rd edition, Jaico Publishing House, 2003	0.0947	0.7870	Idelchik I.E, Handbook of Hydraulic Resistance, 3 rd edition, CRC press, 1994	0.0970	0.3929	Idelchik I.E, Handbook of Hydraulic Resistance, 3 rd edition, CRC press, 1994, calculated by MARS-LBE 3.11	0.0974			
10-1 → 10-2							0.4140	Idelchik I.E, Handbook of Hydraulic Resistance, 3 rd edition, CRC press, 1994, calculated by MARS-LBE 3.11	0.0974	0.9482	Idelchik I.E	0.0909
10-2 → 11-1	0.4978	Idelchik I.E, Handbook of Hydraulic Resistance, 3 rd edition, Jaico Publishing House, 2003	0.0947							0.4818	B.S.Massey	0.0909
11-1 → 11-2										0.0042	Trubenok, V.D.	0.0909
11-2 → 12-1	0.4978	Idelchik I.E, Handbook of Hydraulic Resistance, 3 rd edition, Jaico Publishing House, 2003	0.0947									
in 12-2												
in 12-4	0.2222	Idelchik I.E, Handbook of Hydraulic Resistance, 3 rd edition, Jaico Publishing House, 2003	0.0947	0.2870	Nippert, H., Über den Stromungsverlust in gekrümmten Kanälen, Forschungsarb. Geb. Ingenieurwes, no. 320, VDI, 1922, 85pp	0.0970	0.3929	Nippert, H., Über den Stromungsverlust in gekrümmten Kanälen, Forschungsarb. Geb. Ingenieurwes, no. 320, VDI, 1922, 85pp	0.0974	0.2633	Nippert H.	0.0909
in 12-5	0.2222	Idelchik I.E, Handbook of Hydraulic Resistance, 3 rd edition, Jaico Publishing House, 2003	0.0947	0.2870	Nippert, H., Über den Stromungsverlust in gekrümmten Kanälen, Forschungsarb. Geb. Ingenieurwes, no. 320, VDI, 1922, 85pp	0.0970	0.3929	Nippert, H., Über den Stromungsverlust in gekrümmten Kanälen, Forschungsarb. Geb. Ingenieurwes, no. 320, VDI, 1922, 85pp	0.0974	0.2633	Nippert H.	0.0909
12-6 → 12-7										0.0042	Trubenok, V.D.	0.0909
12-7 → 13-1	0.4718	Idelchik I.E, Handbook of Hydraulic Resistance, 3 rd edition, Jaico Publishing House, 2003	0.0947				0.0098	Idelchik I.E, Handbook of Hydraulic Resistance, 3 rd edition, CRC press, 1994, calculated by MARS-LBE 3.11	0.0974	0.1969	B.S.Massey	0.1627

in 13-1	0.1960	Idelchik I.E, Handbook of Hydraulic Resistance, 3 rd edition, Jaico Publishing House, 2003	0.1695	0.3900	Emerson – Fisher, Control valve handbook, 4 th edition / ISA 75.01.01 – 2007, Flow equation for sizing control valves (tuning according to phase I)	0.0000	0.5162	Idelchik I.E, Handbook of Hydraulic Resistance, 3 rd edition, CRC press, 1994, calculated by MARS-LBE 3.11	0.1743	0.2438	Idelchik I.E	0.1627
13-1 → 13-2							0.0129	Idelchik I.E, Handbook of Hydraulic Resistance, 3 rd edition, CRC press, 1994, calculated by MARS-LBE 3.11	0.0974			
13-2 → 14-1	0.4487	Idelchik I.E, Handbook of Hydraulic Resistance, 3 rd edition, Jaico Publishing House, 2003	0.0947							0.0042	Trubenok, V.D.	0.1627
in 14-2												
14-3 → 14-4										0.0042	Trubenok, V.D.	0.0909
14-4 → 15-1	0.4978	Idelchik I.E, Handbook of Hydraulic Resistance, 3 rd edition, Jaico Publishing House, 2003	0.0947									
15-1 → 15-2	0.4972	Idelchik I.E, Handbook of Hydraulic Resistance, 3 rd edition, Jaico Publishing House, 2003	0.0947				0.7436	Idelchik I.E, Handbook of Hydraulic Resistance, 3 rd edition, CRC press, 1994, calculated by MARS-LBE 3.11	0.0974	1.2900	Verein Deutscher Ingenieure, VDI	0.0909
in 15-2	9.0360	Rehme, K., Pressure Drop Correlations for Fuel Element Spacers, Nuclear Technology, Vol.17, pp.15-23, 1973	0.0169	13.084 0	Rehme, K., Pressure Drop Correlations for Fuel Element Spacers, Nuclear Technology, Vol.17, pp.15-23, 1973	0.0170	6.5287	Rehme, K., Pressure Drop Correlations for Fuel Element Spacers, Nuclear Technology, Vol.17, pp.15-23, 1973	0.0174	1.35406*6	Idelchik I.E	0.0909
15-2 → 15-3	0.3526	Idelchik I.E, Handbook of Hydraulic Resistance, 3 rd edition, Jaico Publishing House, 2003	0.0943				0.4068	Idelchik I.E, Handbook of Hydraulic Resistance, 3 rd edition, CRC press, 1994, calculated by MARS-LBE 3.11	0.0969	1.2900	Verein Deutscher Ingenieure, VDI	0.0214
15-3 → 15-4										0.0042	Trubenok, V.D.	0.0905

15-4 → 16-1	0.4978	Idelchik I.E, Handbook of Hydraulic Resistance, 3 rd edition, Jaico Publishing House, 2003	0.0943									
in 16-2	0.2222	Idelchik I.E, Handbook of Hydraulic Resistance, 3 rd edition, Jaico Publishing House, 2003	0.0943	0.2920	Nippert, H., Über den Stromungsverlust in gekrümmten Kanälen, Forschungsarb. Geb. Ingenieurwes, no. 320, VDI, 1922, 85pp	0.0966	0.3999	Nippert, H., Über den Stromungsverlust in gekrümmten Kanälen, Forschungsarb. Geb. Ingenieurwes, no. 320, VDI, 1922, 85pp	0.0969	0.2633	Nippert H.	0.0905
in 16-4												
16-5 → 16-6										0.0042	Trubenok, V.D.	0.0905
16-6 → 17-1	0.4718	Idelchik I.E, Handbook of Hydraulic Resistance, 3 rd edition, Jaico Publishing House, 2003	0.1687				0.0098	Idelchik I.E, Handbook of Hydraulic Resistance, 3 rd edition, CRC press, 1994, calculated by MARS-LBE 3.11	0.0969			
in 17-1	0.1960	Idelchik I.E, Handbook of Hydraulic Resistance, 3 rd edition, Jaico Publishing House, 2003	0.0943	0.3900	Emerson – Fisher, Control valve handbook, 4 th edition / ISA 75.01.01 – 2007, Flow equation for sizing control valves (tuning according to phase I)	0.0000	0.5163	Idelchik I.E, Handbook of Hydraulic Resistance, 3 rd edition, CRC press, 1994, calculated by MARS-LBE 3.11	0.1735	0.4406	B.S.Massey, Idelchik I.E	0.0905
17-1 → 17-2							0.0129	Idelchik I.E, Handbook of Hydraulic Resistance, 3 rd edition, CRC press, 1994, calculated by MARS-LBE 3.11	0.0969	0.0042	Trubenok, V.D.	0.0905
17-2 → 18-1	0.4487	Idelchik I.E, Handbook of Hydraulic Resistance, 3 rd edition, Jaico Publishing House, 2003	0.0943									
in 18-2												
18-3 → 18-4	0.4978	Idelchik I.E, Handbook of Hydraulic Resistance, 3 rd edition, Jaico Publishing House, 2003	0.0943							0.0042	Trubenok, V.D.	0.0905

18-4 → 8-1	0.4648	Idelchik I.E, Handbook of Hydraulic Resistance, 3 rd edition, Jaico Publishing House, 2003	0.0943	0.0171	Idelchik I.E, Handbook of Hydraulic Resistance, 3 rd edition, CRC press, 1994	0.0970	0.0171	Idelchik I.E, Handbook of Hydraulic Resistance, 3 rd edition, CRC press, 1994, calculated by MARS-LBE 3.11	0.0969			
in 8-2	10.2020	Idelchik, I.E., Determination of the resistance coefficients during discharge through orifices	0.0826	10.4250	Idelchik, I.E., Determination of the resistance coefficients during discharge through orifices, Gidrotekh. Stroit., no. 5, 31-36, 1953	0.2250	11.6540	Idelchik, I.E., Determination of the resistance coefficients during discharge through orifices, Gidrotekh. Stroit., no. 5, 31-36, 1953	0.0849	0.4460	Idelchik I.E	0.0905
8-3 → 19-2	0.4318	Idelchik I.E, Handbook of Hydraulic Resistance, 3 rd edition, Jaico Publishing House, 2003	0.0826	0.1050	Idelchik I.E, Handbook of Hydraulic Resistance, 3 rd edition, CRC press, 1994	0.0850	0.0226	Idelchik I.E, Handbook of Hydraulic Resistance, 3 rd edition, CRC press, 1994, calculated by MARS-LBE 3.11	0.0969	0.0042	Trubenok, V.D.	0.0905
19-2 → 20-1	0.4978	Idelchik I.E, Handbook of Hydraulic Resistance, 3 rd edition, Jaico Publishing House, 2003	0.0943									
in 20-2	0.7200	Idelchik I.E, Handbook of Hydraulic Resistance, 3 rd edition, Jaico Publishing House, 2003	0.0943	1.2900	Verein Deutscher Ingenieure, VDIWärmeatlas 3.0, Springer Verlag, Berlin Heidelberg, 2006	0.0969	1.4232	Verein Deutscher Ingenieure, VDIWärmeatlas 3.0, Springer Verlag, Berlin Heidelberg, 2006	0.0969	1.2900	Verein Deutscher Ingenieure, VDI	0.0905
20-3 → 20-4										0.0042	Trubenok, V.D.	0.0905
20-4 → 21-1	0.4978	Idelchik I.E, Handbook of Hydraulic Resistance, 3 rd edition, Jaico Publishing House, 2003	0.0943									
in 21-2	0.2222	Idelchik I.E, Handbook of Hydraulic Resistance, 3 rd edition, Jaico Publishing House, 2003	0.0943	0.2920	Nippert, H., Über den Stromungsverlust in gekrümmten Kanälen, Forschungsarb. Geb. Ingenieurwes, no. 320, VDI, 1922, 85pp	0.0970	0.3864	Nippert, H., Über den Stromungsverlust in gekrümmten Kanälen, Forschungsarb. Geb. Ingenieurwes, no. 320, VDI, 1922, 85pp	0.0969	0.2633	Nippert H.	0.0905
in 21-4	0.2222	Idelchik I.E, Handbook of Hydraulic Resistance, 3 rd edition, Jaico Publishing House, 2003	0.0943	0.2920	Nippert, H., Über den Stromungsverlust in gekrümmten Kanälen, Forschungsarb. Geb. Ingenieurwes, no. 320, VDI, 1922, 85pp	0.0970	0.3999	Nippert, H., Über den Stromungsverlust in gekrümmten Kanälen, Forschungsarb. Geb. Ingenieurwes, no. 320, VDI, 1922, 85pp	0.0969	0.2633	Nippert H.	0.0905

21-5 → 21-6										0.0042	Trubenok, V.D.	0.0905
21-6 → 22-1	0.4978	Idelchik I.E, Handbook of Hydraulic Resistance, 3 rd edition, Jaico Publishing House, 2003	0.0943				0.0098	Idelchik I.E, Handbook of Hydraulic Resistance, 3 rd edition, CRC press, 1994, calculated by MARS-LBE 3.11	0.0969			
in 22-1	0.1960	Idelchik I.E, Handbook of Hydraulic Resistance, 3 rd edition, Jaico Publishing House, 2003	0.1687	0.3900	Emerson – Fisher, Control valve handbook, 4 th edition / ISA 75.01.01 – 2007, Flow equation for sizing control valves (tuning according to phase I)	0.0000	0.5162	Idelchik I.E, Handbook of Hydraulic Resistance, 3 rd edition, CRC press, 1994, calculated by MARS-LBE 3.11	0.1735			
22-1 → 22-2							0.0129	Idelchik I.E, Handbook of Hydraulic Resistance, 3 rd edition, CRC press, 1994, calculated by MARS-LBE 3.11	0.0969			
22-2 → 23-1												
in 23-2	0.6940	Idelchik I.E, Handbook of Hydraulic Resistance, 3 rd edition, Jaico Publishing House, 2003	0.0943	1.2900	Verein Deutscher Ingenieure, VDI Wärmeatlas 3.0, Springer Verlag, Berlin Heidelberg, 2006	0.0970	1.4232	Verein Deutscher Ingenieure, VDI Wärmeatlas 3.0, Springer Verlag, Berlin Heidelberg, 2006	0.0969	1.2900	Verein Deutscher Ingenieure, VDI	0.0905
in 23-3	0.1359	Idelchik I.E, Handbook of Hydraulic Resistance, 3 rd edition, Jaico Publishing House, 2003	0.0943	0.1060	Nippert, H., Über den Stromungsverlust in gekrümmten Kanälen, Forschungsarb. Geb. Ingenieurwes, no. 320, VDI, 1922, 85pp	0.0970	0.2327	Nippert, H., Über den Stromungsverlust in gekrümmten Kanälen, Forschungsarb. Geb. Ingenieurwes, no. 320, VDI, 1922, 85pp	0.0969	0.1579	Nippert H.	0.0905
in 23-5	0.1359	Idelchik I.E, Handbook of Hydraulic Resistance, 3 rd edition, Jaico Publishing House, 2003	0.0943	0.1060	Nippert, H., Über den Stromungsverlust in gekrümmten Kanälen, Forschungsarb. Geb. Ingenieurwes, no. 320, VDI, 1922, 85pp	0.0970	0.2327	Nippert, H., Über den Stromungsverlust in gekrümmten Kanälen, Forschungsarb. Geb. Ingenieurwes, no. 320, VDI, 1922, 85pp	0.0969	0.1579	Nippert H.	0.0905
23-5 → 23-6										0.0042	Trubenok, V.D.	0.0905